University of Arkansas, Fayetteville

ScholarWorks@UARK

Graduate Theses and Dissertations

12-2016

Growth of GeSn and GePb Alloy Films Using Thermal Evaporator

Hakimah Alahmed
University of Arkansas, Fayetteville

Follow this and additional works at: https://scholarworks.uark.edu/etd

Part of the Electronic Devices and Semiconductor Manufacturing Commons

Citation

Alahmed, H. (2016). Growth of GeSn and GePb Alloy Films Using Thermal Evaporator. *Graduate Theses and Dissertations* Retrieved from https://scholarworks.uark.edu/etd/1861

This Thesis is brought to you for free and open access by ScholarWorks@UARK. It has been accepted for inclusion in Graduate Theses and Dissertations by an authorized administrator of ScholarWorks@UARK. For more information, please contact scholar@uark.edu.

Growth of GeSn and GePb Alloy Films Using Thermal Evaporator

A thesis submitted in partial fulfillment
of the requirements for the degree of
Master of Science in Microelectronics-Photonics

by

Hakimah Alahmed
King Faisal University
Bachelor of Science in Physics, 2011

December 2016
University of Arkansas

This thesis is approved for recommendation to the Graduate Council.

Dr. Hameed Naseem
Thesis Director

Dr. Surendra Singh
Committee Member

Dr. Shui-Qing (Fisher) Yu
Committee Member

Dr. Rick Wise
Committee Member

The following signatories attest that all software used in this thesis was legally licensed for use by Hakimah Alahmed for research purposes and publication.

______________________________	______________________________
Ms. Hakimah Alahmed, Student	Dr. Hameed Naseem, Thesis Director

This thesis was submitted to http://www.turnitin.com for plagiarism review by the TurnItIn company's software. The signatories have examined the report on this thesis that was returned by TurnItIn and attest that, in their opinion, the items highlighted by the software are incidental to common usage and are not plagiarized material.

______________________________	______________________________
Dr. Rick Wise, Program Director	Dr. Hameed Naseem, Thesis Director

Abstract

Silicon is the most important semiconductor material used in microelectronic devices. As the number of transistors keep doubling every 24 months (Moore's law), transistors continue scaling down in size, electrical interconnect is reaching its limits to keep up with the scaling down rate in integrated circuits. These limitations are related to interconnect density and power consumption. Hence, replacing electrical interconnect with optical interconnect on the chip or between chips has the ability to overcome these limitations. However, silicon has poor light emitting efficiency, and other substitutes such as III-V materials are not suitable due to high cost, lattice mismatch, and thermal mismatch with Si. Recently researchers have been developing novel group IV alloys from silicon, germanium, and tin to overcome these problems.

In this research a less developed group IV alloy, GePb, as well as GeSn, have been studied for the development of optoelectronic devices. A physical vapor deposition method is used to evaporate the solid sources in a thermal evaporator chamber to deposit the films on a Si substrate. The GeSn and GePb samples were deposited at room temperature then annealed in a Fisher Scientific furnace at different temperatures (300-600 °C) and times (15-60 min). Material and optical characterization of the samples was performed using Raman spectroscopy, X-ray diffraction, photoluminescence, and scanning electron microscopy.

Acknowledgement

Firstly, I would like to thank God for giving me the health, patience, and power to keep following my dream and goals. Second, I would like to thank Dr. Hameed Naseem, for his support in my Master's work. He has motivated me and kept pushing me forward to success. I would not be able to achieve my goals without his help and support. He always seeks for my straightness and tries to guide me to the right way. Also, when I asking questions, he prefers that I tried my best searching for the answers to advance my research skill. I feel that he makes me a better student and taught me how to face my weakness and come up with solutions. I would like to thank Dr. Fisher Yu for his support and motivation. Also, he allowed me to use his characterization lab to get training for the Raman spectroscopy. I am thankful for my committee members Dr. Fisher Yu, Surendra Singh, and Dr. Rick Wise who helped me achieve my goals and were patient and supportive. I have a special thanks to Dr. Rick Wise for his great help, motivation, and support.

I would like to thank my postdoctoral, Dr. Murtada Alhur, who gave me the time and effort to complete my research. Aslo, he spent a lot time training me on the thermal evaporator, sample cleaning process, and Raman spectroscope. Thank you is not enough for him. I am very thankful to Salman who gave me his time and answered my questions, corrected my mistakes, and proof read my thesis. Even though he was very busy, he tried to give me help and support anyway. He followed my progress and kept advising me to do my best in each part of my research. I am lucky to have had Dr. Hussam helping me on my research and teaching me how to analyze data. I would like to thank Dr. Yu's group: Sattar, Amir, and PC who helped me a lot with the optical characterization. I am thankful for Dr. Mourad, and Andrian who helped me with

the material characterization, XRD and SEM. I am thankful for my friend, Fahimah, who tried her best answering my questions and discussing my work. I want to thank my family: my mother, Fatima Almubarak, my father, Ahmed Alahmed , and my siblings for their motivation and support to study aboard. Lots of thanks, for my supportive friends. Thanks for King Abdullah Scholarship Program, which opens the opportunity for me to complete my study in the U.S. Also, thank you to all of the University of Arkansas faculty and students.

Dedication

To my mother, father, and sisters.

Table of Contents

Chapter 1: Introduction 1
1.1 Motivation 1
1.2 Optical Interconnect 2
1.3 Germanium Alloys 3
1.4 Thesis Organization 4
Chapter 2: Theoretical Framework 5
2.1 Crystal Structure 5
2.2 Ge alloys Structure 7
2.3 Solubility of Pb and Sn in Ge 10
2.4 Epitaxial Growth 10
2.5 Strained Lattice 12
2.6 Film Depositing 13
2.6.1 Thin Film Deposition 13
2.6.2 Chemical vapor deposition (CVD) 15
2.7 Evaporation Sources 17
2.7.1 Evaporation 17
2.7.1.1 Sputtering 19
2.7.1.2 Physical Vapor Deposition (PVD) 19
2.7.1.3 Electron Beam (E-beam) Evaporation 21
2.7.1.4 Thermal Evaporator 23
2.8 Materials Background. 25
2.8.1Germanium (Ge) 25
2.8.2 Tin (Sn) 26
2.8.3 Lead (Pb) 26
Chapter 3: Literature Review 27
3.1 Growth of GePb 27
3.2 Growth of GeSn 29
Chapter 4: Experimental Methodology and Equipment 31
4.1 Experimental Procedures 31

4.1.1 Sample Cleaning 31
4.1.2 Deposition Process 32
4.1.3 Sample Annealing Process 33
4.1.4 Wet Etching Process 36
4.2 Equipment 36
4.2.1 Deposition Equipment 36
Chapter 5 Results and Discussion 49
5.1 The Fabrication Process of Ge Alloy 50
5.1.1 Fabrication Process of GeSn 50
5.1.2 Fabrication Process of GePb 52
5.2 GeSn Result 53
5.2.1 Raman Spectroscopy 53
5.2.1.2 Annealing Temperature Study 55
5.2.1.3 GeSn on Glass Substrate 56
5.2.2 Photoluminescence Spectra (PL) 57
5.2.3 X-Ray Diffraction (XRD) Result 59
5.3 GePb Results 60
5.3.1 Raman Spectroscopy 60
5.3.1.2 Annealing Time tudy 62
5.3.2 GePb Photoluminesces spectra result 65
5.3.4 X-Ray Powder Diffraction (XRD) result 70
5.3.5 GePb SEM Results 71
Chapter 6: Conclusion 79
References 80
Appendix A: Description of Research for Popular Publication: Faster Electronic Devices for a Bright Future 85
Appendix B: Executive Summary of Newly Created Intellectual Property 87
Appendix C: Potential Patent and Commercialization Aspects of Listed Intellectual 88
Property Items 88
Appendix D: Broader Impact of Research 89
Appendix E: Microsoft Project for MS MicroEP Degree Plan 90

Appendix F: Identification of All Software Used in Research and Thesis Generation 93

List of Figures

Figure 2.1. Lattice structure (a) Ge diamond structure, (b) Pb FCC structure……………………5

Figure 2.2. Schematics of band structures of Ge, Sn, GeSn……………………………………....6

Figure 2.3. Group IV hydride…………………………………..…………………………….....8

Figure 2.4. Group IV element lattice sizes………………………………..………………....8

Figure 2.5. Cluster calculation and Vegard's law of GeSn and GePb…………………………...10

Figure 2.6. (a) band gap structure of GePb with different composition (0.5-2%), (b) the band gap at (L, Γ and X valleys) with the concentration dependence…………………………...10

Figure 2.7. Phase diagram of (a) GePb and (b) GeSn. ……………………………………..11

Figure 2.8. Schematic of lattice match, strain, and relaxe……………..…………………………...14

Figure 2.9. Sketch of thin films nucleation and growth phenomena. …………………………...15

Figure 2.10. Diagram determines angles and parameters used in the deposition derivation rate in evaporation..……………………………………..………………………………16

Figure 2.11. Different types of PVD………………………………………………………….18

Figure 2.12. Physical deposition phases………………………………………………………20

Figure 2.13. E-beam evaporator. ………………………………………………………….…..22

Figure 2.14. Simple drawing of thermal evaporator system. ……………………………….....24

Figure 2.15. Different sources for thermal evaporation of materials. …………………………...25

Figure 4.1. Fabrication process of GePb/GeSn.……………………………………………….38

Figure 4.2. Fabrication process of GePb/GeSn….………………………………………….....39

Figure 4.3. Fisher Scientific furnace.………………………………...……………………..41

Figure 4.4. Schematic diagram of Raman spectroscope set-up. ……………………………...42

Figure 4.5. Raman spectroscopy system.……………………………………………………...43

Figure 4.6. Diagram of photoluminescence set-up……………………………………………44

Figure 4.7. Photoluminescence system. ………………………………………………………………45

Figure 4.8. A picture of XRD system…………………..……………………………………..46

Figure 4.9. Bragg's low: X-ray interaction with the atoms……………………………………..47

Figure 4.10. SEM system……………………………………………………..……………..48

Figure 4.11. A schematic of SEM system…………………………………………………..49

Figure 5.1. GeSn sample surface changes during the fabrication. ……………………………...52

Figure 5.2. GePb sample surface changes during the fabrication………………………………53

Figure 5.3. Comparison of the Raman spectroscopy of Ge reference and GeSn annealed for 1 hour at 400 °C under N_2 environment on a Si substrate…………………………………...55

Figure 5.4. Raman spectroscopy of GeSn at different annealing temperature (300-600 °C) for 1 hour under N_2 environment…………………………………………………………...57

Figure 5.5. Comparison of the Raman spectroscopy of Ge reference and GeSn annealed for 1 hour at 400 °C under N_2 environment on glass substrate.…………………………………57

Figure 5.6. Photoluminescence spectra for Ge reference, GeSn film on Si and glass annealed at 400 °C for one hour under N_2 environment……………………………………….. 58

Figure 5.7. Photoluminescence spectra for GeSn film on glass annealed at 400 ºC and 500 ºC for 1 hour under N_2 environment…………………………………………………………..59

Figure 5.8. XRD patterns for GeSn/Si annealed at 300 ºC for 1 hour under N_2 environment…..60

Figure 5.9 Comparison of the Raman spectroscopy of the Ge reference and the GePb sample annealed for 1 hour at 400 °C under N_2 environment on a Si substrate…………….……...62

Figure 5.10. Raman spectroscopy of Ge reference and GePb on Si substrate at different annealing temperature (300-600 °C) for 1 hour under N_2 environment…….…………62

Figure 5.11. Raman spectroscopy of the Ge reference and GePb annealed at 300 °C for 15-30-60 min under N_2 environment on a Si substrate………….…………………….. 64

Figure 5.12. Raman spectroscopy of the Ge reference and GePb annealed at 400 °C for 15-30- 60 min under N_2 environment on a Si substrate……………………………………..65

Figure 5.13. Raman spectroscopy of the Ge reference and GePb annealed at 500 °C for 15-30-60 min under N2 environment on a Si substrate……………………………………...65

Figure 5.14 Raman spectroscopy of the Ge reference and GePb annealed at 600 °C for 15-30-60 min under N_2 environment on a Si substrate..…………………………………………66

Figure 5.15. Raman spectroscopy of the Ge reference and GePb annealed at 600 °C for 15-30-60 min under N2 environment on a Si substrate….……………………..……………..66

Figure 5.16. Photoluminescence spectra for GePb films on Si substrates at different annealing temperatures (300-600ºC) for one hour under N2 environment……………………………….68

Figure 5.17. Photoluminescence spectra for GePb films on Si substrate at 400 ºC for different annealing time (15-60 min) under vacuum.…………………………………………………...68

Figure 5.18. XRD patterns for GePb/Si annealed at 400 ºC for 1 hour under N_2 environment…69

Figure 5.19. XRD patterns for GePb/Si annealed at 400 ºC for 1 hour under N_2 environment…70

Figure 5.20. Wide scan of XRD patterns of GePb/Si annealed at 400 ºC for 1 hour under N_2 environment………..…..…………………..……………………………………………71

Figure 5.21. XRD powder data base for (a) Ge and (b) Pb.……………………………………72

Figure 5.22. SEM images of Ge-Pb-Si (as grown sample) before annealing and etching process……………………………………………………………………………………….73

Figure 5.23. SEM pictures of GePb annealed at 400 ºC for 15 min……………………………74

Figure 5.24. SEM images of GePb annealed at 400 ºC for 30 min…………………………......75

Figure 5.25. SEM images of GePb annealed at 400 ºC for 60 min…………………………......76

Figure 5.26 (a) and (b) are EDx images for GePb/Si annealed at 400 ^{o}C for 60 min, (c) GePb mapping……………………..…………………………………………...……...77

Figure 5.27. SEM images of GePb shows layer inversion.……………………………………..78

Figure 5.28. SEM images of GePb annealed at 400 ºC for 60 min with layer thickness……….79

List of Tables

Table 2.1. Ge, and Sn lattice constant and band energy………..………………………………...7

Table 4.1. Parameters for Ge-Pb growth using thermal evaporator.…………………………….35

Table 4.2. Parameters for Ge-Sn growth using thermal evaporator…………………………….37

Table 4.3. Parameters for Ge-Pb-Sn growth using thermal evaporator………………………….38

Chapter 1: Introduction

1.1 Motivation

Silicon (Si) is the dominant material that can be found in every technical device such as phones, and computer chips, and other microelectronic systems. Si is very important as a semiconductor material for several reasons. Silicon is the second most abundant element on the earth after oxygen (O) with 28% [1]. This is what makes silicon very cheap. It is widely used in electronic devices such as the fabrication of integrated circuits (IC), transistors, diodes, and solar cells. The lattice structure of crystalline Si easily allows impurities in the substitutional site with high doping concentration of 10^{21} atoms/cm^3 [1]. This mean silicon has high carrier (holes/electrons) mobility, which typically leads to better device performance. Finally, silicon dioxide has good properties for chip design and it is the most extensively used insulator in IC technology. Even though there are a few materials that share some of the desirable properties of Si, such as Ge and GaAs, none of these materials have all of these properties together except Si. As a result of that, in fabrication of microelectronics, Si is the ideal choice of semiconductor.

In 1965, Moore, the founder of Intel, predicted that the number of transistors placed into the chip would nearly double every 24 months [2]. His prediction has become a law and in order to keep the rate of progress, the size of the transistors has decreased over time. There are two main aspects related to processing and fundamental materials that need to be considered in order to maintain Moore's law on track. First, decreasing the size of transistors increases the speed of data processing. However, data transfer delay (Resistance-Capacitance RC) will not decrease at the same rate as the increase in data processing speed. For example, when doubling the number of transistors on the chip, the data processing speed will double. However, the length of the metallic interconnects remains the same and results in delaying data transfer ratio even though

the data processing speed increases. In addition, there is a limitation of the electrical interconnect scaling due to the physical properties of the electrical wire. Therefore, wires do not perform well with the transistors and cause interconnection delay. Another issue of wire interconnect, is power consumption. To transport signals, electrical lines should be charged no less than the signaling voltage. Nowadays, the energy needed for charging and discharging the lines can simply exceed what is used for switching a logic gate. Therefore, replacing electrical interconnect with optical interconnection is good to keep up Moore's law. The main reason that makes the optical interconnect a better choice than electrical interconnect, is its capability of transferring more data via modulation which results in decreasing the number of wire connections needed.

1.2 Optical Interconnects

Lately, researchers have paid attention to the use of optical interconnect to benefit connection of devices on a chip. In addition, these days, circuits have more complex interconnects which make optical interconnects a priority over electrical interconnects. Optical interconnects can take less area than the electronic counterparts if it is used for replacing the top layers of metal contact. Also, optical interconnects are able to transmit the data at much higher rate than electrical interconnects and use less power [3]. Moreover, optical interconnection ensures less loss for data in a long distance chip [4]. However, implementing optical interconnects on a chip requires many optoelectronic devices such as modulators, lasers, waveguides, and detectors. Since these devices are based on light emitting approach, another challenge arises. Integrating optical interconnects with silicon, which has indirect band-gap, means very low light emitting efficiency. Therefore, researchers have been using group III-V compounds such as GaAs which have high light emitting efficiency compared to Si. However,

GaAs is produced at high cost and does not match Si technology because of thermal mismatch between them. Since Si has low light emitting efficiency, researchers are focusing on group IV alloys especially germanium (Ge).

Generally, there are three main approaches that can be used to achieve direct bandgap transition in Ge in order to enhance the light emission/absorption efficiency: heavy n-type doping, biaxial tensile-strain, and Ge alloys.

1.3 Germanium Alloys

Recently, germanium alloys have grabbed researchers' attention due to its ability to display direct band gap and its compatibility with silicon technologies. Ge reveals very little difference between the direct band (Γ-valley) with 0.8 eV and the indirect band (L-valley) with 0.67 eV. This would make it easier for Ge alloys to achieve a direct band gap. Tin (Sn), which is also in group IV, comes in two forms which are β-tin and α-tin. The α-Sn is a semimetal with diamond cubic structure and conduction band minimum at Γ point equal to 0.41 eV below the valence band.

When Sn is incorporated in Ge, both the Γ and L valley decrease at the same time although more so in the Γ valley which leads to direct bandgap materials. In addition, increasing the percentage of Sn atoms in the Ge alloy would lead to even lower band gap energy and a higher potential for a direct band gap [5]. Theoretical study on GePb also shows that the same trend in bandgap change happens by using Pb alloying in Ge [6]. The alloy of germanium-tin (GeSn) or germanium-lead (GePb) would help make the Ge band gap a direct one. In addition, they support more optical and electrical properties, since they give great combinations and high

performance semiconductors [6]. Researchers are looking for low cost materials with high light emitting efficiency; with Ge alloys this goal can be reached.

GeSn and GePb alloys were deposited by a thermal evaporator (PVD) system on a Si substrate and annealed at 300-600 ^{o}C. The quality of the crystal of GeSn and GePb was characterized by Raman spectroscopy. Photoluminescence (PL) was used to examine the optical properties of the alloys. X-ray diffraction (XRD) was used to study the composition of the material and strain. Scanning electron microscopy was used to determine surface texture, composition, and average layer thickness.

1.4 Thesis organization

This thesis includes six chapters. Chapter 1 starts with an introduction and explanation of the motivation behind utilizing Ge alloys, and different methods for obtaining a direct band gap. The related theoretical framework is included in the second chapter. In the third chapter, literature review is included. Chapter 4 discusses the experimental fabrication methods and concentrates on equipment used in this research for characterization. Results of both alloys (GeSn and GePb) are discussed in Chapter five. Chapter six, the final chapter, gives the conclusion of this research and suggests future work.

Chapter 2: Theoretical Framework

2.1 Crystal Structure

Atoms in materials are bonded through sharing electrons that are available in the valence band. Depending on the number of electrons available, they can form different numbers of bonds. The crystals are formed when the atoms bonded together are arranged in an ordered structure. When a set of atoms or molecules are arranged identically at the lattice point, crystal structure will form [7]. Depending on the number of electrons available in the valence band to form the bonds and their orbital, they form different types of crystal. All group IV elements (C, Si, Ge, and Sn) form diamond cubic crystal structure with (sp^3 hybridized bonding between atoms) except for Pb which forms as face centered cubic (FCC) crystal structure.

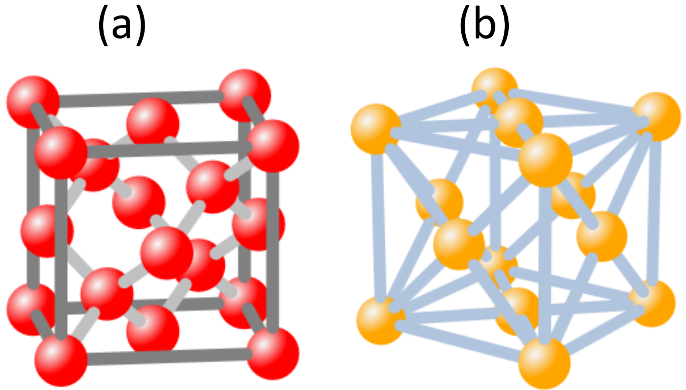

Figure 2.1. a) Diamond crystal, and b) Face center cubic lattice structure.

2.2 Ge Alloys Structure

2.2.1 Si-Ge-Sn Band Structure

Ge band structure has two valleys, the lower one has a minimum at L point at 0.67 eV and the other one has a minimum at Γ point at 0.8 eV. This makes it possible to get direct band

gap since the gap is small. It is easier for the electron to migrate to the lower level, which makes indirect band gap. However, alloys of Ge can provide direct bandgap. The difference in the energy for the two valleys is very small, only 0.13 eV. Therefore, if this small energy barrier can be overcome by electrons present in the Γ valley, the emitting efficiency of light will be significantly raised due to the rate of radiative recombination for band-to-band recombination in the direct transition which is 10^5 times higher than the indirect transition. In addition, this minor amount of energy change opens the door for more options of making direct band gap of Ge via bandgap engineering [5]. See Figure 2.1 for energy band diagram for germanium, tin, and germanium tin.

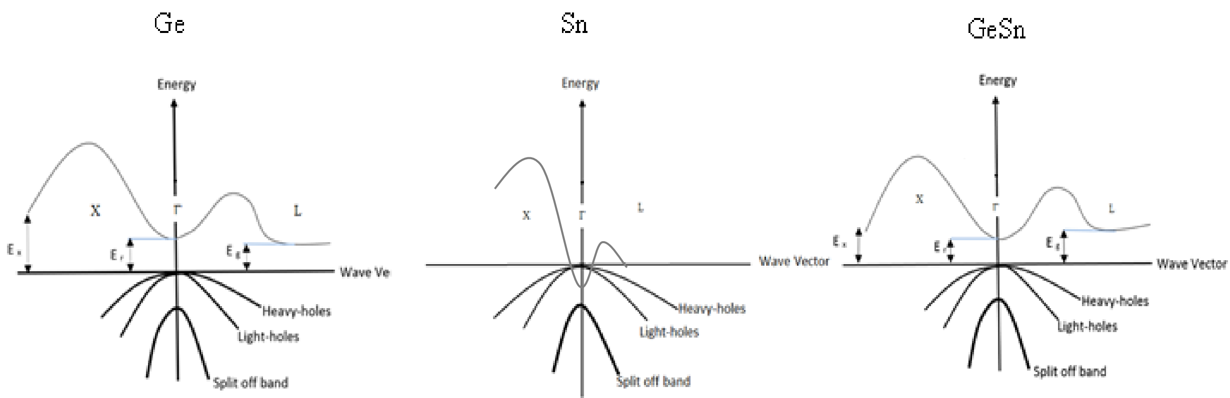

Figure 2.2. Schematics of band structures of Ge, Sn, GeSn.

Gamma (Γ), is the direct bandgap transition, whereas L and X represent the indirect transition. After Sn is incorporated with Ge, GeSn has a lower band gap in the Γ valley since GeSn alloys decrease the band gap energy in general, yet the direct one decreases faster than indirect one. This can result in direct band gap of GeSn. Ge with Sn or Pb alloys can make a great combination because they create a high performance semiconductor with higher light emitting efficiency. This is because of a controlled bandgap and the opportunity for high carrier

mobility. Thus, Ge with direct bandgap is capable of making laser target in the optical interconnection in the chip.

Using Vegard's law, band gaps and lattice constants for GeSn and GePb can be calculated. Equation 2.1 and Equation 2.2 show the calculation of Γ energy change as a function of Ge and Sn. In those equations, the predicted values of band gaps and lattice constants for the research samples can be calculated.

$$E_g^{GeSn} = (1-x)E_g^{Ge} + E_g^{Sn}.x - 1.94\ eV.x.(1-x) \quad \text{(Equation 2.1)}$$

$$a_g^{GeSn} = (1-x)a_g^{Ge} + a_g^{Sn}.x - 0.0468\ nm.x.(1-x) \quad \text{(Equation 2.2)}$$

E_g^{Ge} and E_g^{Sn} are the band gap energy, and a_g^{Ge}, and a_g^{Sn} are the lattice size while 1.94eV, and 0.0468 nm are the bowing parameters for Γ valley $E_g^{Ge} = 0.8$ eV and $E_g^{Sn} = -0.41$ eV. Table 2.1 illustrates the lattice constants of Ge, Sn, and GeSn materials

Table 2.1 Ge and Sn lattice constant and band energy [8].

Material	Band gap (eV)	Lattice constant (nm)	Band gap type
Ge	0.67	0.5658	Indirect
Sn	-0.41	0.6489	Direct

2.2.2 Si-Ge-Pb Band Structure

In order to be able to develop Vegard's law for bandgap and lattice size of the GePb alloy, the energy band diagram and the lattice constant of Pb are needed. However, as Pb does not form the same crystal structure, the available data could not be used the same way it could be used for Sn. In order to do so, it is required to know if Pb can form the sp^3 hybrid bonding the same way as C, Si, Ge, and Sn do. As the crystal structure of Pb does not show that possibility,

the Pb hydride was studied as compared with C, Si, Ge, and Sn hydride. Figure 2.3 shows that an unstable compound of plumbane does form which is similar to methane, silane, germane, stannane. This implies that Pb could be modeled in diamond lattice structure as it forms the tetrahedral sp^3 hybrid bonding.

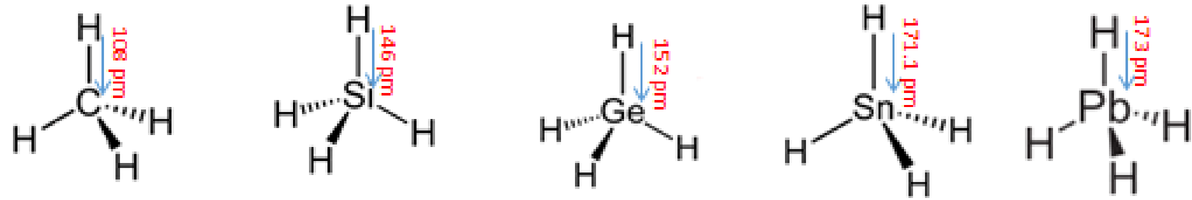

Figure. 2.3. Group IV hydrid.

In order to estimate the lattice size of Pb in diamond structure, the lattice size of C, Si, Ge, and Sn were compared with their covalent bond size and hydride bond size. Using the covalent bond size and hydride bond size of Pb, the diamond lattice size of the Pb was estimated to be 6.82 Å (See Figure 2.4).

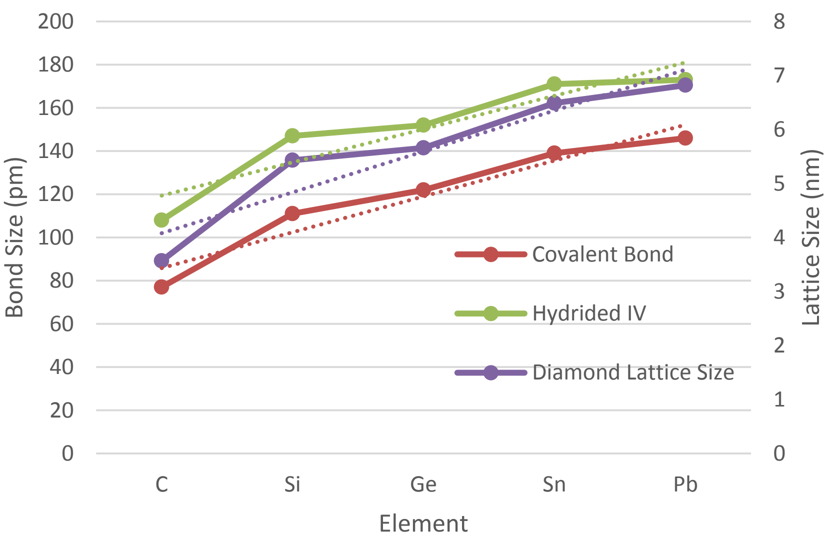

Figure 2.4. Group IV element lattice sizes.

Using Vegard's law, the lattice size of GePb is estimated by the following relationship:

$$a_{g}^{GePb} = (1\text{-}x)a^{Ge} + a^{Pb}.x \qquad \text{(Equation 2.3)}$$

where a^{Ge} = 5.568 A and a^{Pb} = 6.82 A. In Figure 2.5, the result of the GePb lattice calculation is compared with the cluster calculation performed using density functional theory (DFT) developed by Huang et al. [6]. However, they only studied three different combinations of 12.5%, 25%, and 50% Pb incorporation in Ge and did not estimate the diamond lattice size of Pb. Figure 2.5 shows the change in the lattice constant of GeSn as a result of Sn incorporation.

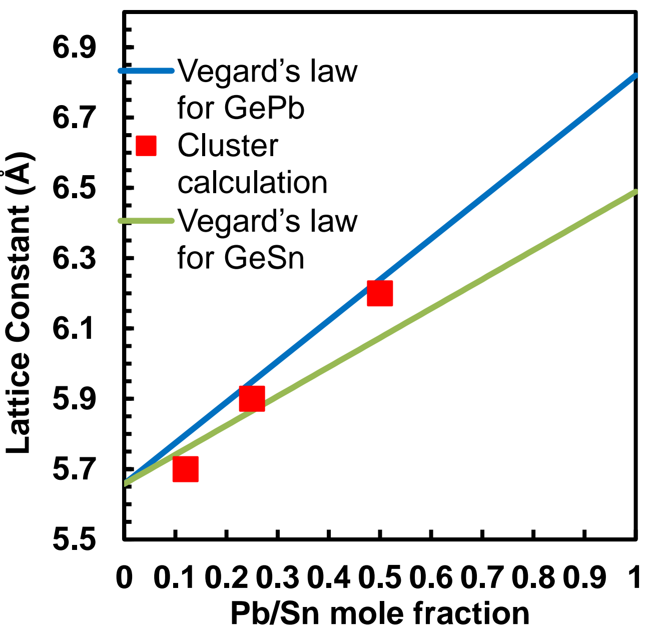

Figure 2.5. Cluster calculation and Vegard's law of GeSn and GePb.

Vegard's law for bandgap calculation of GePb has not been develped due to unavailablity of Pb band strucutre in diamond lattice. However, the preliminary study by Huang et al. [6] stated that the GePb alloy band gap experienced transition from indirect to direct as the Pb composition increased. In addition, they specified that 1.5 % of Pb is able to convert the indirect Vegard's law for bandgap calculation of GePb has not been develped due to unavailablity of Pb

bandgap to a direct bandgap. However, their results have not been verified experimentally. Figure 2.6 shows their results.

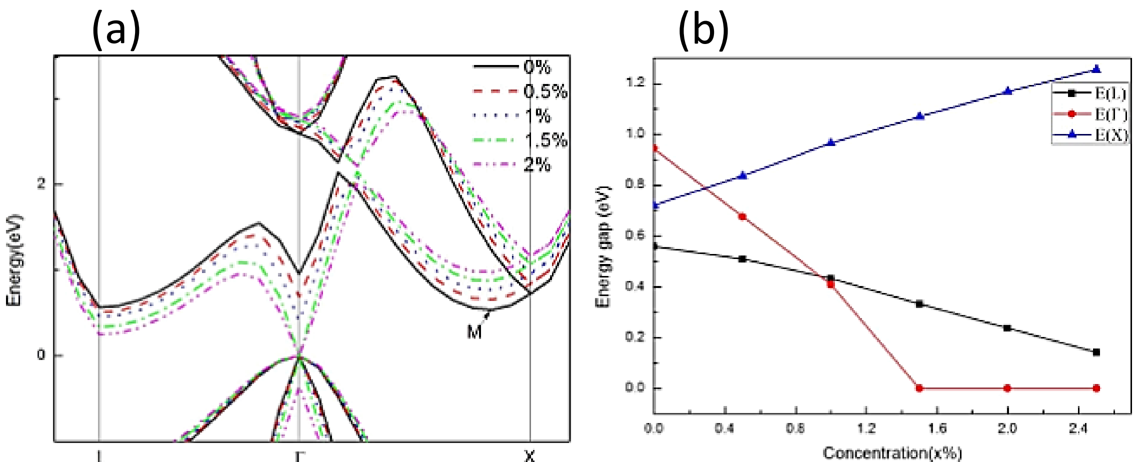

Figure 2.6. (a) band gap structure of GePb with different composition (0.5-2%), (b) the band gap at (L, Γ and X valleys) with the concentration dependence [6].

2.3 Solubility of Pb and Sn in Ge

Obtaining high Sn or Pb composition in $Ge_{1-x}Sn_x$ and $Ge_{1-x}Pb_x$ alloys is very challenging, because of the equilibrium solid solubility limitation of < 1% for both Pb in Ge and Sn in Ge, and vice versa. Therefore, incorporation of these elements in Ge is only possible in conditions away from thermal equilibrium. Figure 2.7 shows the phase diagram of GePb and GeSn.

2.4 Epitaxial Growth

The process of growing a crystal on top of another crystal while the orientation is specified by the main crystal is called epitaxial growth [11]. In other words, growing a single crystal layer over a substrate that is also single crystal is called epitaxy [12]. Epitaxial growth is The process of growing a crystal on top of another crystal while the orientation is specified by

required in many applications, such as the making of different layers in semiconductor thin films and is particularly utilized to engineering optoelectronic devices.

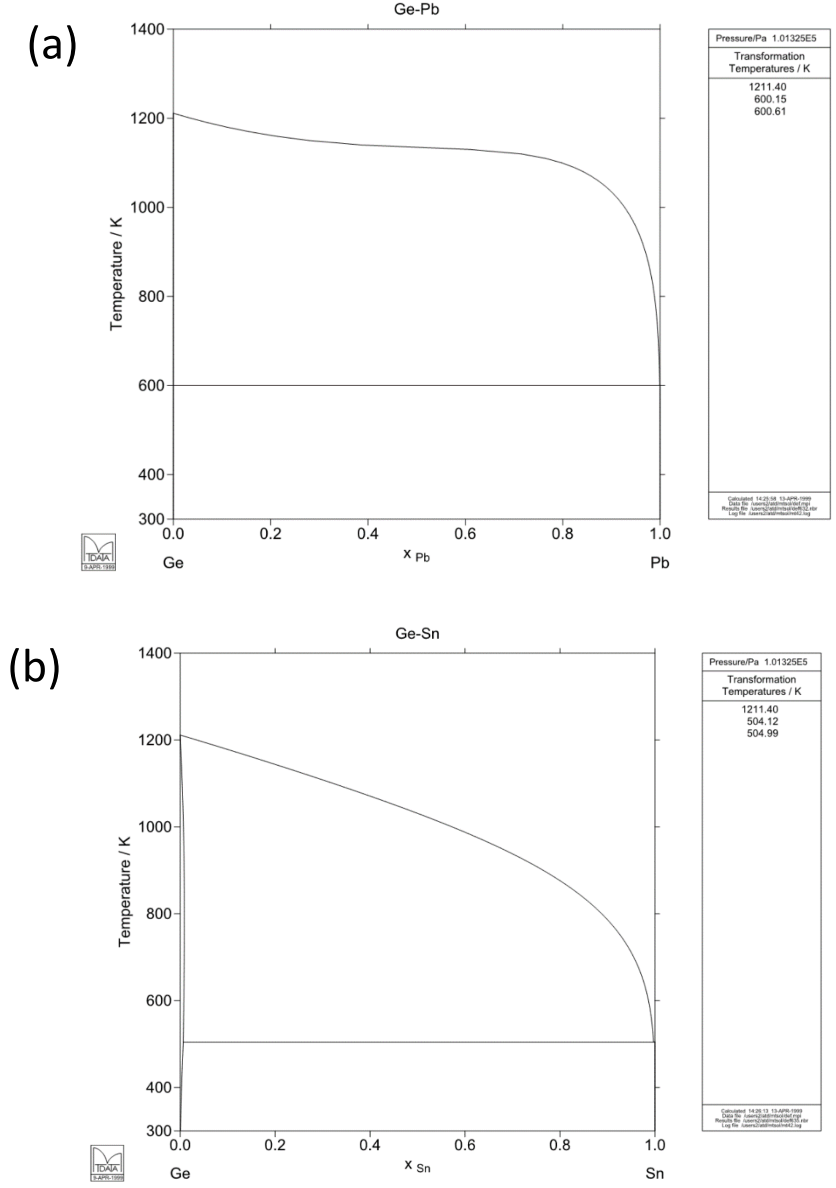

Figure 2.7. Phase diagram of (a) GePb and (b) GeSn [9] [10].

In the epitaxial films, the atoms have a specific location related to the underlying (main) crystal. The outcome of this procedure is the development of crystalline wafers that can either be created on the same substrate material with exactly the same chemical composition and In the

arrangement of atoms or on a different substrate. In addition, crystalline wafers can be composed of just one layer, or several deposition layers.

There are two types of epitaxy: homoepitaxy and heteroepitaxy. In the first type, the substrate and the growth layer are made of the same materials, whereas in the second type, the materials of the epitaxy films are different from the substrate [11]. The homoepitaxy method is utilized more in the growth of silicon on a silicon substrate. In this method, the epitaxially grown layers are capable of being doped independent of the substrate, and epitaxial films more pure than the substrate. Heteroepitaxy is used more in optoelectronics and bandgap engineering, and a good example of heteroepitaxy materials is GaAs on Si. Unfortunately, layer by layer growth, as in the case of heteroepitaxy, leads to mismatched lattice bonds, which results in strained growth and sometimes causes interfacial defects [12].

2.5 Strained Lattice

In several applications, near-matched lattices are the most desired since it reduces defects and raises electron mobility. When the mismatch becomes larger, there is a potential of the alloy material to expand to suit the lattice structure of the wafer substrate. These scenarios, called pseudomorphic, happen in the initial steps of film formation and occur with materials of similar lattice assembly.

One example is the silicon germanium structure. When strain accommodation is not likely, dislocation occurs, and defects at the interface might take place. This can cause the upper lattice to relax. As a result, the film reverts to its usual lattice structure on top of the interface. A schematic of lattice matched, strained, and relaxed films is shown in Figure 2.8. The equation below can determine lattice misfit.

$$f = [(a_{\circ}(s) - a_{\circ}(f))/a_{\circ}(f)] \qquad \text{(Equation 1.4)}$$

$a_{\circ}(s)$, $a_{\circ}(f)$ are the lattice constants of both the film and substrate [13].

In the case of lattice mismatch less than 9%, the first layer of the film will produce pseudomorphically. So, very thin films will elastically strain to obtain an interatomic space similar to that of the substrate. In addition, when the thickness of the film increases, the increasing strain will cause sequences of mismatching dislocations, separated by areas of quite acceptable fit. In this way, they are considered to be in equilibrium [13].

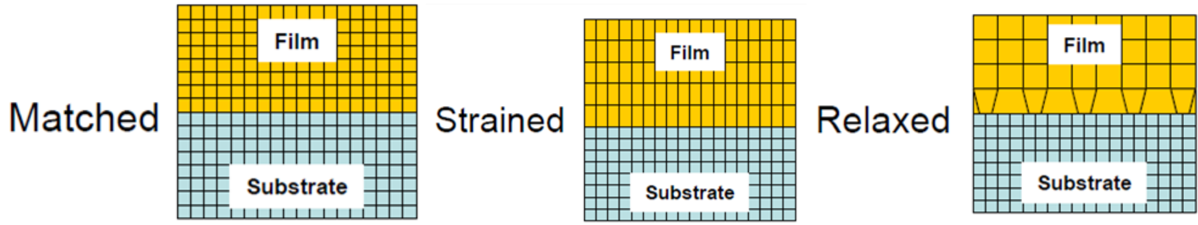

Figure 2.8. Schematic of lattice matched, strained, and relaxed [14].

2.6 Film Deposition

Physical Vapor Deposition (PVD) and Chemical Vapor Deposition (CVD) are two techniques that can accomplish a vapor phase deposition of thin films. In the deposition via PVD, the metal species transforms to its' molecular or atomic form, and then it is deposited on the sample substrate and on the chamber lid or walls. In this process, there is not any chemical reaction on the depositing substrate or even in the gas phase [14].

2.6.1 Thin Film Deposition

Placing an extremely thin layer of material, from a few nanometers to around a hundred micrometers thickness, on a substrate area to be coated or deposited, is called thin film

deposition [14]. Thin film deposition on a surface is expected to occur in the following order. When atoms and molecules touch the surface, they are physically absorbed (physisorbed). Based on the energy of the incident particle and the substrate energy, the surface either absorbs the incident atoms or it is absorbed chemically (chemisorption). In both the physical and the chemical method of absorption, the surface mobility of the atoms is sufficient to transfer about on the growth area. In this phase, atoms combine to make a nucleus that can randomly collect or separate on the whole area.

At this point, the size of the nuclei rises over critical size (meaning that increasing the surface energy resulting from the expanded size becomes greater than the stable energy which occurs due to the decreasing in the energy). Thus, the nuclei become steady and are able to continue growing. Moreover, once the nuclei hit other ones, they combine and begin forming a film. The roughness of the surface relies on some deposition circumstances such as evaporation rate, heat, and other evaporated materials [13]. This is shown in Figure 2.9.

PVD sources such as thermal evaporator or e-beam can be considers as point sources. Therefore, having a the substrate located too far from the source,> 30 cm will result in non-uniform film deposition.

The mass deposition per unit area, R_d may calculated as

$$R_d = (M_e / r^2) \cos \theta \cos \phi. \quad [13] \qquad \text{(Equation 2.5)}$$

Where M_e is the total mass of the evaporated area while r, θ, and ϕ are shown in Figure 2.10.

This equation is called the cosine law. It is important to rotate the substrate area to obtain satisfactory deposition uniformity on big parts of the substrate. Due to the difficulty of water

water vapor, it is necessary to prevent the chamber from being exposed to ambient air in order to increase the pumping rapidity. A liquid nitrogen trap inside the chamber also helps to get rid of moisture and works to prevent leaking oil in the back flow from the pump into the chamber [13].

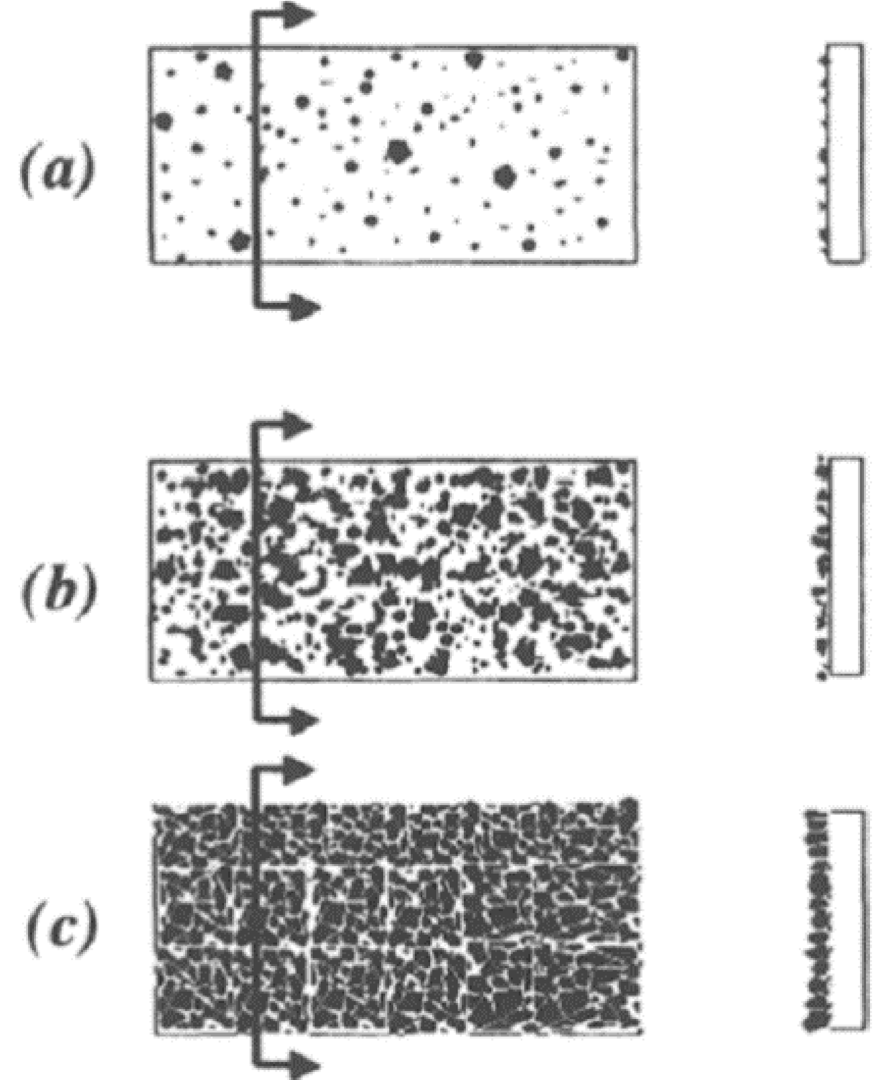

Figure 2.9 Sketch of thin films nucleation and growth phenomena [13].

2.6.2 Chemical Vapor Deposition (CVD)

This system process depends on certain chemicals reacting with each other to combine and create the growth of thin layer of films. Reactive gases pass over the hot substrate on a

furnace in the CVD system. This method is very beneficial for growing different materials and it shows more developed step coverage than the PVD deposition system. However, the physical deposition works on some metals whereas CVD system cannot use certain metals. Usually the reactor in CVD consisted of a tube furnace and a vacuum pump scheme, in case the system is functioning at lower than the atmospheric pressure. The geometries of the reactor impact film parameters and deposition; therefore, it is crucial to characterize the exact reactor equipment consistently in every laboratory. Many vacuum systems like the common one utilized in the etching processes or sputtering, can be implemented in a plasma enhanced CVD (PECVD) system. The main benefit of using a PECVD system is that lower temperatures can be successfully used, in comparison to higher temperature usage in furnace procedures.

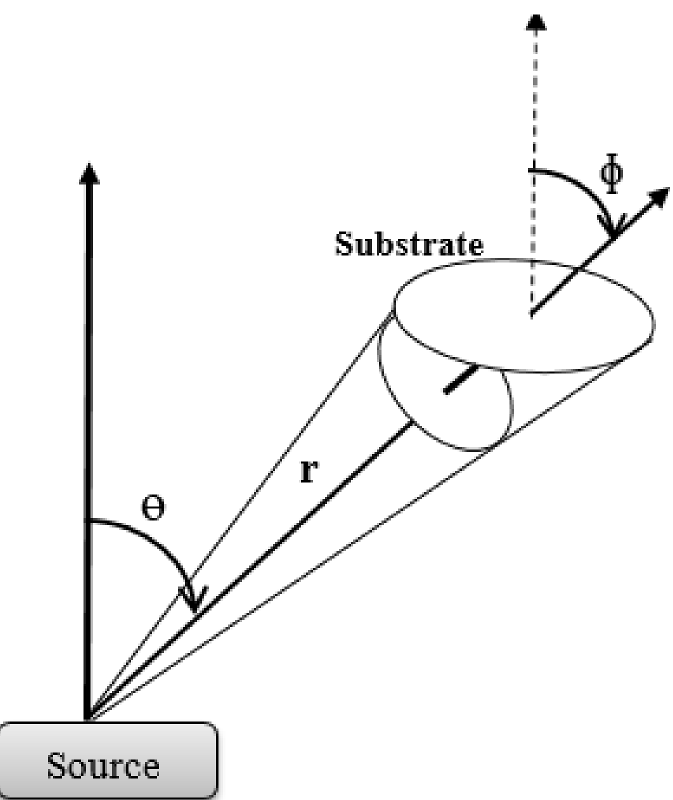

Figure 2.10. Diagram that determines angles and parameters used in the deposition derivation rate in evaporation.

In the integrated circuit, during the metallization phase of the fabrication system, the metals generally will not with stand high-temperature furnace processes. When depositing nitride or oxide passivation coatings following metallization, for instance, PECVD delivers a low temperature as an alternate step. However, one of the disadvantages of this process is that oxide layers deposited by CVD are fundamentally less dense than when the layers are deposited via thermal oxidation.

In contrast, in the CVD technique, there is a chemical reaction between the depositing surface and gaseous species which create the thin film. Although there are many essential benefits of using the CVD method such as useful step coverage and conformal coating that are not obtainable in PVD, over all, the CVD of metals is under developed and requires a long

process to improve [13]. The two main types of PVD are evaporation and sputtering, as displayed in Figure 2.1. Evaporation and sputtering systems have mainly been used for thin films metallization [13].

2.7 Evaporation Sources

PVD sources come in two forms: sputtering and evaporation.

2.7.1 Evaporation

For the deposition of thin films, evaporation is a simple technique. In this system, vapor is delivered from materials that are placed in a source heated by one of the techniques in Figure 2.11. For instance, when heating Al or Au, they melt right away. After providing more heat energy, the metal atoms obtain enough kinetic energy to escape from the melted surface. Then, the atoms start to spread in all different directions bearing them far from the source. If these

atoms strike cooler walls of the chamber or surface, thin films of the evaporated materials (e.g. Al or Au) are formed by the condensing atoms [13].

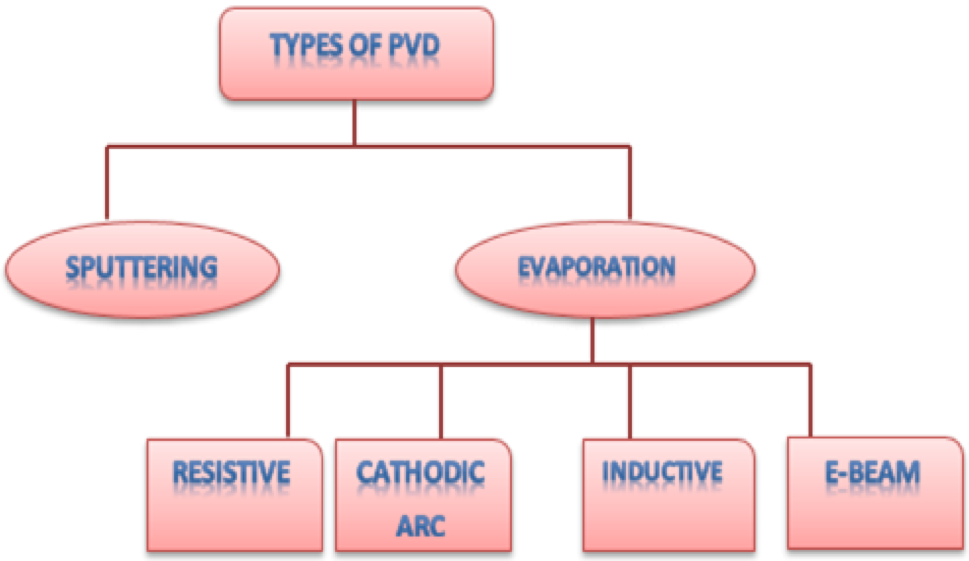

Figure 2.11. Different types of PVD.

As known, most metals evaporate at temperatures ranging from 500°C up to 2000 °C, so there is a big concern that the metal or the material may react with the ambient gas while evaporation occurs. For instance, if Al is the metal being used, during the evaporation process there is a high possibility of Al reacting with the ambient gas, including oxygen or moisture in air creating aluminum oxide instead of pure aluminum. Therefore, it is important to have an evacuation system within a metal evaporation system in order to rid the chamber of any gases or moisture that may react with the materials. An additional benefit of a vacuum system is that during evaporation, the metal atoms do not hit any gaseous atoms before condensing on the substrate surface, which guarantees a higher deposition rate. In addition, it helps the atoms strike certain desired parts and not others [13].

2.7.1.1 Sputtering

Sputtering is a procedure used to deposit a thin layer of material on a substrate surface. The initial step in the procedure is making vaporous plasma and then accelerating ions from the plasma to the target materials. The target source is eroded via the received ions by energy that is transformed and then ejected in the shape of neutral particles in a cluster of atoms (individual atoms or molecules). When ejecting, the neutral atoms move in a direct line, except when they encounter other atoms or any close surface. For instance, if the substrate area is a silicon wafer that is located in the area of the ejected particles a thin layer of the target materials will cover the silicon wafer.

In essence, plasma can be defined as the "fourth state of matter", besides the well-known three states: solid, liquid, and gas. In fact, vaporous plasma is an active state at which neutral gas photons, ions, atoms, and electrons occur in a close balanced condition together. Using energy sources, such as a direct current (DC), or radio frequency (RF), is necessary to feed the plasma and maintain its condition while the plasma is missing energy. This dynamic state is produced by applying gas such as argon (Ar) in the pre-pump vacuum chamber and then allowing the chamber pressure to reach a specific level (0.1 Torr, for instance). Then by vacuum feedthrough, live electrodes can be introduced inside the low-pressure gas environment [15].

2.7.1.2 Physical Vapor Deposition (PVD)

PVD is a process utilized in order to deposit very thin layers of metals, usually varying in thickness from a nanometer to several micrometers. The processes of this vacuum deposition system are safe for the environment. It includes three main stages: a) materials are evaporated from a solid source supported by either gaseous plasma or by using vacuum with high

temperature dependence; b) the vapor is then transported to the substrate surface in a vacuum or partial-vacuum; c) and, particles finally condense on the substrate area to produce thin films (see Figure 2.12).

Many of PVD systems use all of the above stages, yet they differ in the method applied to produce and deposit metals. Thermal evaporation and sputtering are the main methods used in PVD systems. In general, the thermal evaporation technique focuses on the evaporation of base material. This is done by heating the metal via suitable approaches in a vacuum. On the other hand, sputtering is a plasma-dependent procedure which produces a vapor coming from the target that strike the substrate surface with fast moving ion, usually argon.

In both evaporation techniques, the generated vapor is then deposited onto the anticipated substrate via a condensation technique. Depositing a thin layer can extend a range of chemical structures depending on the original materials in the source [16].

PVD utilizes different vacuum deposition systems to deposit thin films via the buildup of a vapor condensing onto different sides of the work area. The coating system includes physical procedures like the high temperature vacuum evaporation and resulting condensation. PVD also includes cathode arc deposition, electron beam physical vapor deposition, evaporation deposition and other vacuum deposition systems [17].

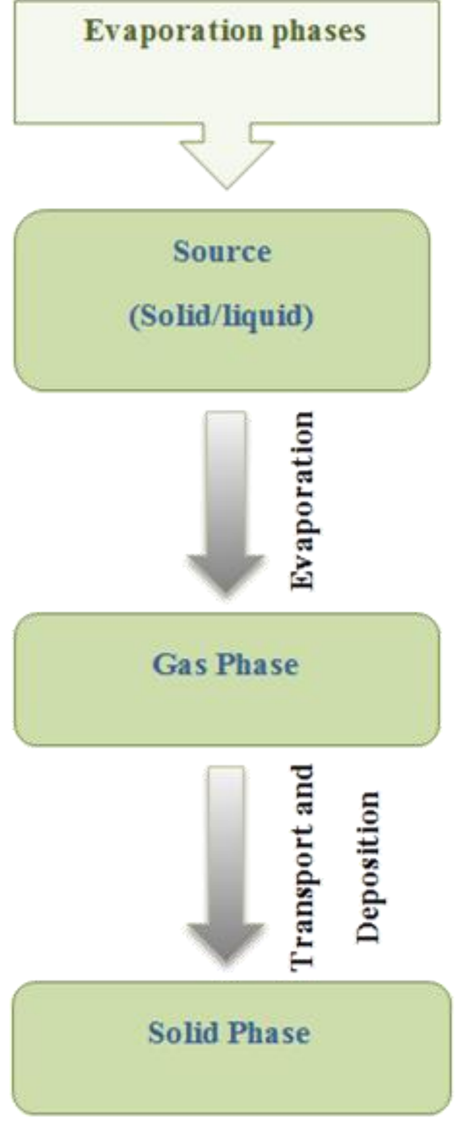

Figure 2.12. Physical deposition phases.

2.7.1.3 Electron Beam Evaporation (E-Beam) Evaporation

E-beam another PVD technique, is produced by a filament and driven by magnetic and electric field. This is in order to attack the source material then evaporate it in a vacuum condition. Once the source materials get hot enough as a result of the energy transferred to the source, surface atoms obtain enough energy to leave. At this time, the atoms attempt to traverse

the vacuum surrounding, when the thermal energy is lower than 1 eV, and deposit as layers on the wafer substrate located above the evaporated metals. The average distance between the substrate and the source is generally between a few centimeters to one meter. A picture of the e-beam evaporator is shown in Figure 2.13.

Figure 2.13. E-beam evaporator [18].

Due to low energy in the thermal system, the chamber pressure should be less than the point at which the mean free-path is longer than the space in between the e-beam source materials and the substrate surface. The mean free-path can be explained as the average distance a molecule or atoms can travel in a vacuum before it hits another atom or particle which disturbs its path to

a certain degree. This value is generally 3×10^{-4} Torr or less.

Other evaporation techniques without ion-beam support can be employed at a pressure less than 1×10^{-4} Torr, but the pressure increases constantly because of the outgassing of several components inside the vacuum chamber. Allowing vaporized atoms to traverse the active distance between the substrate and the source materials undisturbed by the rest of the remaining atoms confirms “line of sight” influx of material that becomes huge when a specific type of mask is applied. Less arrival energy is considered beneficial for a substrate with more sensitivity, though the radiation coming from the powerful energy of electron beam transfer under the substrate area naturally will dominate [19].

2.7.1.4 Thermal Evaporator

Another common PVD system is the thermal evaporator method. This method is used when it is crucial to apply very thin films in a high vacuum setting because this system provides high temperatures through applying Joule heating to a strong metal. When applying a high current through a resistive component like a light bulb, the filament will get hot. Gold and aluminum are heavy filaments and can be used as the metal wire. The metal wire will initially heat up and increase the filament temperature, then the metal evaporates from the filament or boats and travels inside the chamber [17].

Basically, the source is heated until the materials inside reach the melting point and become liquid. This material is usually placed inside the bottom of the chamber, in a boat or crucible. Therefore, when these materials evaporate, the vapor will rise above the source and touch the inverted substrate which is on the top, opposite from the source. At this phase, the substrate

surface is coated and thin films are created. See a simple drawing of a thermal evaporator system in Figure 2.14 [20].

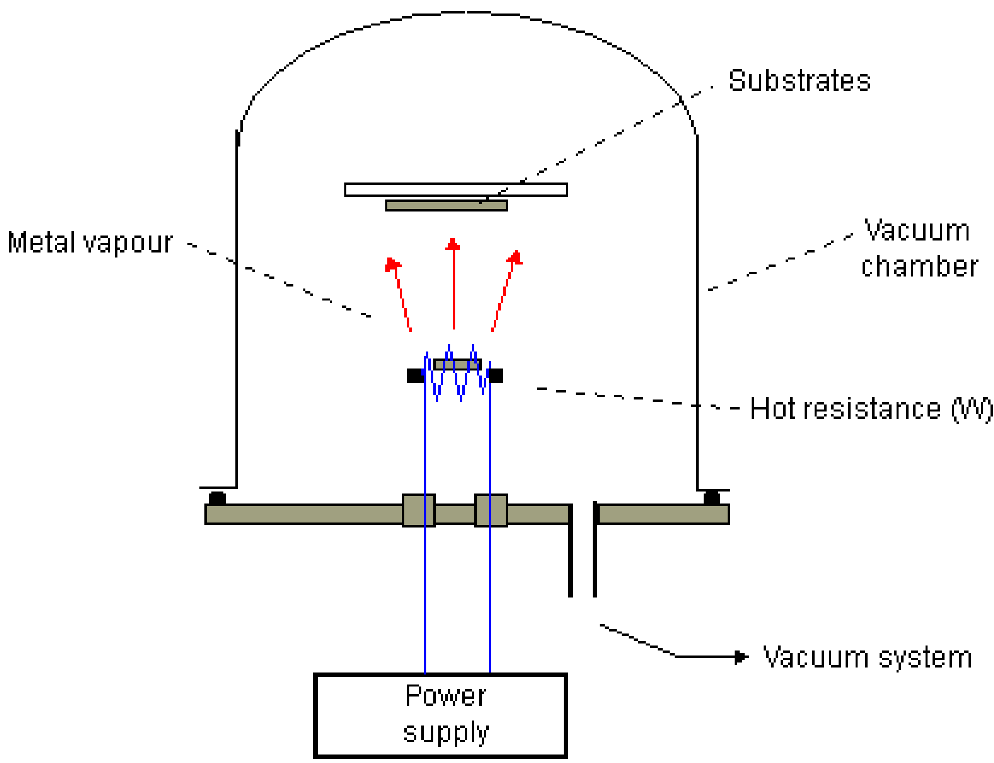

Figure. 2.14. Simple drawing of thermal evaporator system [21].

In the thermal evaporator system, a large electric current at a small voltage is delivered through a rigid metallic filament heater or in metal boats. These filaments or metal boats can come in a various form as shown in Figure 2.15.

The filament and spiral are individually prepared from multi-strand tungsten (W) rope and are very appropriate for aluminum vapor in general. Dimple boats and crucibles are usually made of tantalum (Ta), tungsten (W), and molybdenum (Mo). Boat filaments made of Mo and Ta work great and can be used several times without causing problems [13]. Moreover, these boat filaments are usually made with an isolating barrier coat of aluminum oxide in order to avoid reaction between the boat filaments and evaporated metal. This also helps to keep the current

from shorting over the heavy molten conductor films being evaporated.

Figure 2.15. Different sources for thermal evaporation of materials [22].

For materials with a very high melting point such as Ta, W, and Mo, a thermal evaporator cannot be used to evaporate them. Electron beam evaporation can be used to evaporate these metals quite easily [13].

2.8 Materials Background

Si and Ge are very popular semiconductors and are the most popular choice for electronic, optoelectronic, and solar cell applications. Also, Ge alloys are recently used in optoelectronic devices to replace GaAs which is much more expensive and incompatible with silicon technology.

2.8.1 Germanium (Ge)

Germanium is in group IV of the periodic table. This element is a metalloid crystalline in its

pure condition. Also, Ge is considered to be a great semiconductor material. There are many applications for the use of Ge. One important use for it is as a transistor in many electronic applications, as an impetus or catalyst, and in fluorescent lights by phosphor. The doping of Ge can be accomplished with gallium, arsenic, and other different elements of group III and V [23]. Even though Ge is very similar to silicon (Si), it is not easy to find Ge naturally, whereas Si is very common on earth. Some of the physical properties of Ge are: its atomic number is 32; its atomic weight is 72.630; it melts at 1211.40 K; its density is 5.3234 g/cm^3; it has diamond cubic structure with band gap 0.67 eV; its thermal conductivity is 60.2 W·m^{-1}·K^{-1}; and, the electrical resistivity at 20 °C is 1 ohm·m for un-doped Ge [24].

2.8.2 Tin (Sn)

Sn and Ge are both group IV, and the atomic number of Sn is 50. It is crystalline, malleable, and its color is a combination of silver and white. It does not require a very high temperature to melt. Its melting point is 231.93 °C (449.47 °F). The thermal conductivity of Sn is 66.8 W·m^{-1}·K^{-1}, and its electrical resistivity at 0 °C is 115 nohm·m. Below 3.72 K, tin converts into a superconductor. Sn has two allotropes, β and α-tin[25]. α-tin forms a diamond structure crystal but is not stable above 13 °C. β-tin is a more stable allotrope of Sn that forms a tetragonal crystal structure. Tin's melting point is 231.9 °C and the boiling point is 2270 °C [24].

2.8.3 Lead (Pb)

Pb is a solid metal element with atomic number 82. It is also in group IV in the periodic table of elements, with an atomic weight of 207.2 g/mol. Its conductivity of electricity is poor and it is very resistant to corrosion. Lead's melting point is 327.46 °C and the boiling point is 1749 °C [26].

Chapter 3: Literature Review

3.1 Growth of GePb

Even though the growth of Ge on silicon is widely studied these days, only a few reports actually talk about the growth of GePb alloys in detail. Most of the studies concentrate on the growth of GeSn and SiGeSn and the optical properties of these alloys.

One of the first reports of Ge-Si properties was published by Olesinski and Abbaschian at the University of Florida in 1984. They studied the germanium-silicon equilibrium phase diagram. The liquid and cubic diamond substitutional solid solution are the two steady states that were formed by Ge-Si and some basic materials properties of Ge and Si [27].

In 2014, Huang, Cheng, Xue, and Li [28] reported that GePb and GeSn can achieve a direct bandgap by using a low concentration of Pb and Sn. Their bandgap calculation of super cell and virtual-crystal structure indicate that GePb alloys shifted to direct bandgap as the concentration of Pb increased. In addition to that, the transitional concentration of GePb alloys is far less than those for the GeSn ones. They used first principle theory to consider the influence of impurity clustering and they also discussed some optical and electrical properties of GeSn and GePb. They used the “Cambridge Serial Total Energy Package” (CASTEP) for the first principles calculations. For achieving the ground state assembly, they utilized the algorithm of Broyden Fletcher Goldfarb Shanno (BFGS). The tolerance for the entire energy difference was 5.0×10^{-7} eV/atom, and their maximum force was equal to 0.02 eV/Å. Their results specified that the transition from indirect band to the direct band requires Sn concentration of the alloy to be more than 6%, while the Pb concentration for indirect to direct band transition was determined to be 0.93% [28].

In 2014 and 2016, Qian et al [29], [30], [31] published three papers on GePb. For the growth of single crystalline GePb, they used sputtering for deposition and laser induced epitaxy for annealing. In their initial studies, they stated that "pulsed laser induced epitaxy" was used to achieve GePb alloys and they were able to achieve substitutional Pb up to 3%. To examine the substitutional Pb, they used high-resolution Rutherford backscattering spectrometry (HRBS). To define the full amount of Pb atoms, they used conventional Rutherford Backscattering (RBS). Their substrate was n-type germanium, which they cleaned with diluted hydrofluoric acid at 1:100 ratios for three minutes. Using sputtering, they deposited GePb with a 30 nm layer thickness at room temperature. The sputter source was a mixture of both Ge and Pb, with 97% of it being Ge and the rest was Pb. SiO_2 of 15 nm thickness was deposited as a second layer without breaking vacuum to avoid surface oxidation. They annealed the amorphous layer of GePb by a KrF pulsed laser with a wavelength 248 nm and a pulse time of 23 ns. The GePb film was crystallized after the laser annealing because of the high temperature produced by the laser.

In their TEM images, they compared the amorphous GePb layer before and after annealing and recrystallizing by the laser. TEM inferred that they obtained epitaxial layers of GePb. They characterized their samples using secondary ion mass spectrometry (SIMS). They concluded that by using sputtering for deposition and a laser for annealing, they were able to get single crystalline GePb films and also achieved almost 3% of lead in the substitutional side [30].

In a later study, Qian et al. [30] used sputtering and laser induced epitaxy to form a GePb single crystalline layer, just like their previous studies. In addition, most of their characterization instruments and parameters stayed the same. Using sputtering, they deposited GePb layers with a thickness of 60 nm for one sample to use for the characterization of secondary ion mass

spectroscopy (SIMS), and the rest of samples at room temperature had a thickness of 40 nm. The chamber pressure was kept at 3×10^{-3} Torr, while the sputtering base pressure was 5×10^{-7} Torr. The sputter source was also a mixture of both Ge and Pb of very high purity. In the pulsed laser annealing process, they used varied laser fluence (300, 350, 400, 450, and 500 mJ/cm^2) with a 248 nm wavelength and diverse capping layers depositions (SiO_2, Si_3N_4, and Al_2O_3). They illustrated single crystalline GePb at various laser fluences and capping deposition layers, yet the 350 mJ/cm^2 fluence was the one that formed a single crystalline layer of GePb [31]. However, the optical properties of GePb were not reported in any of their studies.

3.2 Growth of GeSn

GeSn alloys have been studied in more detail using a variety of methods such as CVD, MBE, PVD, etc. Here, GeSn films achieved using PVD are focused on. In 2013, Haofeng et al. [32] achieved a substitutional crystalline GeSn alloy with 8.7% atomic percent of Sn on a SiO_2 substrate with 10 nm layer thickness. The crystallinity of GeSn was formed at low temperatures ranging from 370 to 470 °C. They used a thermal co-evaporation PVD system to deposit Ge and Sn. Using cross sectional scanning electron microscopy (SEM), they were able to measure the thickness of thin films. They etched the segregated tin on the annealed GeSn films with a hydrochloric acid solution HCl:H_2O (37.2%). The thickness of germanium was 100 nm, while the GeSn alloy was almost 300 nm. They also used Raman spectra with an excitation laser operating at wavelength of 514 nm.

Overall, they obtained high crystalline GeSn, and improved the optical and electrical properties of the thin films at low temperatures not exceeding 470 °C. They also found that when increasing the Sn concentration, the crystallization temperature goes down. The band gap of the

GeSn films becomes much lower than the pure germanium, varying from 0.8 eV for the pure Ge to 0.5 eV for the alloyed thin film [32].

In 2014, Ruben et al. [33] examined optical and structural properties of amorphous and crystalline GeSn annealed at 500 °C on a Si substrate. They used an ultra-high vacuum (UHV) system to deposit Ge and Sn which they evaporated in different single effusion cells. The thickness of their amorphous GeSn ranged from 37 nm up to 65 nm. The chamber base pressure was 2×10^{-10} Torr. After annealing at 500 °C for one minute under a nitrogen environment, the amorphous material became single crystalline GeSn.

They obtained GeSn with minimal concentration of Sn (4.5% and 11.3%). In the sample with a concentration of 4.5%, Sn seemed to form as substitutional in both the as-deposited GeSn and in the crystalline form with no clustering of Sn. Conversely, for crystalline GeSn at concentration of 11.3% Sn, they found the segregation of Sn and observed the presence of β-Sn by Extended X-ray Absorption Fine Structure (EXAFS). Their indirect amorphous GeSn changed to direct crystalline GeSn [33].

Chapter 4: Experimental Methodology and Equipment

This chapter starts with the experimental processes that were followed during the deposition and growth of Ge alloys. Then it illustrates the equipment and characterization tools used in the process of characterizing the films.

4.1 Experimental Procedures

4.1.1 Sample Cleaning

First, to clean the Si (100) substrate, piranha solution was used to remove the organic material and metals from the sample substrate. Piranha etch is a mixture of two components, sulfuric acid (H_2SO_4) and hydrogen peroxide (H_2O_2) combined with a 1:1 ratio. The solution was prepared in the acid bench at University of Arkansas, High Density Electronics Center (HiDEC) clean room. Glass containers were used for preparation of piranha solution, as plastic containers could melt due to the heat generation during the process. It was necessary to add H_2SO_4 first then slowly add H_2O_2. After that, the silicon wafers were placed in the solution using a suitable holder and a timer was set for 10 minutes.

Hydrofluoric acid solution (HF) was later used to remove the oxide layer from the samples. This was also prepared in the acid bench in the clean room. This solution contains HF and deionized water (HF: H_2O with 1:10 ratio). Opposite from the piranha solution, HF solution should be prepared in a plastic container because HF is capable of dissolving glass. Si samples were dipped in the HF solution for 2 minutes then rinsed with DI water and dried using a nitrogen gun. After the cleaning process was completed, samples were kept in the container until the next step.

4.1.2 Deposition Process

To grow GeSn and GePb on Si, a thermal evaporator was used to deposit the thin films under a high vacuum at room temperature. Then samples were annealed at different annealing temperatures and times. Etching was the last step before characterization, and hydrochloric acid (HCl) and acetic acid (CH_3COOH) were two solutions used for etching the metal.

Before putting the glass or Si substrates on the substrate holder, the glass substrates were cleaned using acetone, and the Si wafers were cleaned following the above mentioned procedure. Moreover, the thermal evaporator chamber was cleaned with 20% potassium hydroxide (KOH) to confirm that there was no contamination from other metals used in previous runs.

4.1.2.1 GePb Deposition

First, the Si and glass substrates were placed on the substrate holder before transferring it to the thermal system. Then, the Ge was placed in one boat and Pb in another before closing the chamber. After turning on the thermal evaporator, the rotary and diffusion pumps were turned on. Next, the handle was switched to the rough pump until the pressure reached 1×10^{-1} Torr, and then the handle was moved again to the backing and vent for five seconds. Following this, the handle was changed once again to the roughing pump until the pressure reached 1×10^{-1} Torr. This same step was repeated to purify the inside of the chamber from moisture before deposition. After the indicator was returned to the roughing pump and the pressure became 6×10^{-2} Torr, the handle was moved to the backing and the gate valve was opened. After the pressure reached 2.25×10^{-5} Torr, liquid N_2 was poured into the trap to decrease the pressure to 5×10^{-6} Torr. At that

point, metal deposition could begin. A current was applied to the filament to heat the boat and evaporate the metal. First the metal (Pb or Sn) was deposited then Ge was deposited.

The layer inversion method that was used for the deposition of GePb required that the metal layer (Pb) be deposited first and then the Ge layer deposited on the top. In this method when the sample is annealed, Ge diffuses through the metal film to the substrate as crystalline Ge while also incorporating as certain concentration of metal. See Table 4.1 for parameter details.

4.1.2.2 GeSn Deposition

The same process was used to grow GeSn, except that the first layer deposited was Sn instead of Pb and the second layer was Ge as it was explained above in the layer inversion method. See Table 4.2 for more parameter details.

As previously mentioned, the layers were deposited at room temperature. The thickness of the layers varied from 50 nm to 200 nm, yet the last 20 experiments had deposited layers all with a thickness of 100 nm. The deposition rate and the amount of time after deposition differed from one run to another. After the deposition was done, chamber temperature was taken for each run. Table 4.3 shows the parameters used for Ge-Pb+Sn on Si sample.

4.1.3 Sample Annealing Process

At the beginning of this research, annealing was done in situ within the thermal evaporator at 200 °C. However, since the annealing temperature could not exceed 300 °C, a Fisher Scientific annealing furnace [34] was used instead for that purpose. The annealing temperatures were varied between 300-600 °C and the annealing time varied from 15 minutes to

60 minutes. Before starting the annealing process, the furnace was purged with dry N_2 gas in order to prevent oxidation of the sample.

Table 4.1. Parameters for Ge-Pb growth using thermal evaporator.

Run number	Layer	Film Thickness (nm)	Power Control	Current (ampere)	Deposition Rate (nm/S)	Deposition Time (Min.Sec)
Rn_1	Pb	100	4	20	________	________
	Ge	100	8	60	________	________
Rn_2	Pb	100	6	30	0.5-1	2.22
Rn_3	Pb	100	5	20-40	1.2-1.3	1.21
	Ge	82	10	60	1.5-2	4
Rn_4	Pb	60	6	40	0.8-0.9	2
	Ge	43	9	60	1-1.5	3
Rn_5	Pb	50	4	30-40	5-6	1.30
	Ge	50	8	60	1.2-1.5	7
Rn_6	Pb	100	5	40	2-4	1
	Ge	100	9	60	1.5-2	6
Rn_7	Pb	100	5	40	2-4	1.5
	Ge	100	9.5	60	0.5-0.6	4
Rn_8	Pb	100	5	40	3-5	0.55
	Ge	100	8-9	60	0.4-0.5	7
Rn_9	**Pb**	100	5	40	2.7	1.15
	Ge	100	8-9	60	0.5	7

Table 4.2. Parameters for Ge-Sn growth using thermal evaporator.

Run number	Layer	Film Thickness (nm)	Power Control	Current (ampere)	Deposition Rate (nm/S)	Deposition Time (Min.Sec)
Rn_1	Sn	50	7	60	0.5	6
	Ge	50	8	60	0.7	7
Rn_2	Sn	100	7	60	0.4-0.5	6
Rn_3	Sn	200	7.5	60	1.6-2	2
	Ge	200	8.5	60	0.6-0.8	5.21
Rn_4	Sn	200	7.7	60	1.5-1.8	2
	Ge	200	8.7	60	0.6	5.21
Rn_5	Sn	200	7.5	60	1.5-1.6	2
	Ge	200	8.8	60	0.7	5
Rn_6	Sn	100	7	60	0.5	4
Rn_7	Sn	100	7.5	58	1	1.30
	Ge	100	9.5	77	1-1.3	4.30
Rn_8	Sn	100	8	60	0.8-1	3.50
	Ge	100	10	60	0.4-0.5	3.40

Table 4.3. Parameters for Ge-Pb-Sn growth using thermal evaporator

Run number	Layer	Film Thickness (nm)	Power Control	Current (ampere)	Deposition Rate (nm/S)	Deposition Time (Min.Sec)
Rn_{Pb+Sn}	Pb+Sn	100	4	40	4	2
	Ge	100	10	60	0.5-0.7	6

4.1.4 Wet Etching Process

HCl and CH_3COOH were both solutions used for metal (Pb or Sn) etching. Both solutions gave nearly identical results, yet HCl was more often used because of the convenience. Also, different HCl concentrations with different etching times were attempted, in order to compare and pick the best concentration. The HCl solution (HCl: H_2O) was prepared in HiDEC clean room with a concentration of 20%, 30%, and 50%, and an etching time of 2 min, 5 min, and 10 min. The 30% etch solution worked very well and all subsequent samples were etched using 30% HCl for 2 minutes. Figure 4.1 shows the fabrication process of GePb/GeSn.

4.2 Equipment

4.2.1 Deposition Equipment

4.2.1.1 Thermal Evaporator

As previously mentioned in Chapter 2, thermal evaporation is a popular method of PVD. A thermal evaporator system includes a vacuum chamber to help with depositing thin films of pure materials onto a substrate. An Edwards Coating System E306A [35] shown in Figure 4.2

was used to deposit thin layers of Ge, Pb, and Sn for subsequent growth of GeSn and GePb.

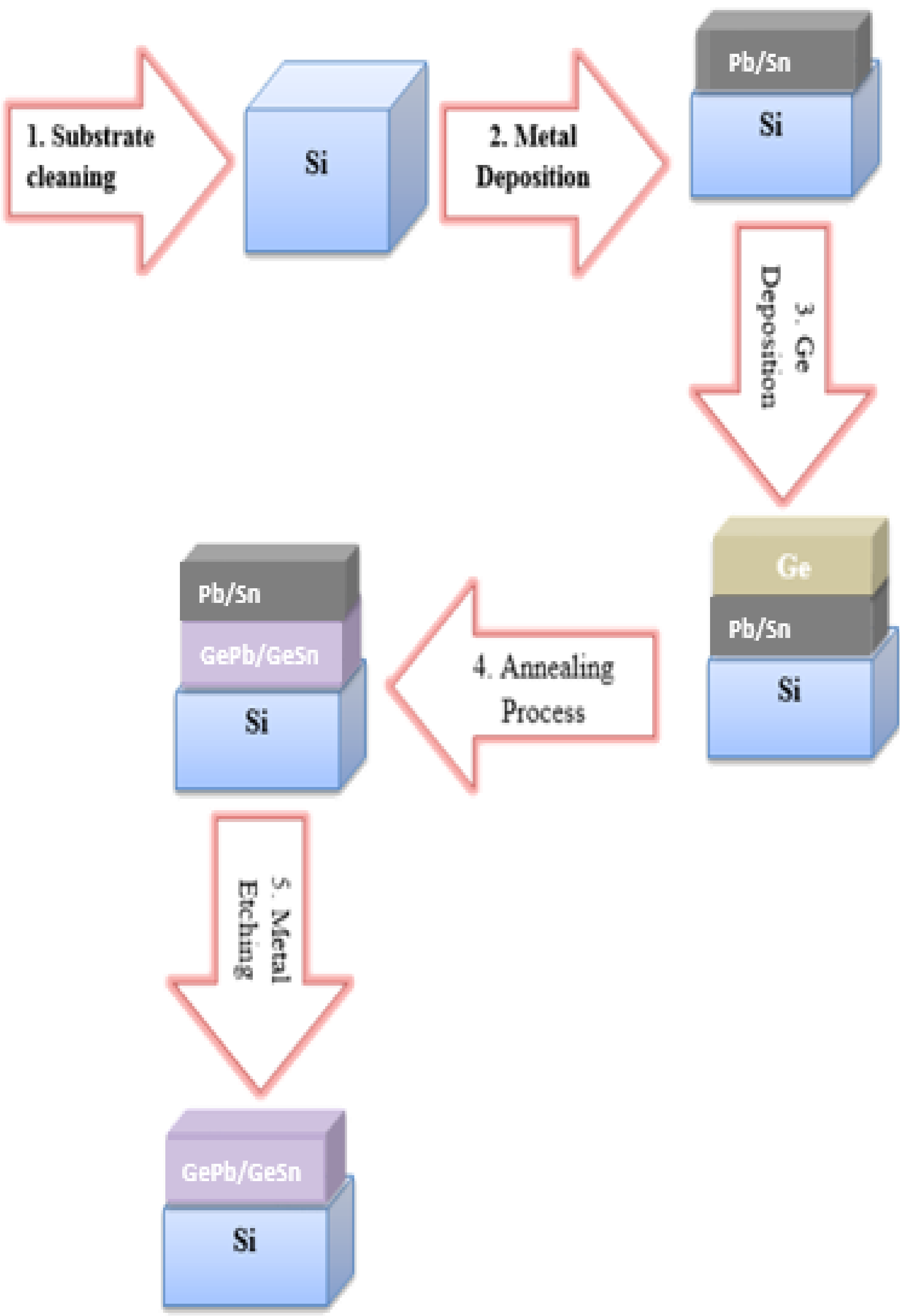

Figure. 4.1. Fabrication process of GePb/GeSn.

Figure. 4.2. Fabrication process of GePb/GeSn (picture taken by the author)

4.2.1.2 Fisher Scientific Furnace

A Fisher Scientific furnace [34] shown in Figure 4.3 in the assembly lab was used to anneal samples under N_2 environment at different annealing time (15-60 mins) and temperatures (300-600 °C).

4.2.2 Characterization Equipment

For sample characterization, Raman spectroscopy, photoluminescence (PL), X-ray diffraction (XRD), and scanning electron microscopy (SEM) were used to examine the sample

crystallinity, band gap energy, and composition.

Figure 4.3. Fisher scientific furnace (picture taken by the author).

4.2.2.1 Raman Spectroscopy

Raman spectroscopy relies on inelastic scattering of monochromatic light, mostly from a laser source. The meaning of the term inelastic scattering is that photon frequency in the incident monochromatic light alters depending on the interaction with samples. When the lattice vibration of the target molecules or crystal interact with incident photons of the laser, the scattered light photons either gain of loose energy corresponding to absorption or emission of a vibration mode quantum. That creates the Raman effect, which gives the reemitted photons frequency shifted (up

or down) in contrast to the prime monochromatic frequency. Raman spectroscopy can also be used to study samples in different phases such as solid, liquid, and gas [36].

Raman spectroscopy contains four main components detector, wavelength selector, light collection optics and illumination structure, and laser source. Usually, the laser beam illuminates the sample in the range of the visible (Vis), ultraviolet (UV), or near infrared (NIR). To get the Raman spectrum of the sample, lens collect the scattered light and then the scattered light is sent via interference filter or spectrophotometer [36]. A schematic diagram of the Raman spectroscopy system setup used in this research is shown in Figure 4.4.

Generally, Raman scattering has sensitivity to degree of crystallinity in materials or alloys. A crystalline material gives a spectrum with intense and sharp Raman peaks while an amorphous material shows wider and less intense peaks. Both states (completely amorphous or completely crystalline) can be deemed spectral extremes. In addition, an intermediate state for Raman spectrum, for instance partly-crystalline, will have features which are intermediate in case of peak intensity and width [37].

Raman shift is the difference in energy between incident and scattered photons in cm^{-1} [37]. Raman shift $\bar{\nu}$ can be calculated by:

$$\bar{\nu} = \frac{1}{\lambda\,\text{incident}} - \frac{1}{\lambda\,\text{scattered}} \qquad \text{(Equation 4.1)}$$

where $\lambda_{incident}$ and $\lambda\ s_{cattered}$ are the wavelength in cm.

Raman spectroscopy can be used in different applications for the following: chemical analysis, microscopic, non-destructive, and imaging. For both qualitative and quantitative data,

Raman analysis is capable of providing important information fast and easy [39].

In semiconductors, a Raman spectroscope (Figure 4.5) is used in several applications such as: characterization of strain or stress, alloy concentration, purity analysis, contamination identification, super-lattice structure, and hetero structure determination, defect analysis, photoluminescence microanalysis, and doping effects [40].

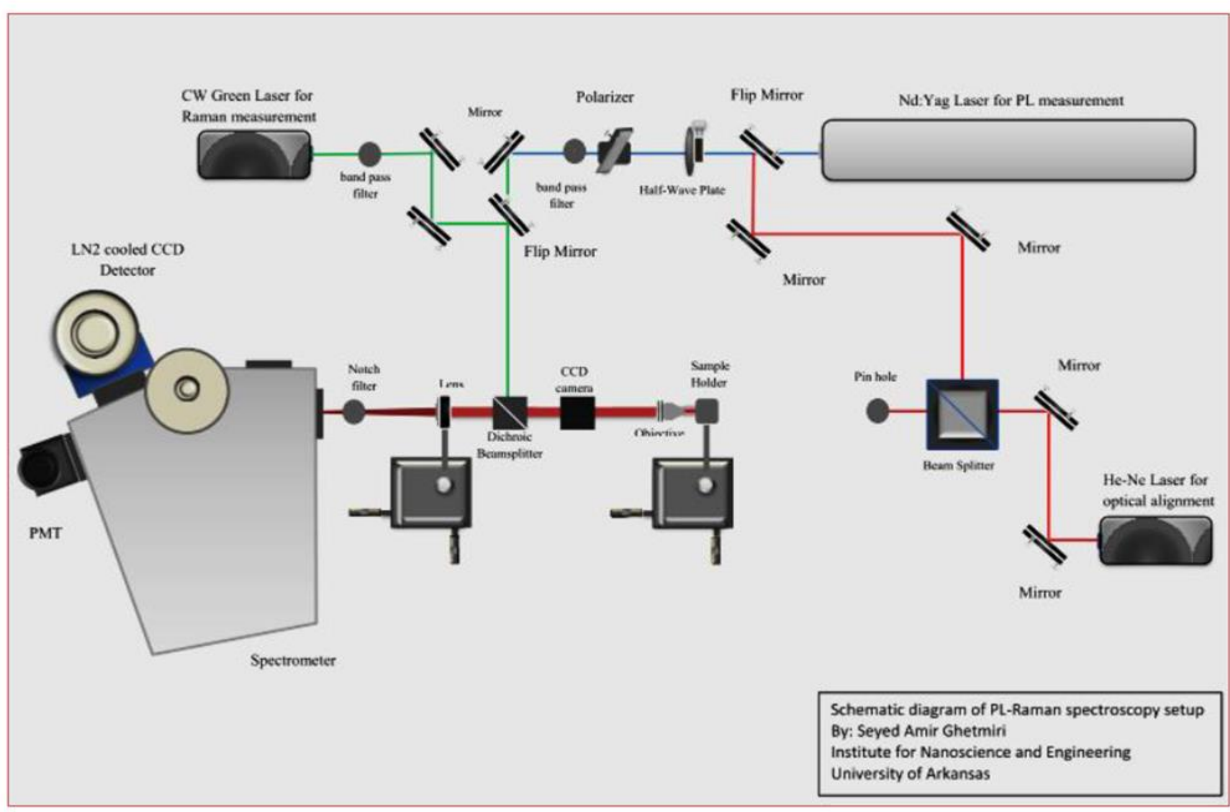

Figure 4.4. Schematic diagram of Raman spectroscope setup [38].

To study the crystallinity of GePb and GeSn thin films, Raman measurements were taken using a helium–neon (He-Ne) laser at wavelength 632.8 nm and 10 mW output power at room temperature. For the last 12 samples measured, another laser was used which was a diode pumped solid state (DPSS) continuous wave (CW) at 532 nm wavelength and power of 500 mW at room temperature.

4.2.2.2 Photoluminescence

Photoluminescence (PL) is a specific type of luminescence. The word photoluminescence includes all devices capable of absorbing light energy and after that, the energy released in the form of light [41]. When light is focused onto a sample, it is absorbed and conveys extra energy into the material in a procedure known as photoexcitation. The sample gives out a portion of that extra absorbed energy in the form of photons or light, and it is said to show photoluminescence [42]. Because of the photoexcitation, electrons in the material may be excited into higher energy states. When these electrons get back to their equilibrium state, the extra energy may be given out as a radiative process (emission of light) or in a non-radiative process [42].

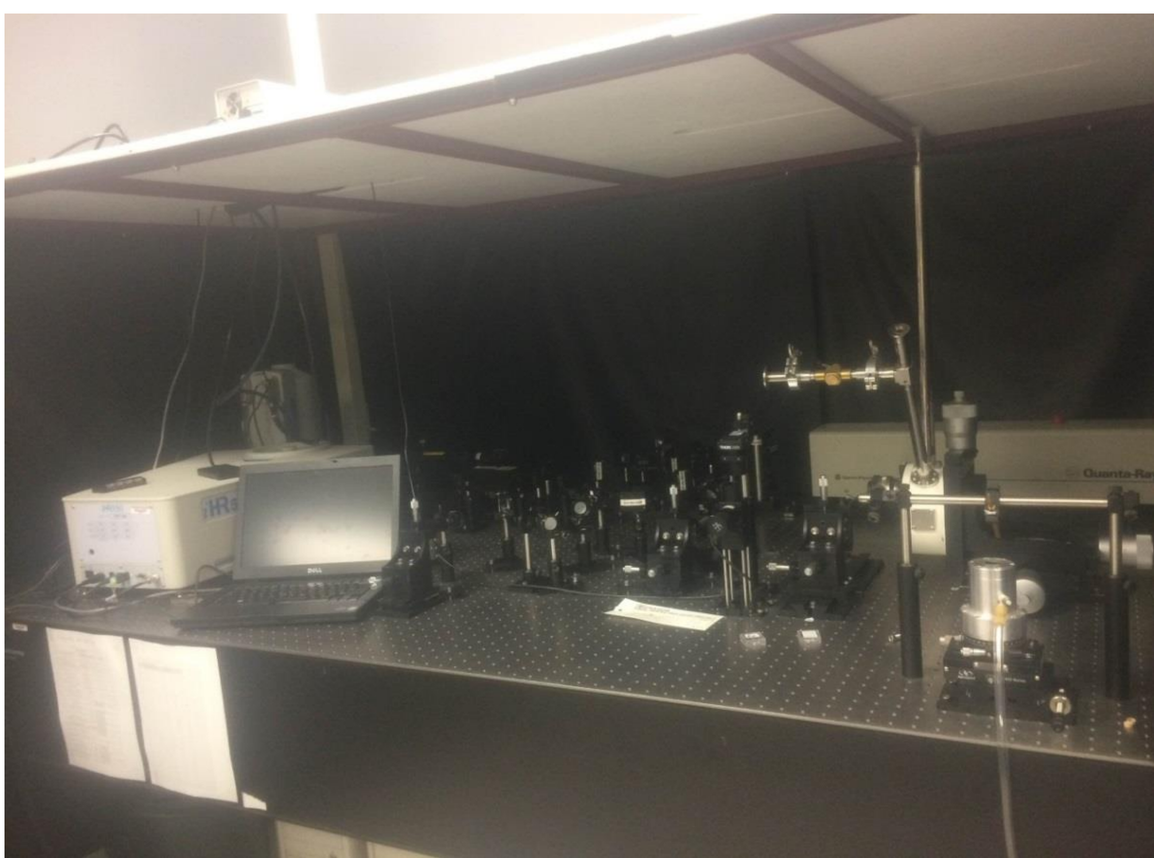

Figure 4.5. Raman spectroscopy system (picture taken by the author).

Fluorescence and phosphorescence are the two kinds of photoluminescence. Fluorescent materials initially absorb light and emit it immediately at various wavelengths, while phosphorescent materials initially absorb small wavelength light and then gradually emit light through time at various longer wavelengths [43].

A laser with a wavelength near the band gap energy of the sample is pointed onto the sample, which can be held by cryostat to be take measurements that taken under low temperature. Once the laser beam falls on the sample, photoluminescence occurs and light is emitted at wavelengths depending on the sample composition.

The sample is placed inside a cryostat, with the reflected beam and photoluminescence emission propagating in various directions. The emitted light is then guided through a fibre optic cable into a spectrometer. A computer is used to interpret the digital information, and can show a PL spectrum [44]. A diagram of photoluminescence set-up is shown in Figure 4.6.

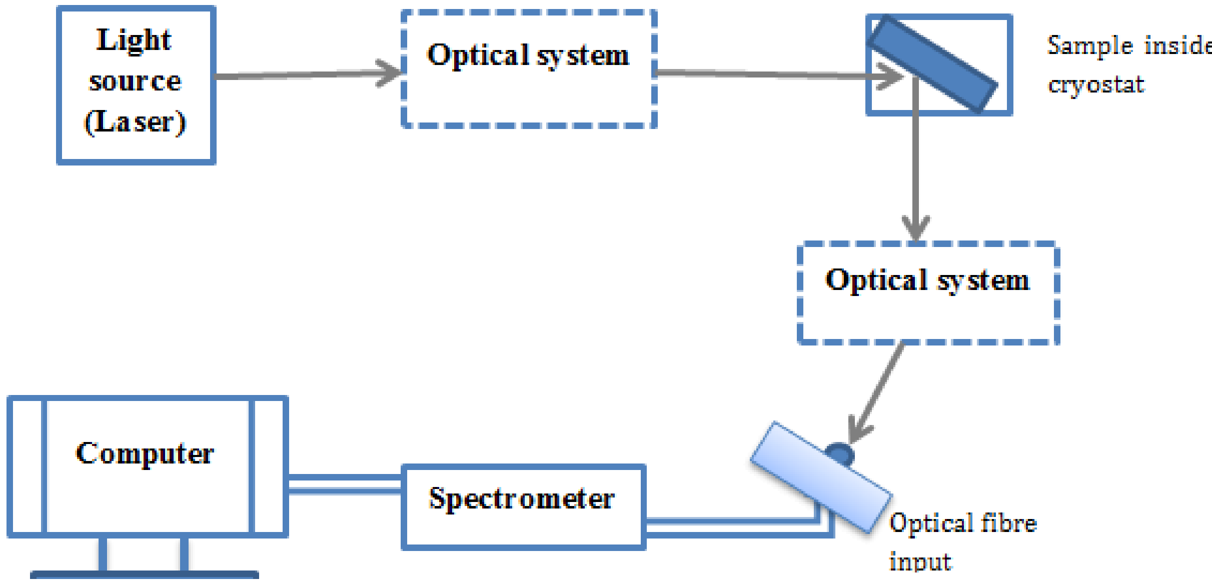

Figure 4.6. Diagram of photoluminescence set-up.

PL can be used to investigate discrete energy levels and to get values for semiconductor sample composition, thickness of quantum well, or sample monodispersity in the case of quantum dots [43].

PL was used in this research to determine the band gap edge. The PL peaks represent direct measurements of the energy level. Diode pumped solid state (DPSS) continuous wave (CW) laser at 532 nm wavelength and power of 500 mW was used at room temperature. A picture of the photoluminescence system used in this research is shown in Figure 4.7.

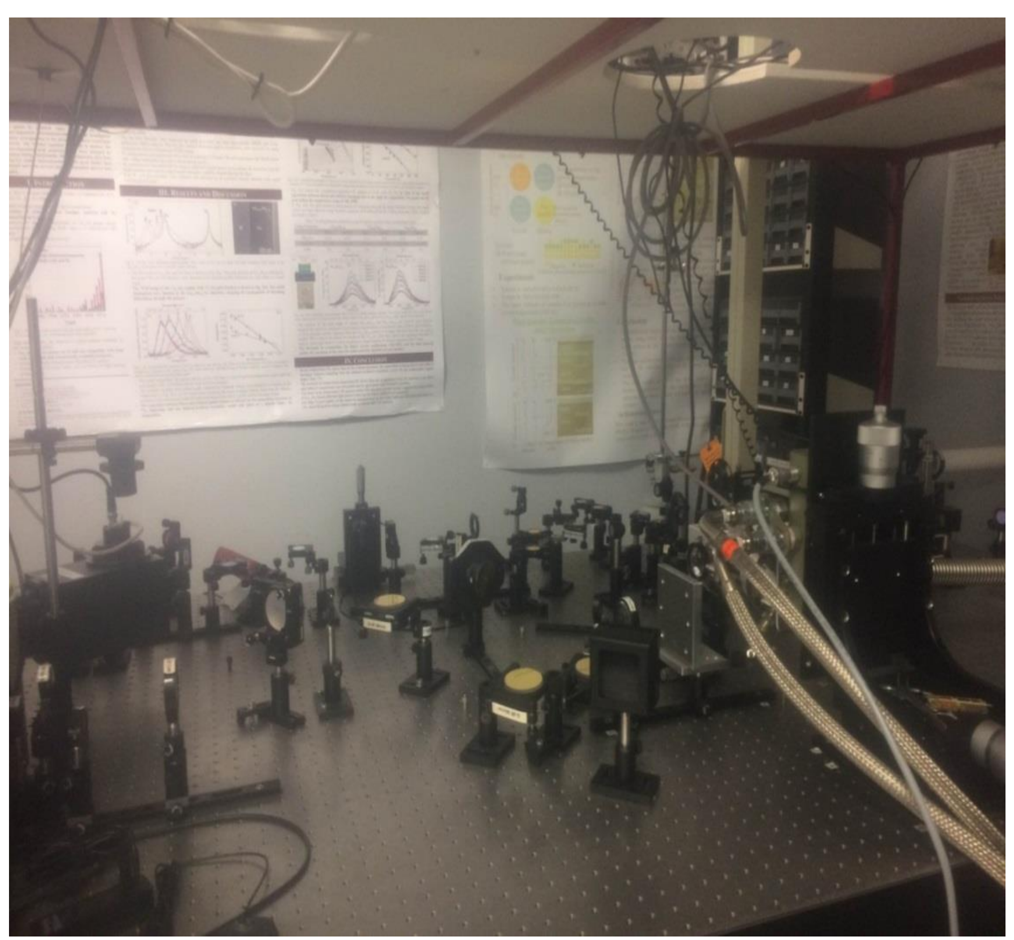

Figure 4.7. Photoluminescence system (picture taken by the author).

4.2.2.3 X-ray Diffraction (XRD)

When the atoms of a crystal scatter X-rays, an interference effect is produced. Therefore, the diffraction pattern offers information about the crystal structure or character of a crystalline substrate [45].

In 1895, X-rays were discovered which helped scientists to analyze the crystalline structure at the atomic scale. There are two primary areas X-ray diffraction has been utilized: as a mark for crystalline materials characterization and for their structure identification [43]. Figure 4.8 shows a XRD system.

XRD can be used for different purposes such as defining the orientation of single crystal or grain, calculating the average spacing between planes of atoms, determining the crystal structure of an unidentified material, measuring internal stress, size, and shape of small crystalline areas [45].

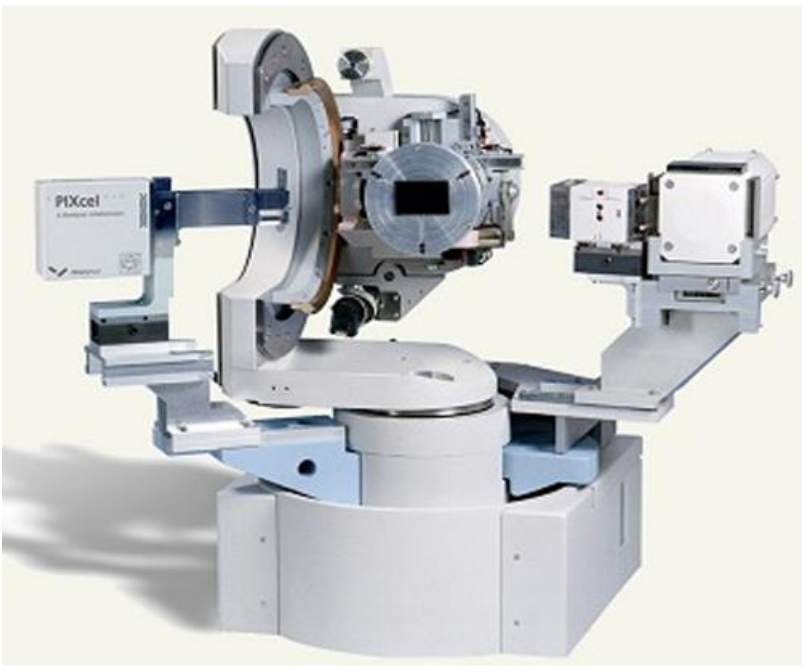

Figure 4.8. A picture of XRD system [46].

4.2.2.3.1 Bragg's law

Diffraction happens only if Bragg's law can be satisfactorily implemented [44]. X-ray reflection from two planes of atoms in a crystal structure are shown in the Figure 4.9.

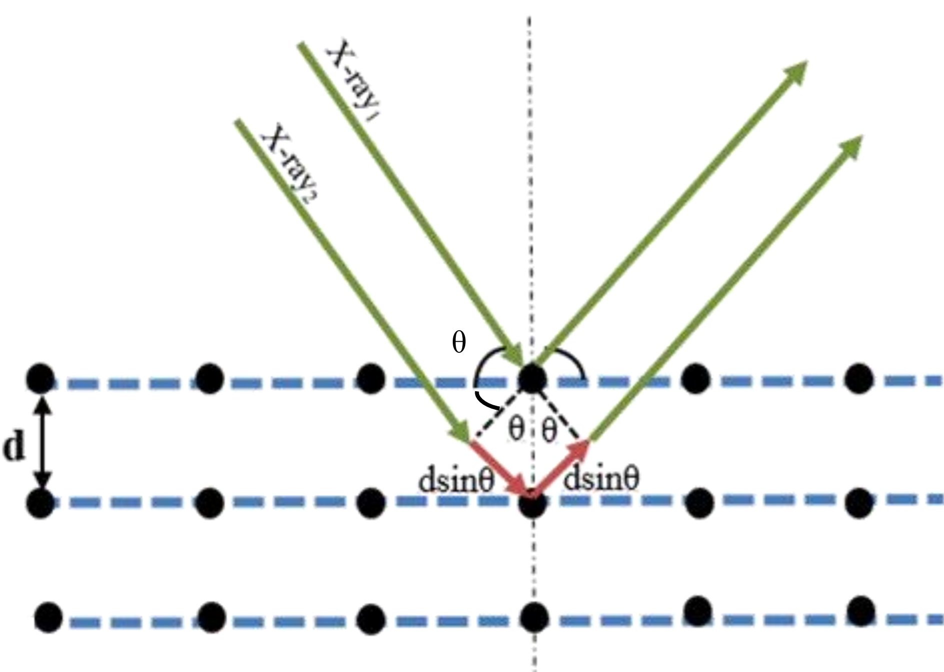

Figure 4.9. Bragg's low: X-ray interaction with the atoms.

Bragg's law states:

$$n\lambda = 2d\sin\theta \qquad \text{(Equation 4.4)}$$

where θ is the reflecting angle, d is the distance between planes, dsinθ is the extra path to reach the atom in the second plane, 2dsinθ is the path difference between the two waves. λ is the wavelength, and n is the number of wavelengths (normally n = 1).

XRD was used in this work to determine the crystal structure and orientation of GePb and GeSn samples. In addition, it was used to measure the d spacing between atoms and to estimate the Pb and Sn composition of the alloy.

4.2.2.4 Scanning Electron Microscopy (SEM)

SEM utilizes an electron beam focused over a substrate area to produce an image. The sample and the beam electrons interact with each other, then generate different signals which can be used to get information about surface morphology and composition [47]. Figure 4.10 shows the SEM used in this research.

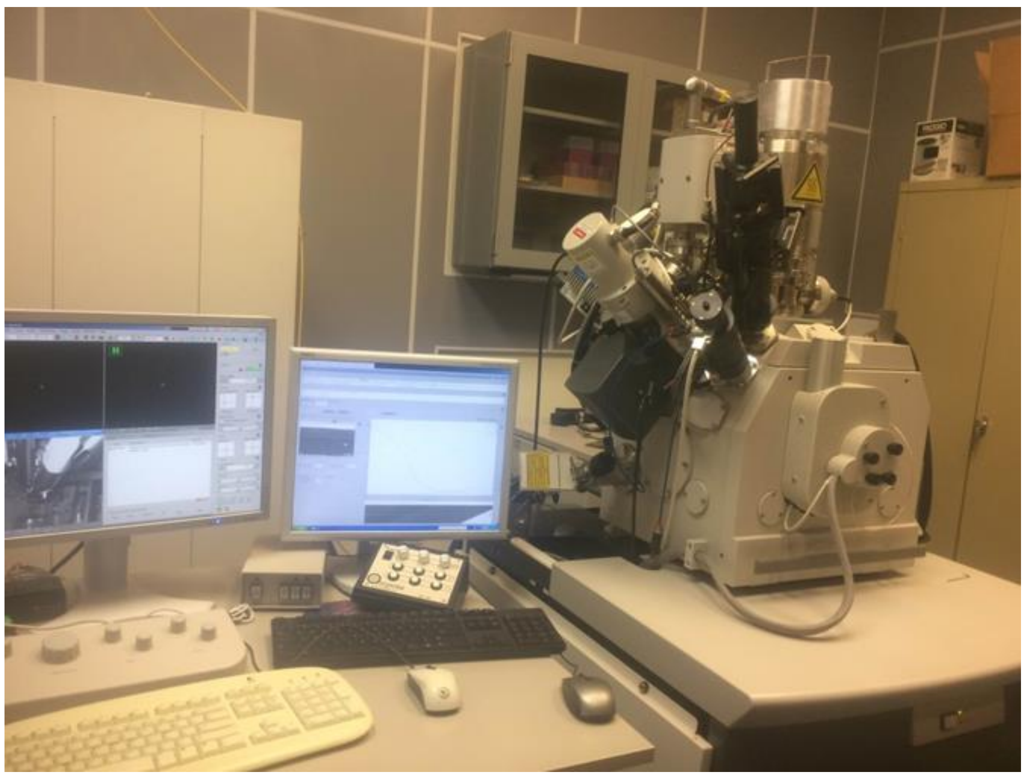

Figure 4.10. SEM system (picture taken by the author).

SEM creates an image with large magnification by replacing electrons instead of using light to produce an image. At the top of the microscope, an electron gun produces a beam of

electrons which follow a vertical track through the microscope. That microscope is operated in a vacuum. The beam goes through electromagnetic fields and magnetic lenses which direct the beam down to the sample. When the beam strikes the sample, electrons and X-rays are produced from the sample. Detectors will collect X-rays, secondary electrons, and backscattered electrons in order to characterize the sample [48]. Secondary electrons emitted from the sample substrate create an image of the sample substrate commensurate with its surface composition and surface morphology. This signal is sent to a screen and creates the final image. The X-ray emission from the sample is characterized to determine the sample composition using energy dispersive analysis of emitted X-rays (EDX). A schematic of an SEM system is shown in Figure 4.11.

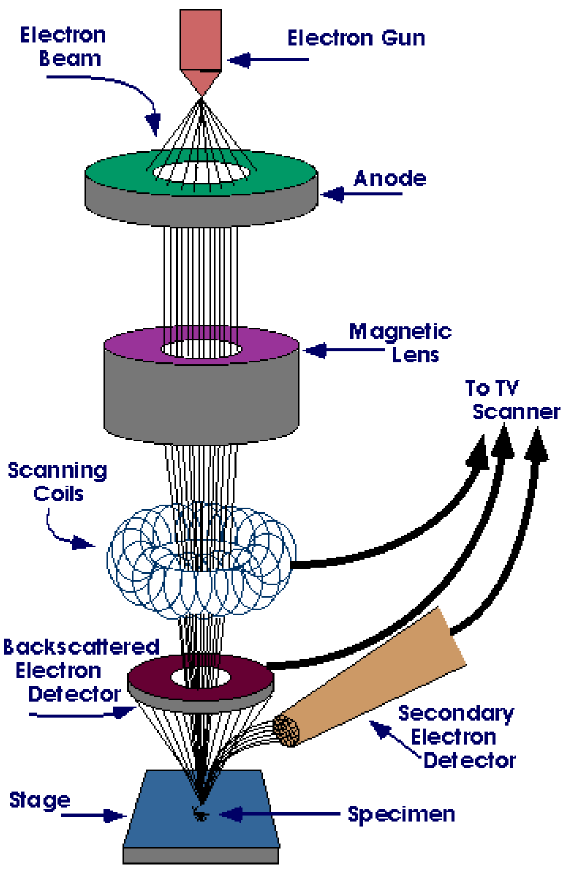

Figure 4.11. A schematic of SEM system [49].

Chapter 5: Results and Discussion

As part of this research, a number of experiments were done in order to grow crystalline GeSn and GePb and to possiblly obtain heteroepitaxy. Additionally, two different substrates were used, glass and Si.

With the PVD system the GeSn and GePb samples were grown thermally. This was by using the thermal evaporator under a high vacuum pressure of 10^{-6} Torr. GeSn and GePb samples were characterized using different characterization methods: Raman spectroscopy, photoluminescence (PL), X-ray diffraction (XRD), and scanning electron microscopy (SEM). Four factors were controlled in the growth: layer thickness, annealing temperature, annealing time, and etching solution. Therefore, those factors were varied in order to find the best growth conditions. However, after trying two different etching solutions hydrochloric acid (HCl) and acetic acid (CH_3COOH), the result was almost exactly the same for both of them. So, the project was completed using only HCl as the etching solution.

There were two main variables used to study the growth of the samples; annealing time and annealing temperature. To study the effect of annealing temperature, a sample from a deposition run was divided and used at four different annealing temperatures (300, 400, 500, and 600 °C), three different times (15, 30, and 60 minutes) for each annealing temperature.

The thickness of each layer was varied between (50-200 nm). However, it was observed that for thickness of 50, 60, and 80 nm, all samples failed to show any shift in the Raman spectroscopy measurement indicating no alloy formation. However, when using 100 nm thickness for each layer, for both Ge-Sn and Ge-Pb, a good shift in the Raman peaks were obtained.

For the thermal process, in order to obtain a pure dry deposition environment, a liquid nitrogen trap was used after the chamber pressure reached 3×10^{-5} Torr. This would preferentially pump out water vapor from the evaporator chamber. The vacuum in the thermal evaporator system provides a pure condition from ambient air particles and other contaminants. This assured clean deposition conditions. All deposition occurred without deliberate substrate heating. However, the substrate temperature was measured to be around (60-80 °C) mainly due to radiation heating from the evaporation boat and convection heating from the evaporated Ge and metal.

Moreover, in the annealing process via Fisher Scientific furnace, N_2 gas was used during annealing to provide a clean dry surrounding.

5.1 The Fabrication Process of Ge Alloy

5.1.1 Fabrication Process of GeSn

As Figure 5.1 shows, the sample with tin on a silicon substrate had a golden color before depositing germanium, but after depositing Ge its color was changed to dark gray. The samples got darker after increasing the annealing time and etching. For the sample annealed for 15 minutes at 300°C, the color did not change more than the un-annealed GeSn. However, after 30 minutes of anneal the sample started to get dark; the one hour annealed sample was almost black with some purple and golden color. Also, increasing the annealing temperature impacted the sample color the same way. For example, the sample annealed at 600 °C was very dark and glittery at the same time while the sample annealed at 400 °C was lighter with gray color and not shiny.

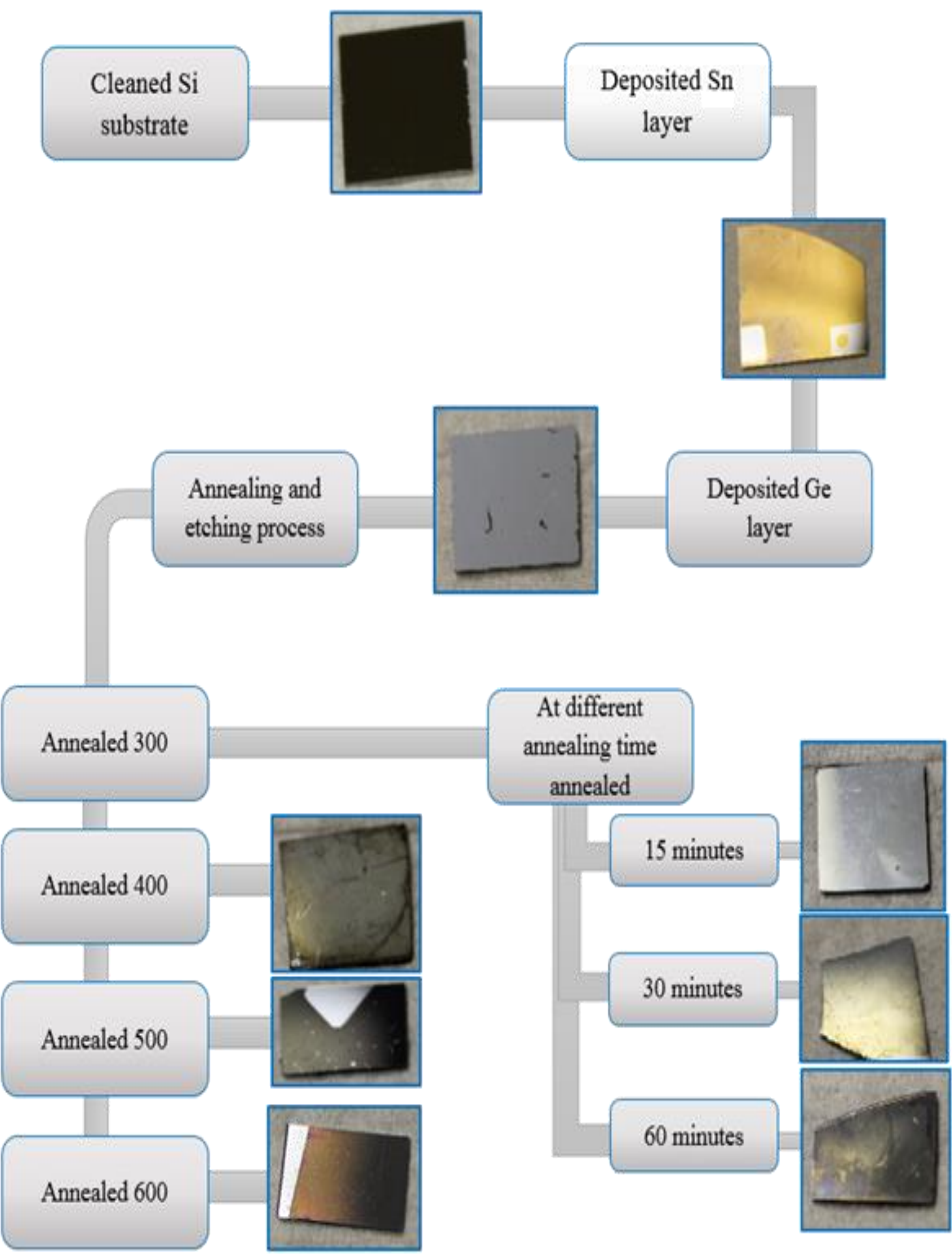

Figure 5.1. GeSn sample surface changes during the fabrication

5.1.2 Fabrication Process of GePb

Figure 5.2 illustrates the noticeable changes of the GePb sample during the fabrication process.

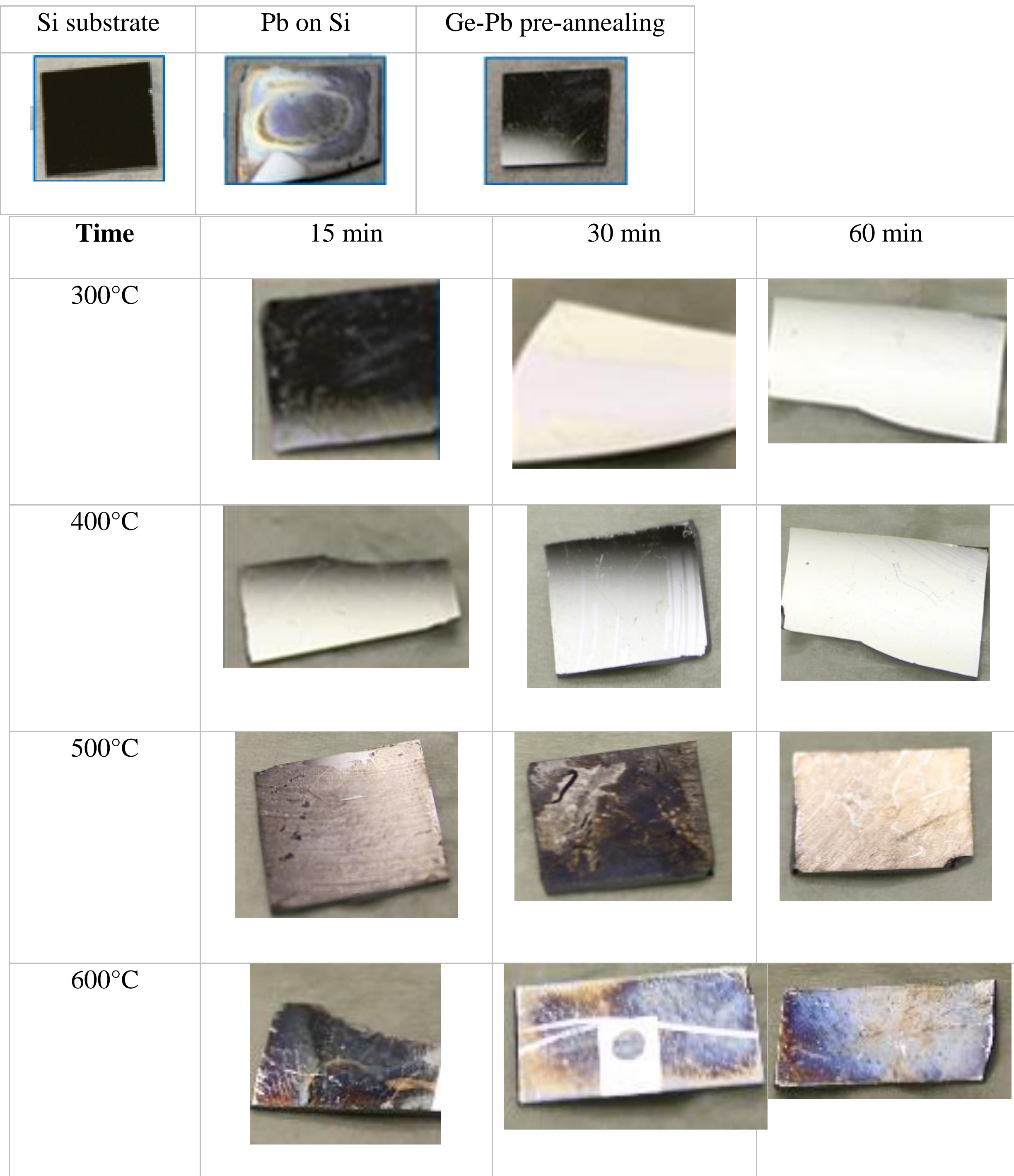

Figure 5.2. GePb sample surface changes during the fabrication process.

GePb sample surface color also changed after the annealing temperature was increased and after etching. Samples annealed at 300 °C and 400 °C did not show a lot of color change, yet the surface was less smooth and less shiny than the un-annealed sample. However, at 500 °C, the samples were rougher with cupreous color. Samples annealed at 600 °C were very dark and had more than one color (brown, blue, and black).

From both GeSn and GePb samples annealed at various temperatures and times, it can be inferred that layer exchanged took place at 300 °C and annealing time above 30 minutes. At high temperature, however, optical interference due to SnO and PbO formation on the surface my have been occurring.

5.2 GeSn Result

5.2.1 Raman Spectroscopy

In this research, Raman spectroscopy was used to determine the alloy composition and crystallinity of the GeSn and GePb films that were deposited on a silicon or glass substrate. After Raman spectroscopy measurement was done using helium–neon (He-Ne) laser at wavelength of 632.8 nm and power of 10 mW, the data was used to generate a graph as shown in Figure 5.3.

The GeSn sample depicted in Figure 5.3 was deposited using thermal evaporator PVD. It was deposited at room temperature under 5×10^{-6} Torr base pressure using layer-by-layer method on a Si substrate. The first layer was tin with 100 nm thickness, deposition rate of 8-10 nm/s, and deposition time of 3 minutes 50 seconds. The second layer was germanium with 100 nm thickness, deposition rate 4-5 nm/s, and deposition time of 3 minutes and 40 seconds. After the deposition was completed, the chamber temperature was 68 °C. Using Fisher Scientific

furnace in the assembly lab, the sample was annealed for 1 hour at 400 °C under nitrogen environment. Then, the sample was etched using a 30% HCl in water solution for 2 minutes. Raman measurements were taken at room temperature.

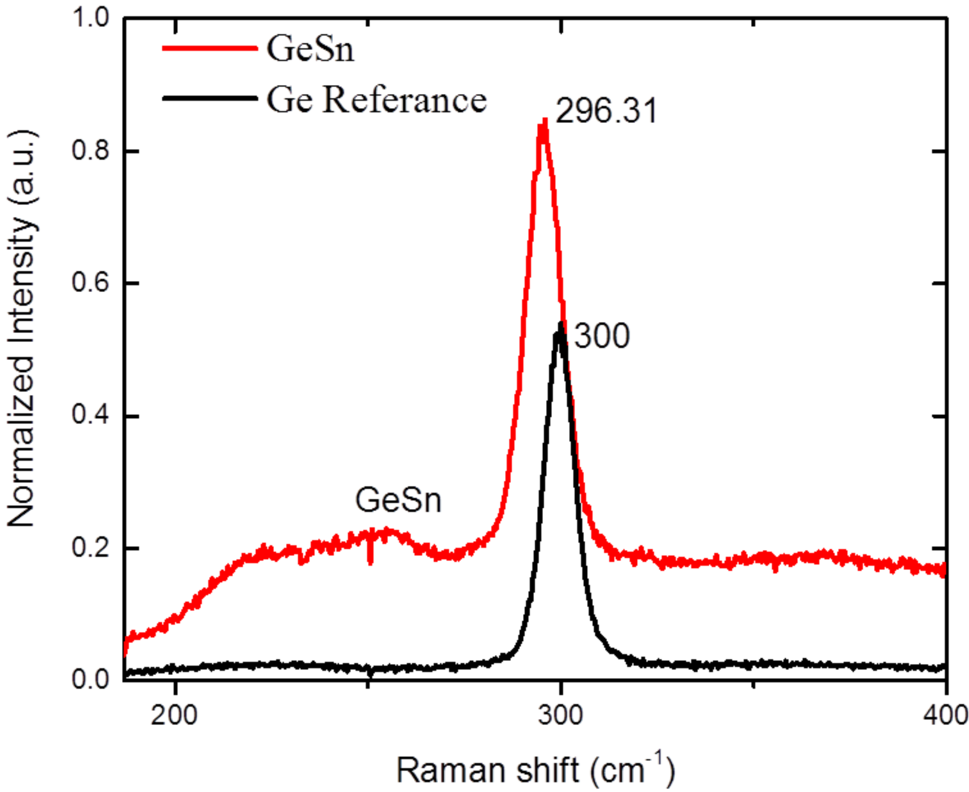

Figure 5.3. Comparison of the Raman spectroscopy of Ge reference and GeSn annealed for 1 hour at 400 °C under N_2 environment on a Si substrate.

As can be seen in Figure 5. 3 the GeSn sample behaved differently than the (001) Ge reference. The Ge-Ge peak was at 300 cm^{-1} while for GeSn sample the peak shifted to the left at 296.31 $cm^{-1.}$ This implies incorporation of Sn in Ge lattice. Left of the shifted peak, the shoulder is in the range of 287 cm^{-1} and Ge-Sn peak from 245 to 274 cm^{-1} refers to the incorporation of Ge-Sn at lower wavelength, because of the variation in the bonding energy of Ge-Ge via Sn atoms. The intensity was normalized to 1 in all Raman graphs, therefore, a low count background peak was observed from 200-250 nm.

5.2.1.2 Annealing Temperature Study

At the same deposition condition, GeSn samples were annealed at different temperatures to study the effect of thermal annealing on the crystallinity of the GeSn. Starting from 300 °C up to 600 °C, the samples were annealed for 1 hour then characterized by Raman scattering spectroscopy. Figure 5. 4 shows, the Raman spectra of GeSn samples on Si substrate annealed at different annealing temperatures. Those samples were cleaned, deposited, and etched under the same condition, the only difference being that each of them was annealed at a different temperature for 1 hour. However, when characterized by Raman spectroscopy, they show shifts in the Ge-Ge peak. Comparing the samples with each other, it is obvious that the sample that was annealed at 400 °C produced larger Raman shift than other samples. This implies that annealing at 400 °C resulted in more incorporation of Sn. This can be due to a segregation of Sn at higher temperature while at lower temperature, such as 300 °C, there was not sufficient incorporation of Sn. From the shape of the Raman peak, it could also be inferred that the films were crystalline.

5.2.1.3 GeSn on Glass Substrate

This sample was different from the previous one in that the substrate was glass. The deposition was done at room temperature while the base pressure was 5×10^{-6} Torr, using the same deposition method as GeSn on silicon. In Figure 5.5, the GeSn on a glass substrate also had a shifted peak compared to the Ge reference. The Ge-Ge peak is ~ 300 cm^{-1} while for GeSn crystalline alloy the peak shifted to the left at 293.20 $cm^{-1.}$ This means that there was an incorporation of Sn in Ge lattice. Ge-Sn peak from 236 to 252.9 cm^{-1} refers to incorporation of Ge-Sn at lower wavelength.

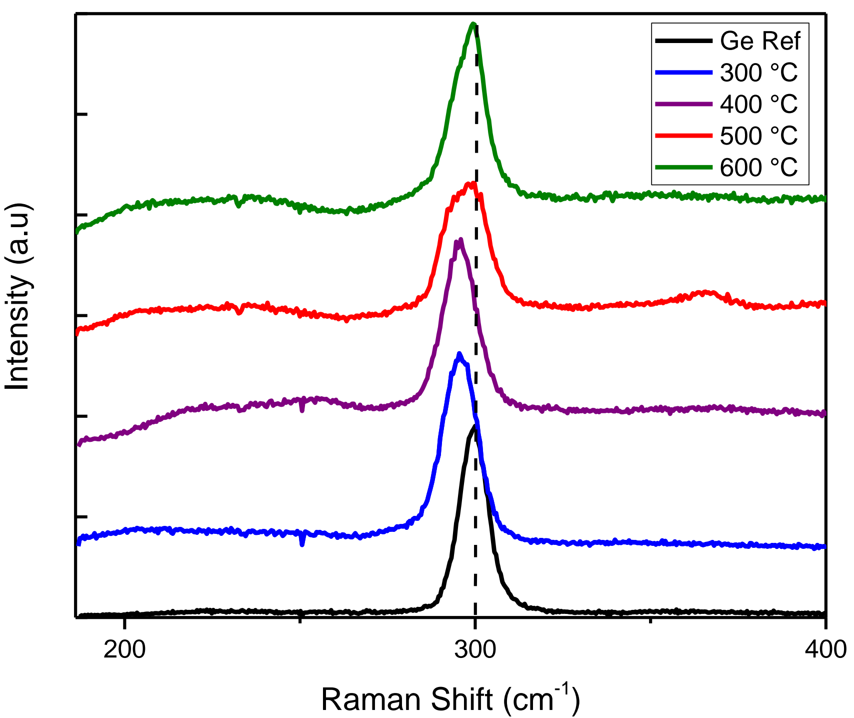

Figure 5.4. Raman spectroscopy of GeSn at different annealing temperature (300-600 °C) for 1 hour under N_2 environment.

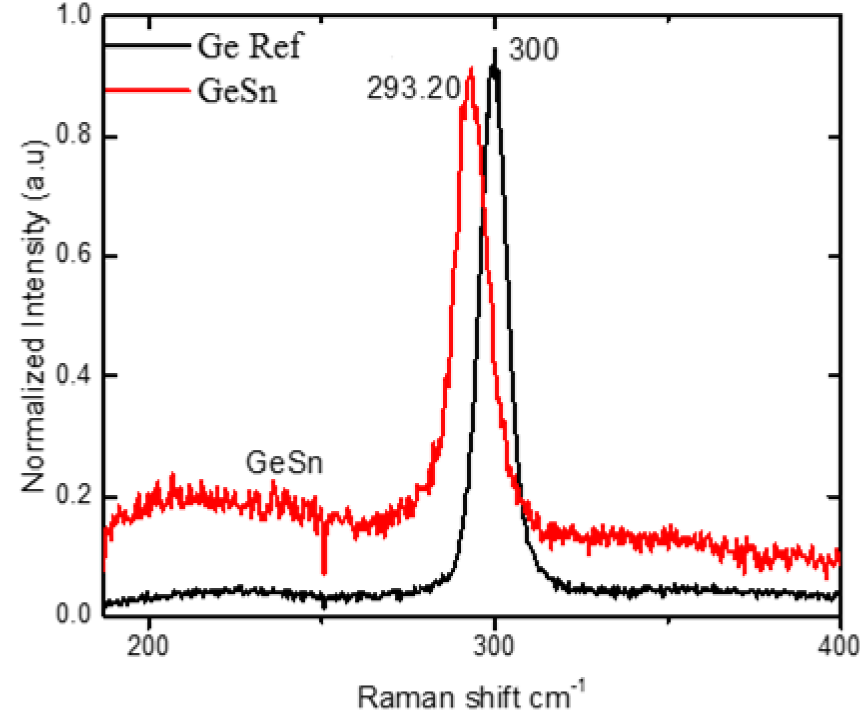

Figure 5.5. Comparison of the Raman spectroscopy of Ge reference and GeSn annealed for 1 hour at 400 °C under N_2 environment on glass substrate.

5.2.2 Photoluminescence Spectra (PL)

In germanium, the L valley is the indirect band gap at an energy of 0.67 eV. While the direct band gap at the Γ valley with energy of 0.8 eV is at standard room temperature. When Sn incorporates in Ge, the conduction band decreases at the Γ valley at a much quicker rate compared to the L valley. In order to determine the bandgap edge for a GeSn sample, photoluminescence spectra (PL) measurements were taken, as illustrated in Figure 5.6.

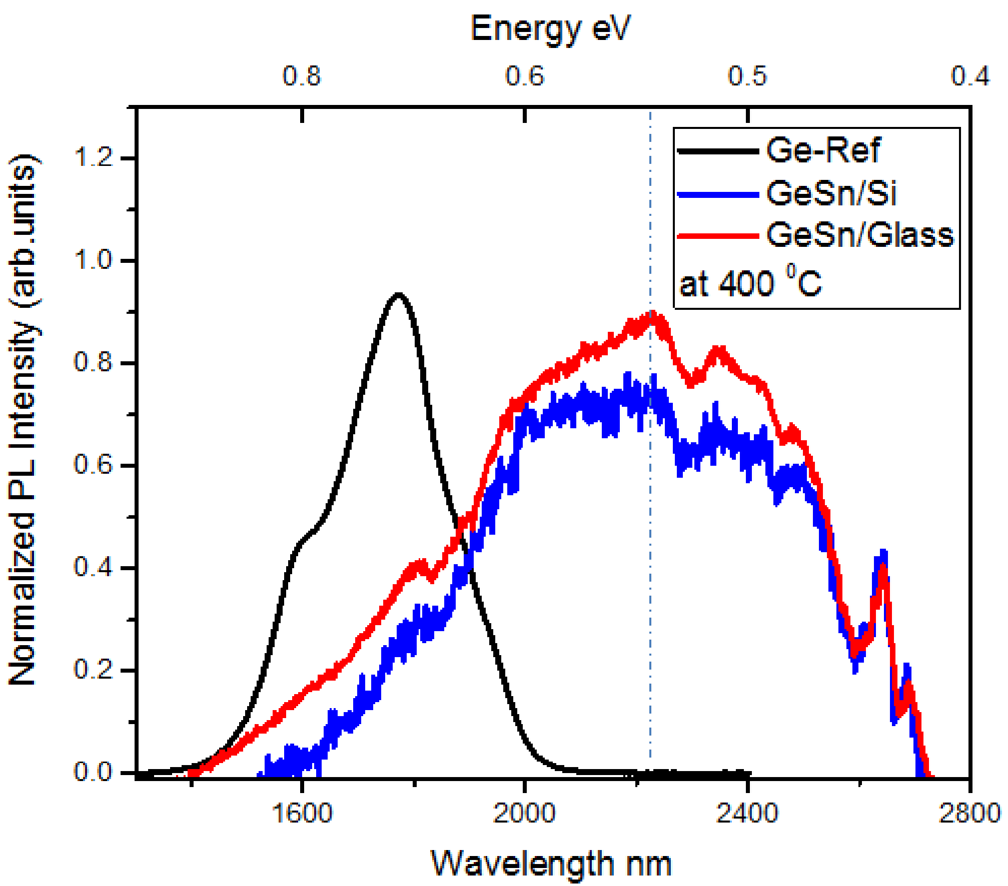

Figure 5.6. Photo luminesces spectra for Ge reference, GeSn film on Si and glass annealed at 400 °C for one hour under N_2 environment.

From Figure 5.6 the Ge reference at wavelength 1784 nm is equal to the band gap energy of E = 0.6950 eV. The band gap energy of GeSn on silicon substrate was E = 0.544 eV which is

lower than the Ge reference. For GeSn on glass substrate, the band gap was E = 0.545 eV. Therefore, PL results indicates that the band gap of Ge reduced by -0.15 eV as a result of alloying with Sn. This was a good sign for direct band gap and crystalline GeSn.

For GeSn on glass substrate annealed at 400 ℃ and 500 ℃, the band gap energy decreased to 0.5565 eV. However, the band gap energy was a little lower for GeSn sample that was annealed for 1 hour at 500 ℃. To the right of both GeSn peaks, there are small curves at 523nm due to the fifth order of the PL wavelength.

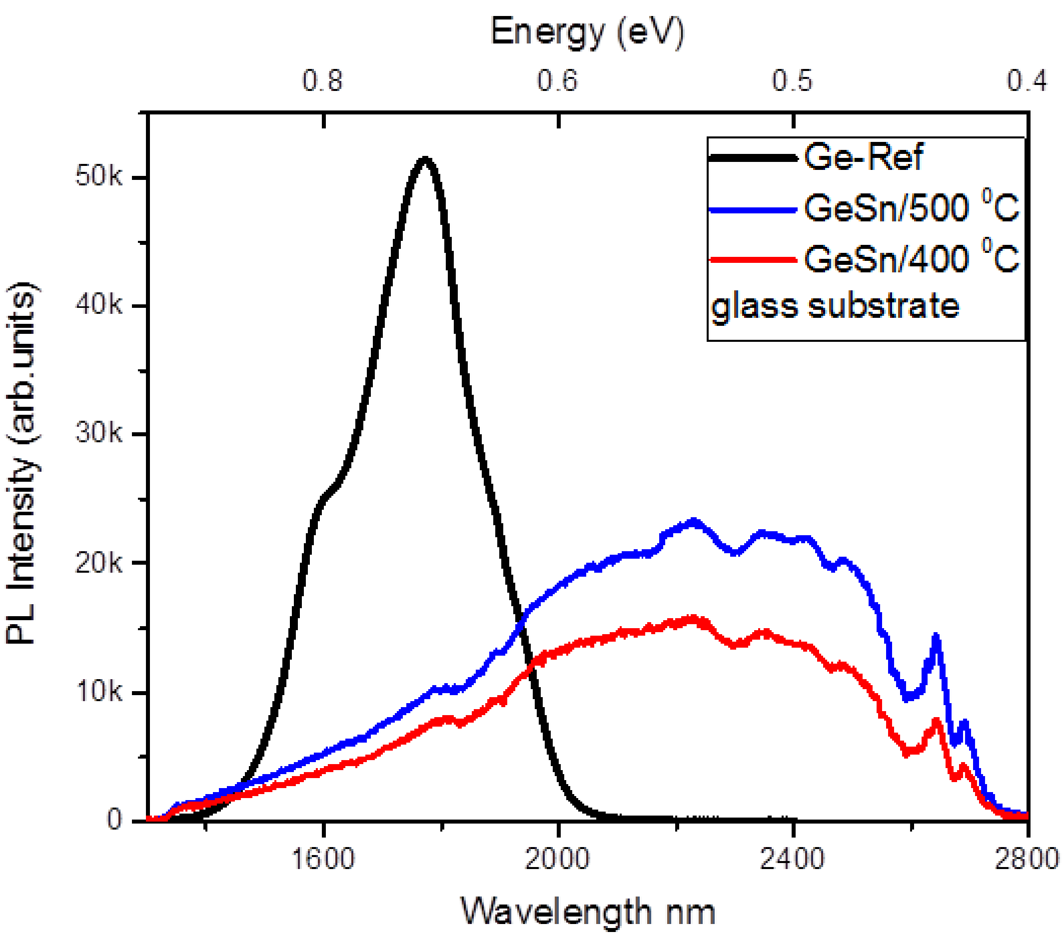

Figure 5.7. Photoluminescence spectra for GeSn film on glass annealed at 400 ℃ and 500 ℃ for 1 hour under N_2 environment.

5.2.3 X-Ray Diffraction (XRD) Result

XRD is used to calculate the typical spacing between planes of a crystal. This is in order to define the orientation of a grain or a single crystal. In addition, it is used to determine the crystal arrangement of a new material [50]. Figure 5.8 illustates the XRD patterns for GeSn/Si annealed at 300 ºC.

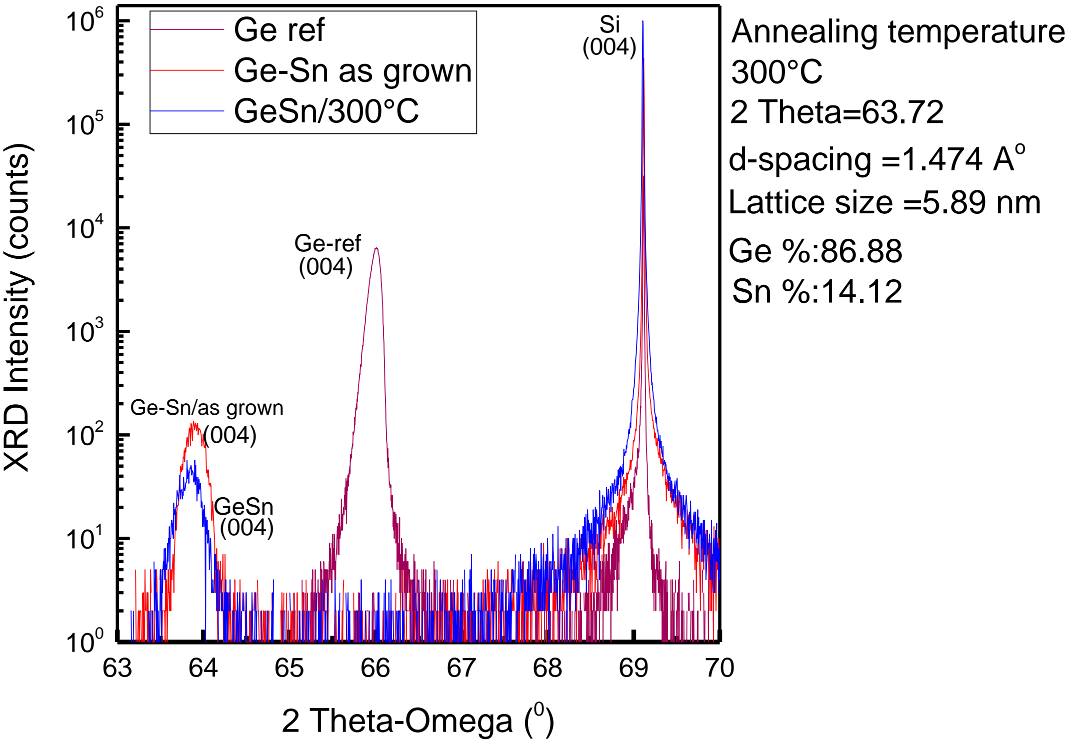

Figure 5.8. XRD patterns for GeSn/Si annealed at 300 ºC for 1 hour under N_2 environment.

This GeSn sample was deposited at room temperature with 100 nm thickness for Ge layer and Sn layer, then the sample was annealed at 300 ºC. The Ge/Sn/Si (as grown) before annealing sample gave a higher intensity peak than GeSn after annealing and etching which gave low intensity peak at the 14% composition level. This could be due to substrate heating during

deposition, which can reach 100 °C and result in crystalline GeSn. Therefore, the annealed sample at 300 ºC gave less quality film than the as grown sample.

5.3 GePb Results

5.3.1 Raman Spectroscopy

GePb was deposited on a Si substrate at room temperature under 5×10^{-6} Torr base pressure. The first layer was Pb with 100 nm thickness for a deposition rate of 0.15-0.2 nm/s and deposition time 1 minute and 30 seconds. The second layer was germanium with 100 nm thickness for a deposition rate of 0.5-0.6 nm/s and deposition time of 7 minutes. After deposition was completed, the chamber temperature was 72 °C. The sample was annealed for 1 hour at 400 °C under nitrogen environment using a Fisher Scientific furnace. Then, the sample was etched using 30% HCl in water solution for 2 minutes.

As can be seen in Figure 5. 9 the GePb sample behaved differently than the Ge reference. The Ge peak was ~ 300 cm^{-1} while for GePb sample the peak shifted to the left at 297.14 cm^{-1}. The left shoulder in the range of 275 cm^{-1} and Ge-Pb peak from 215 to 268 cm^{-1} refers to incorporation of GePb at lower wavelength. The intensity was normalized in all Raman graphs.

5.3.1.1 Annealing Temperature Study

GePb samples were annealed at different annealing temperatures to study the effect of thermal annealing on the crystallinity of the $Ge_{1-x}Pb_x$. The samples were annealed from 300 °C to 600 °C for 1 hour then characterized using Raman scattering spectroscopy.

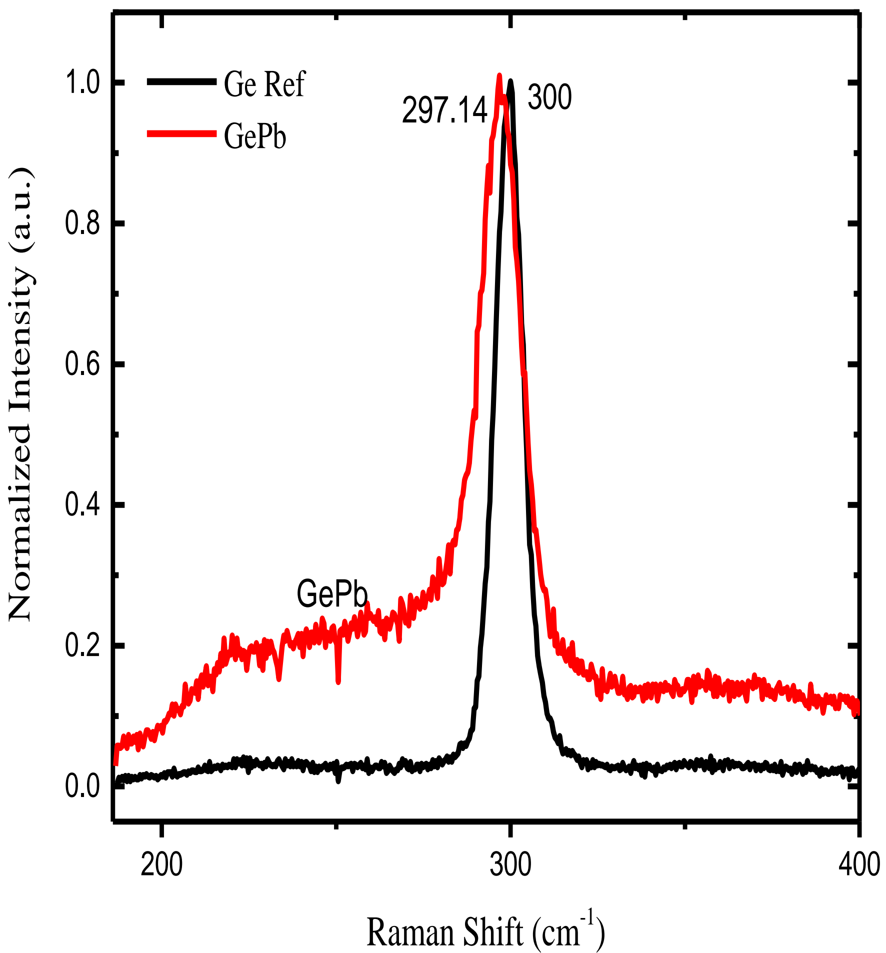

Figure 5.9 Comparison of the Raman spectroscopy of the Ge reference and the GePb sample annealed for 1 hour at 400 °C under N_2 environment on a Si substrate.

Figure 5.10 shows Raman spectra for the GePb samples on Si substrate. These samples were produced at the same conditions, except that each of them was annealed at a different temperature for 1 hour. Then, they were characterized by Raman spectroscopy. For 300 °C, there was almost no shifting at all, only the peak was a little wider. However, the graph shows shifting in the Ge peak at other samples. When comparing samples, the sample that was annealed at 400 °C showed more shifting than other samples at other annealing temperatures. This implies that annealing at 400 °C creates more incorporation. At lower temperatures such as 300 °C there was not sufficient incorporation between Ge and Pb as seen from the absence of any shift.

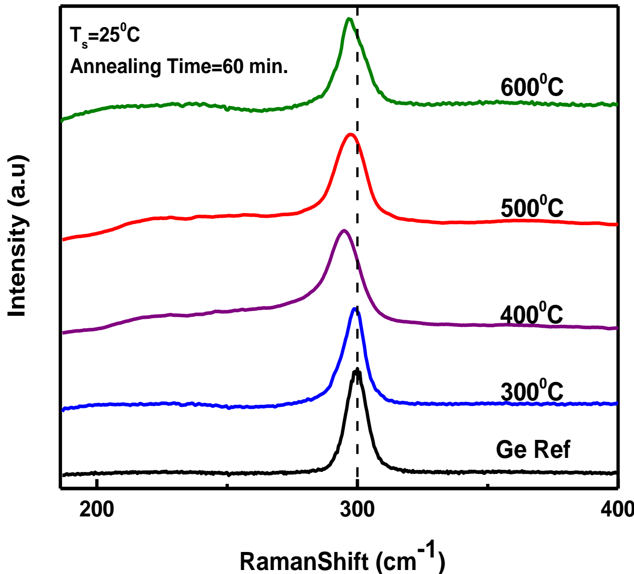

Figure 5.10. Raman spectroscopy of Ge reference and GePb on Si substrate at different annealing temperature (300-600 °C) for 1 hour under N_2 environment.

5.3.1.2 Annealing Time Study

For further investigation, GePb samples were annealed at different times for each annealing temperature to study the effect of the annealing time on the crystallinity of Ge_{1-x}-Pb_x. This was done by annealing each sample from 300 °C up to 600 °C at different times 15,30, or 60 minutes.

Figure 5.11 shows the Raman spectra for four Ge-Pb samples. Those GePb samples were grown on Si substrate at room temperature and annealed at 300°C for different annealing time 15, 30, or 60 minutes. At this temperature for those altered times, there was not any good shifting; all peaks were very similar to each other. This means, at 300 °C, there was not sufficieant growth and Pb did not incorporate in Ge.

Figure 5.12 shows the Raman spectra for four GePb samples. Those samples were all processed under the same condition, except that each of them was annealed for a different time.

However, unlike the 300 °C annealed temperature, growth on Si substrate for 400 °C at different times 15, 30, or 60 minutes showed very good shifting.

After characterization was done by Raman spectroscopy, the result showed shifting for both 30 and 60 minutes annealing time while the shifting did not exist at 15 minutes. Although at 60 minutes there was shifting, yet it was less than the shifting obtained at 30 minutes. This indicates that there was more incorporation of Pb in Ge.

Figure 5.13 shows Raman spectra of four GePb samples annealed at 500 °C for different annealing times (15-60 minutes). The growth process for those sample is very similar to the previous two except the annealing temperature was changed to 500°C. The result was similar to those in Figure 5.12; no shifting appeared, but these samples had more noise and the peaks in samples annealed at 300 °C for a different time were sharper and much smoother. This means at higher temperature 500 °C there was no growth and Pb did not show incorporation in Ge. This could be due to Pb segregation at temperature 500 °C.

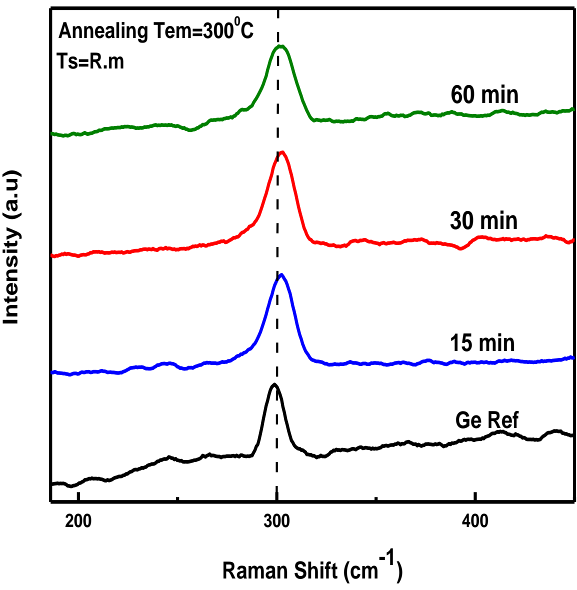

Figure 5.11. Raman spectroscopy of the Ge reference and GePb annealed at 300 °C for 15-30-60 min under N_2 environment on a Si substrate.

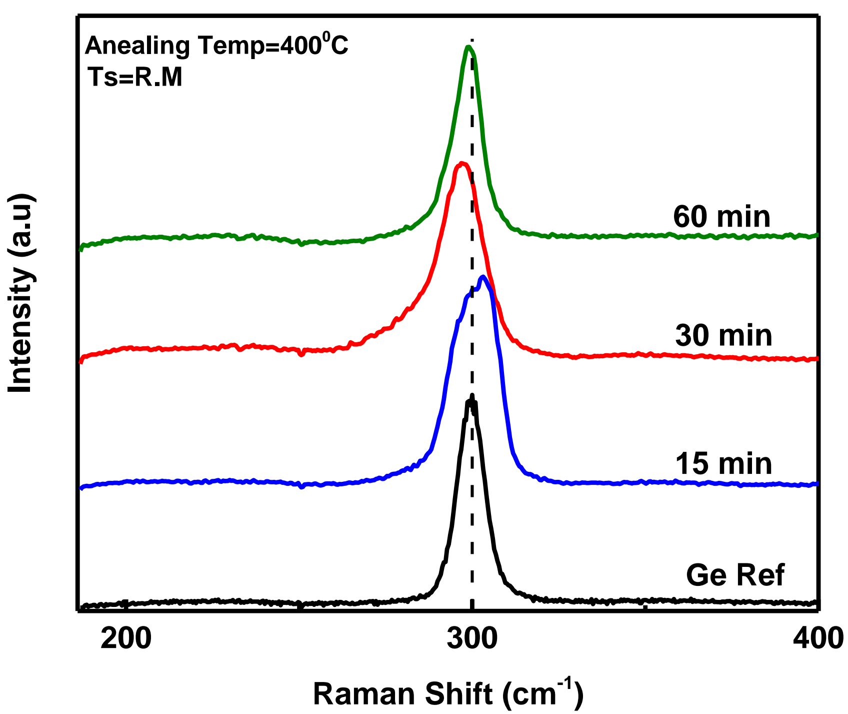

Figure 5.12. Raman spectroscopy of the Ge reference and GePb annealed at 400 °C for 15-30-60 min under N_2 environment on a Si substrate.

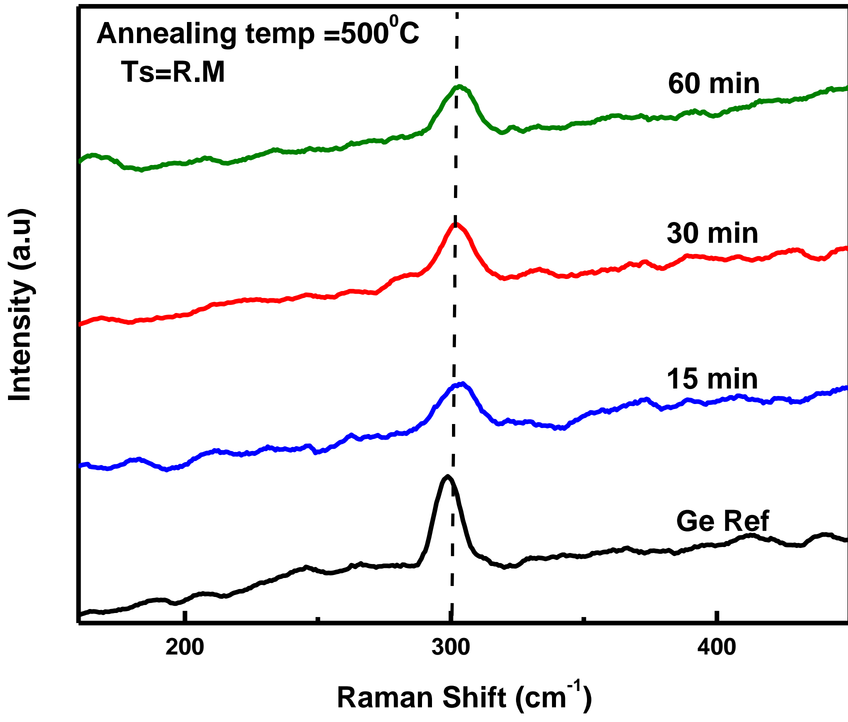

Figure 5.13. Raman spectroscopy of the Ge reference and GePb annealed at 500 °C for 15-30-60 min under N_2 environment on a Si substrate.

For GePb annealed at 600 °C, the annealing time was varied (15, 30, 60 minutes) as illustrated in Figure 5.14. The results are similar to the samples annealed at 300 °C and 500 °C for the same times. There was almost no shifting, but the peaks for 600 °C annealing were sharper and smoother than for those annealed at 300 °C and 500 °C. Also, this could be due to Pb segregation at temperature ≥ 500 °C**.** Overall, Raman Spectroscopy indicated that annealing at 400 °C for 30 minutes was the ideal annealing temperature and time for growth condition of GePb.

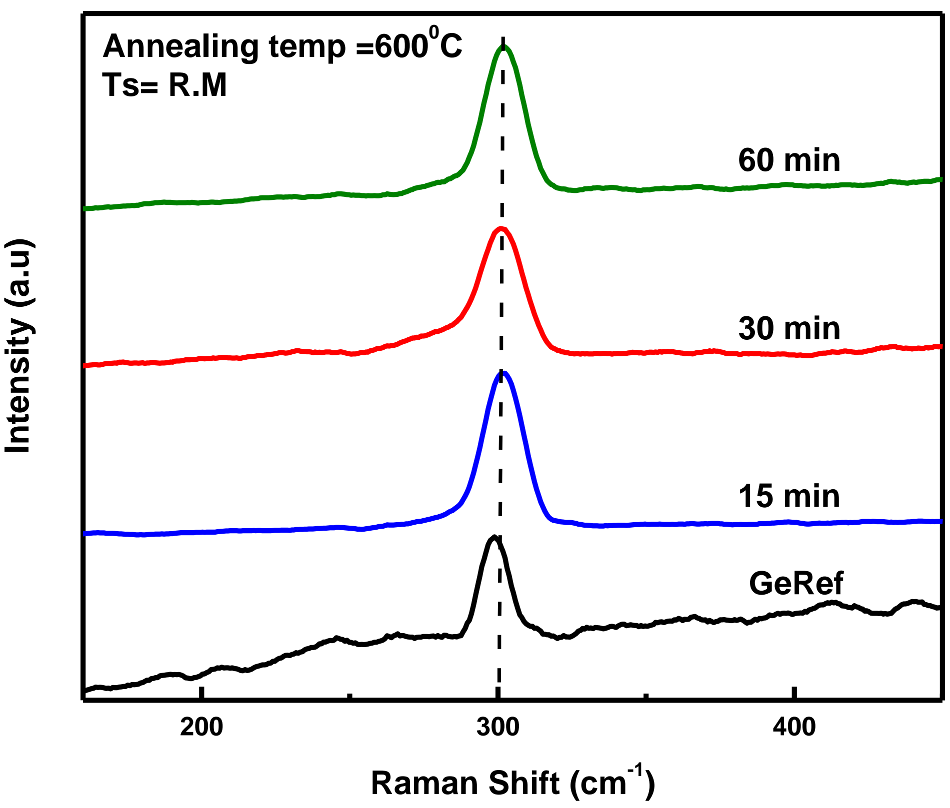

Figure 5.14 Raman spectroscopy of the Ge reference and GePb annealed at 600 °C for 15-30-60 min under N_2 environment on a Si substrate.

5.3.2 GePb Photoluminescence Spectra Result

After Raman measurements the same samples at the same growth, annealing, and etching

condition were taken to the photoluminescence spectra to see the optical properties of the samples and ensure the results of the Raman spectroscope.

From Figure 5.15, the band gap energy of GePb sample on silicon substrate was E = 0.5428 eV (equal to 2284nm) while the band gap energy for the same sample on glass substrate was E= 0.5659 eV (equal to 2191nm). The band gap energy of the Ge reference was almost 0.79 eV, which was much bigger than the band gap energy of the GePb samples on silicon and glass substrate at 400 °C. PL measurements show that the films produced had good optical properties.

Figure 5.15 shows that annealing at 400 ºC for 30 and 60 minutes gave a wider range of wavelengths and a smaller band gap energy, which means a smaller band gap than other samples which used different annealing temperatures.

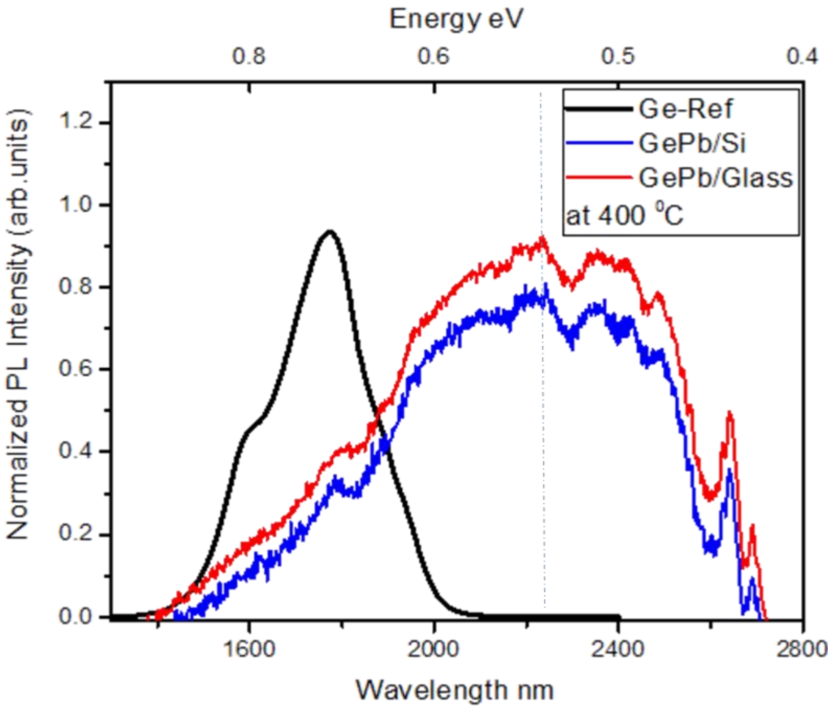

Figure 5.15. Photoluminescence spectra for Ge reference, GePb film on Si substrate, and GePb film on Glass substrate.

Figures 5.16, and 5.17 confirm the Raman measurements in that the PL measurements for 400 ºC annealing at 30 and 60 minutes on silicon substrate showed a wider peak and less bandgap energy than a 15 minutes annealing time. The band gap energy of GePb annealed for 60 minutes was E = 0.5472 eV (equal to 2266nm). The bandgap energy for the sample annealed for 30 minutes was E = 0.5428 eV (equal to 2284nm), which showed that annealing for 30 minutes or 60 minutes at 400 ºC was the preferred to get direct bandgap Ge alloys.

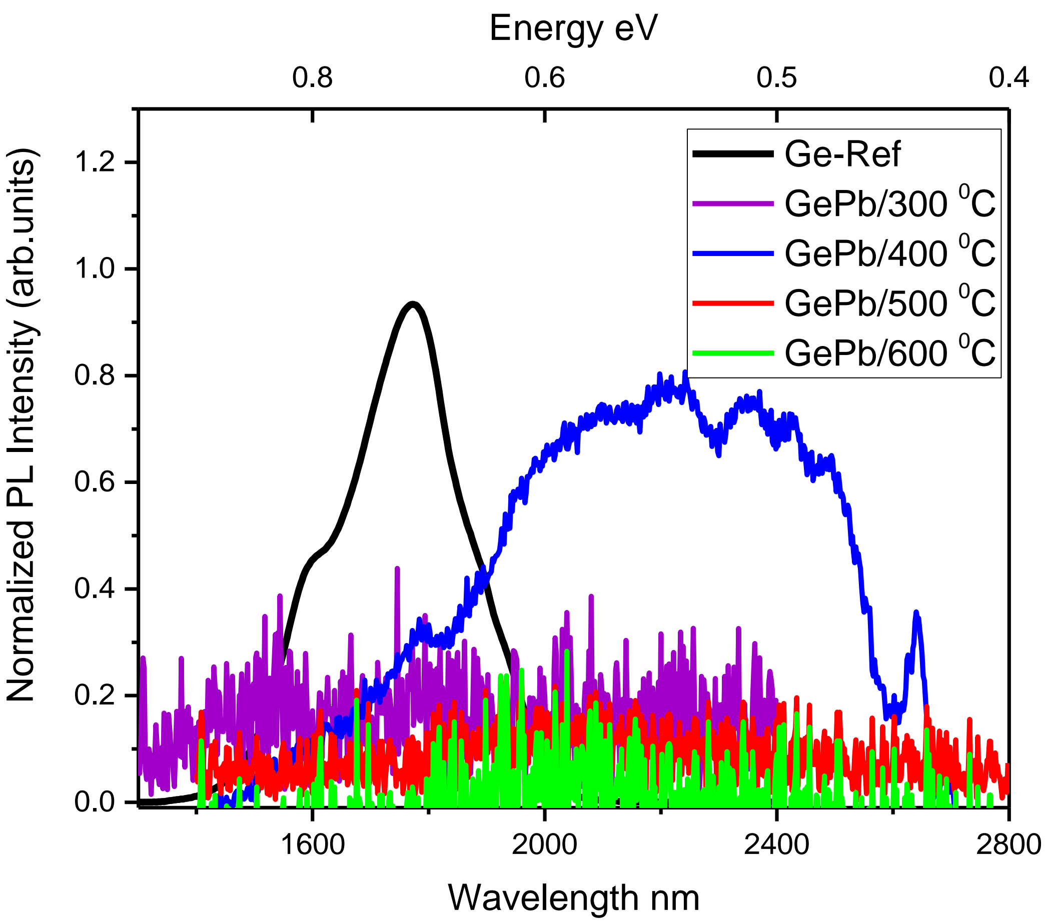

Figure 5.16. Photoluminescence spectra for GePb films on Si substrates at different annealing temperatures (300-600 ºC) for 1 hour under N_2 environment.

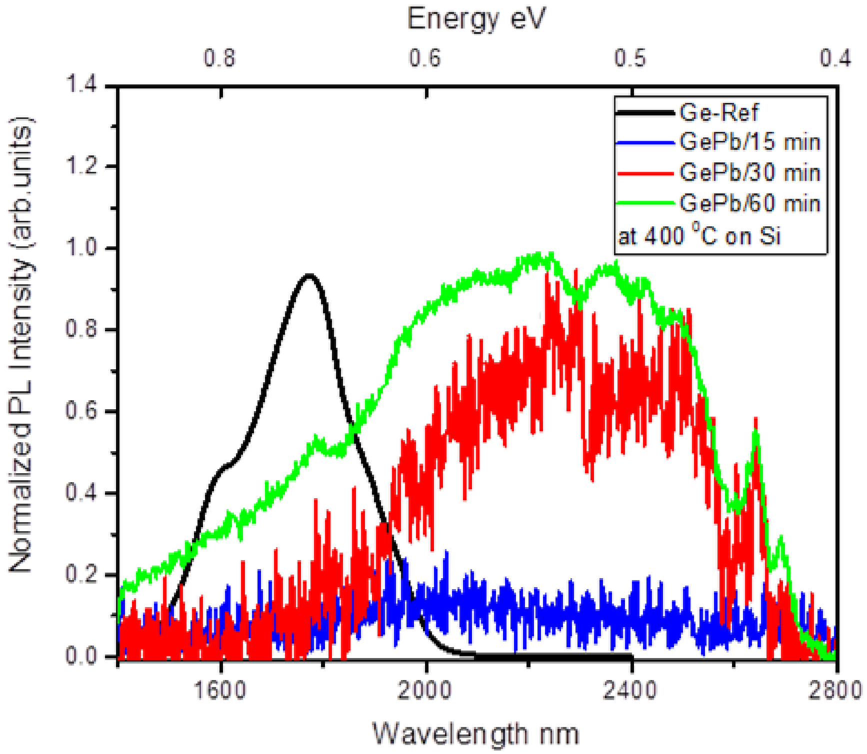

Figure 5.17. Photoluminescence spectra for GePb films on a Si substrate at 400 ºC for different annealing time (15-30-60 min) under vacuum environment.

5.3.3 X-Ray Diffraction (XRD) result

XRD measuerments shown in Figure 5.18 and Figure 5.19 were taken for two samples one on a silicon substate and the other on a glass substrate. Both were deposited at room temperatue in a high vcuum enviernment by a thermal evaporator. Those samples have thickness of 100 nm of Ge, and the same amount of Pb. They were annealed at 400 ºC for 1 hour under nitrogen environment. Even though the GePb un-annealed sample gave more shifting to the left, it had less quality indicated by the lower intensity of the peak. The XRD measurements in Figure 5.19 were taken for GePb on glass substrate with 400 ºC annealing temperature. However, GePb on Si substrate showed higher peak intensity at the same peak position, 2theta omega = 65.2^{o} and a higher XRD intensity implied a better quality GePb film.

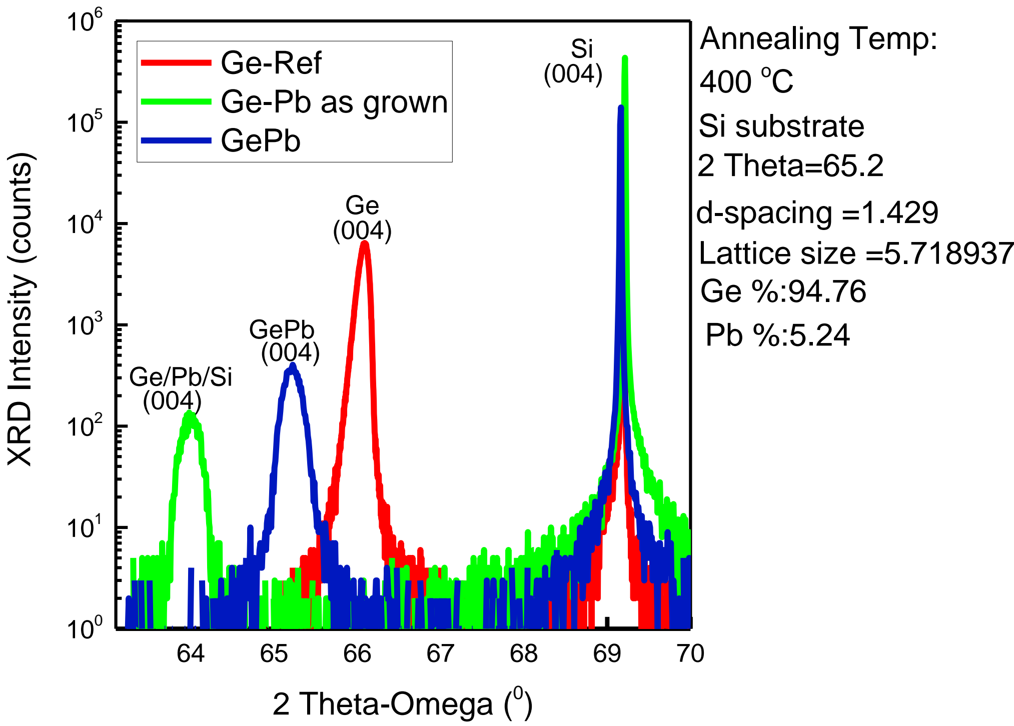

Figure 5.18. XRD patterns for GePb/Si annealed at 400 ºC for 1 hour under N_2 environment.

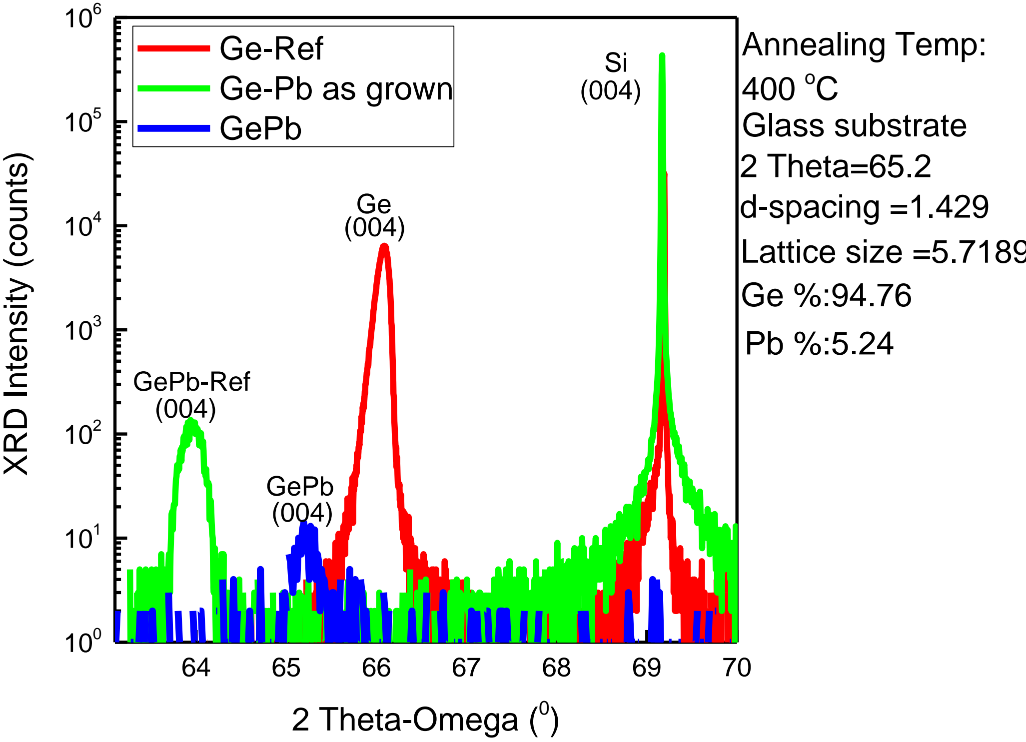

Figure 5.19. XRD patterns for GePb on a glass substrate annealed at 400ºC for 1 hour under N_2 environment.

5.3.4 X-Ray Powder Diffraction (XRD) Result

In order to investigate how much Ge was in different orientation peaks, a wide scan of GePb XRD was carried out as shown in Figure 5.20. XRD powder diffraction pattern for both Ge and Pb were taken from the XRD powder data base and plotted in Figure 5.21 a and b. In a randomly oriented Ge or GePb polycrystalline film, the (004) peak is expected to be only about 7% of the (111) peak, whereas, in the GePb film of this research, the ratio was formed to be 133% . This resulted in a 94% preferential growth of (004) orientation from this film. In other words, epitaxial growth was obtained.

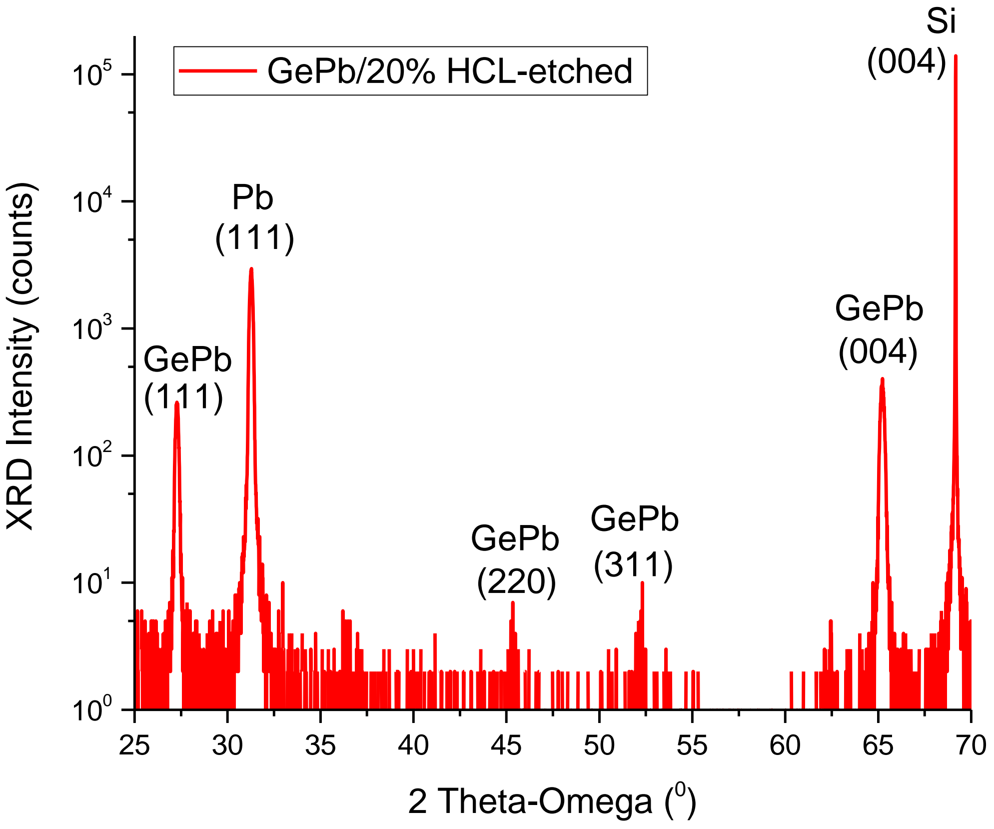

Figure 5.20. Wide scan of XRD patterns of GePb/Si annealed at 400ºC for 1 hour under N_2 environment.

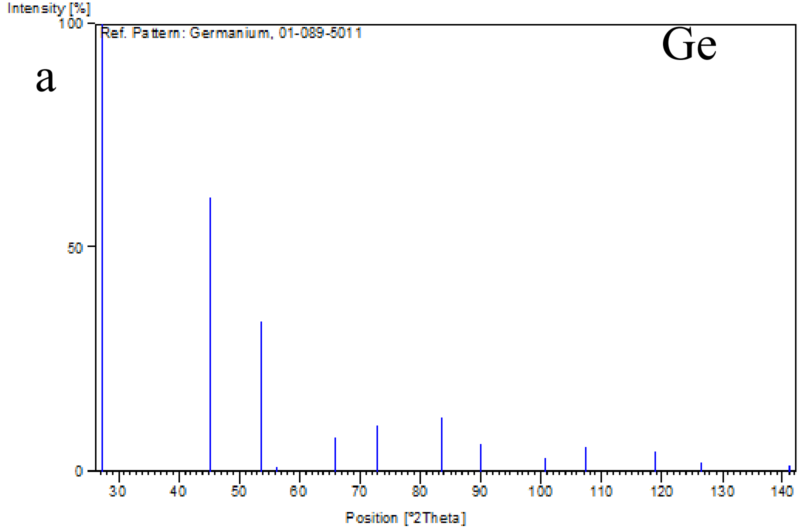

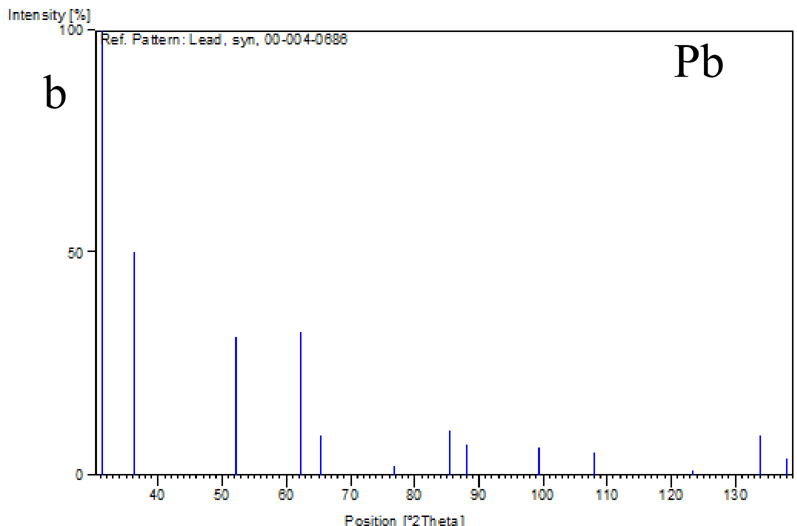

Figure 5.21. XRD powder data base for (a) Ge and (b) Pb.

5.3.5 GePb SEM Results

SEM images were taken for Ge/Pb/Si samples (un-annealed and un-etched) as shown in Figure 5.22, and then images were taken after annealing and etching at different annealing time

15, 30, or 60 mins as shown in Figures 22- 26. Those samples were deposited at room temperature under nitrogen environment, and then annealed at 400 ºC.

Figure 5.22 shows a SEM image of a Ge-Pb-Si sample before annealing and etching. From the contras difference and the existence of small patches of grey in a higher magnification field, it appears that some interaction had already taken place between Pb and Ge before annealing. The overall surface looked very smooth except for some protrusions that may have arisen from the sputtering of Pb during evaporation.

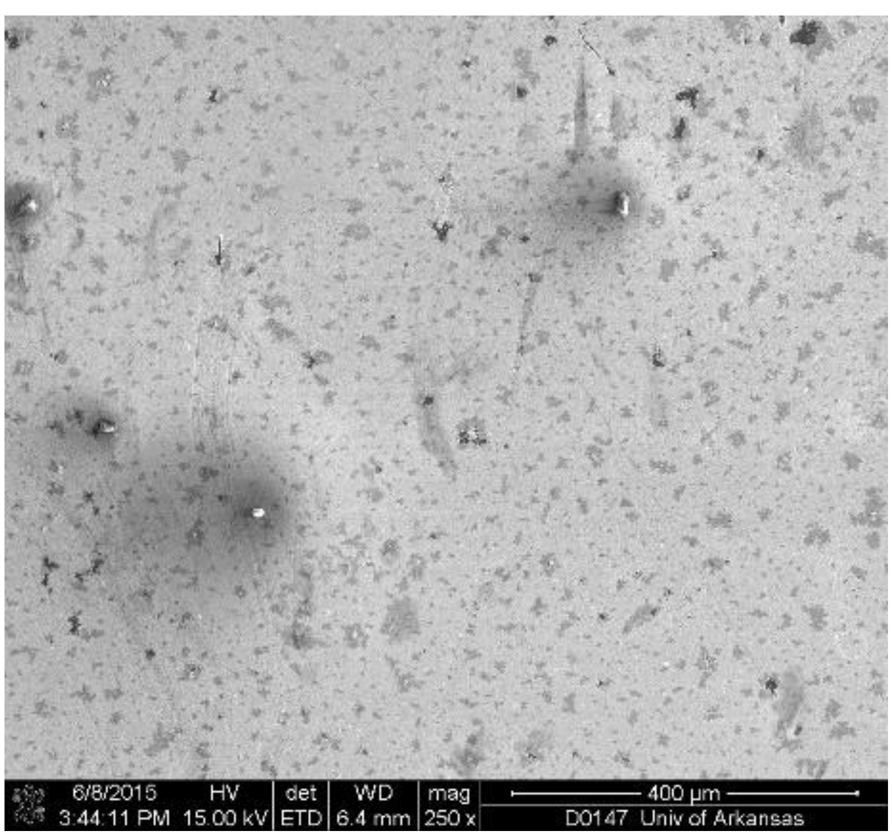

Figure 5.22. SEM images of Ge-Pb-Si (as grown sample) before annealing and etching process.

Figure 5.23 shows SEM images at 300x and 5000x of a GePb film which was deposited on Si substrate at room temperature then annealed for 15 minutes at 400 ºC. It may be noted that Pb was etched away from the sample before SEM were taken. Figure 5.23 (a) shows the surface

of the GePb sample with 350x magnification. The surface of the sample still had some of the Pb protrusion, which could have been because of some Pb drops that did not go away after etching the sample, but the surface was not very rough. Figure 5.23 (b) was taken at a higher magnification of 5000x and shows microstructures of dimension 2-10 μm. This may have been due to insufficient annealing time to make the grains much bigger.

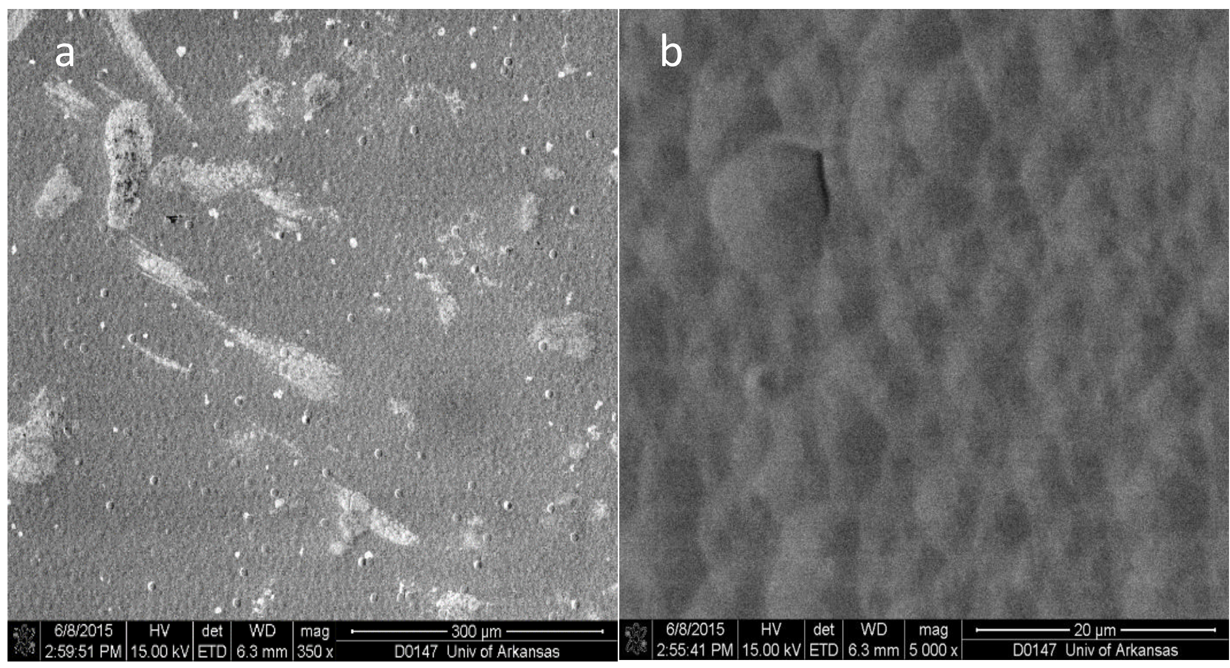

Figure 5.23. SEM pictures of GePb annealed at 400 ºC for 15 min.

Figure 5.24 (a) and (b) shows SEM images of GePb on Si substrate that was annealed for 30 minutes at 400 ºC under N_2 environment. The result of SEM shows that the sample had big grains. Image (b) is for the same sample but with higher magnification of 5000x and shows the size of one of the grains to be 42 μm. This means that annealing GePb sample for 30 minutes at 400 ºC resulted in a polycrystalline GePb material with huge grain sizes.

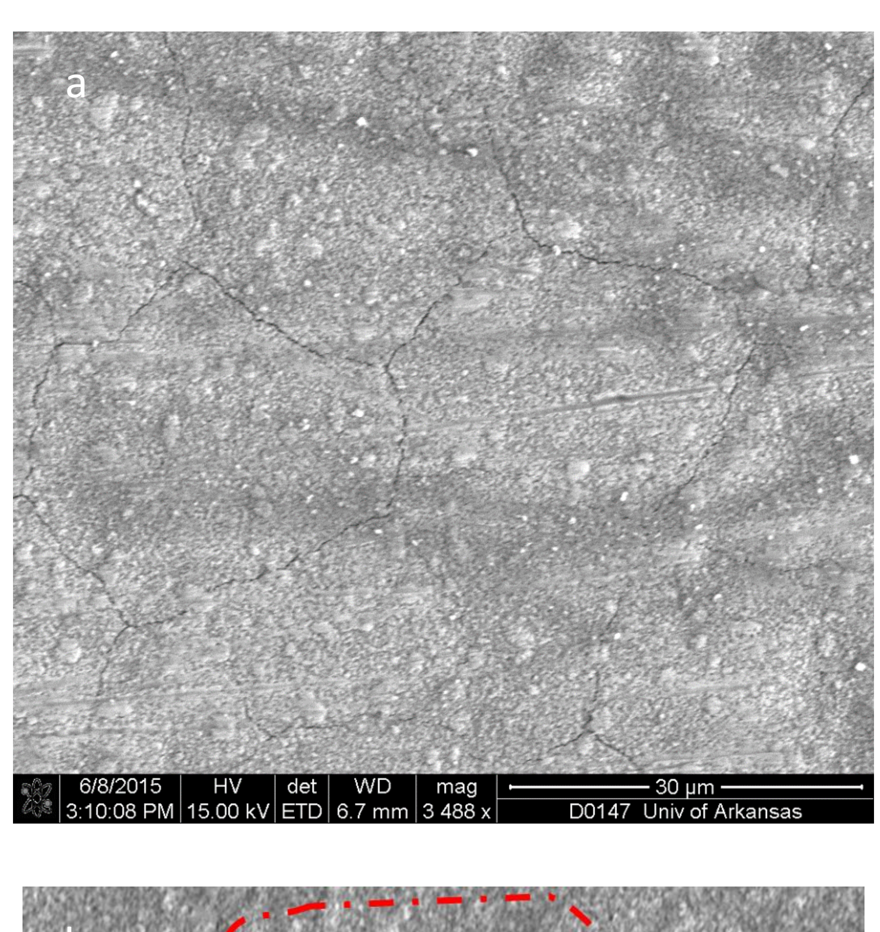

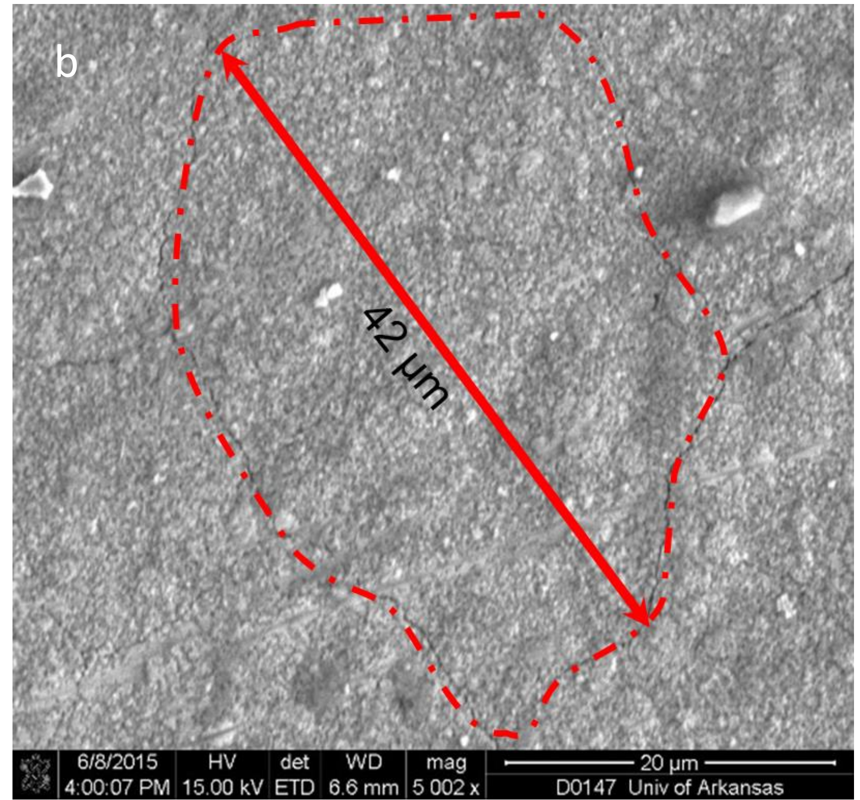

Figure 5.24. SEM images of GePb annealed at 400 ºC for 30min.

Figure 5.25 (a) and (b) shows SEM images of GePb annealed for 60 minutes at 400 ºC on Si substrate. The SEM results show that the sample had small grains and a smooth surface. Image (a) shows a smooth surface and magnification of 5000x while image (b) is taken with higher magnification of 50,000x. Figure 5.25(b) shows a pitted surface which may have been caused by Pb segregation during subsequent etching. The size of the grains was very small compared to the grains of GePb sample annealed for 30 minutes. Both samples were grown at the same condition with the same layer thickness of 100 nm for each layer of Ge and Pb. This means annealing GePb sample for 30 minutes and 60 minutes at 400 ºC resulted in a polycrystalline GePb material, but the grain size of the sample annealed for 30 minutes was bigger than the grain size of the sample annealed for 60 minutes. Therefore, 30 minutes annealing seemed to be the most suited time, and 400 ºC is the preferred annealing temperature for GePb.

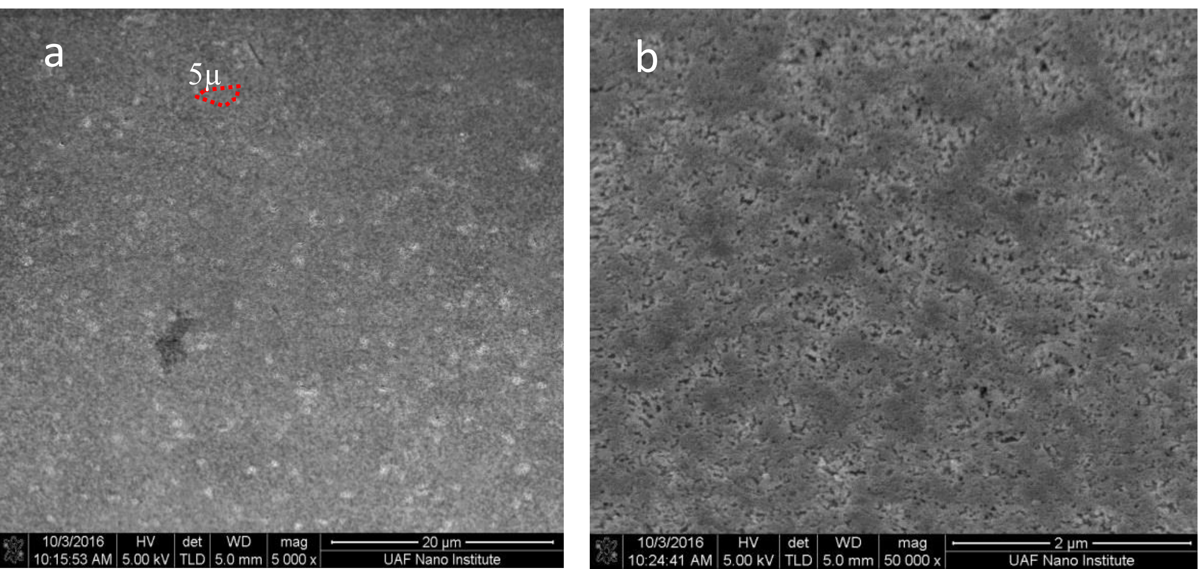

Figure 5.25. SEM images of GePb annealed at 400 ºC for 60min.

Energy Dispersive X-ray (EDX) images and mapping were taken for the GePb sample annealed for 1 hour at 400 ºC in order to determine the type of materials in the GePb films

surface and how Ge and Pb were distributied in the surface. Ge and Pb was equally distributed in the film and the film was homogeneous as Figure 5.26 shows.

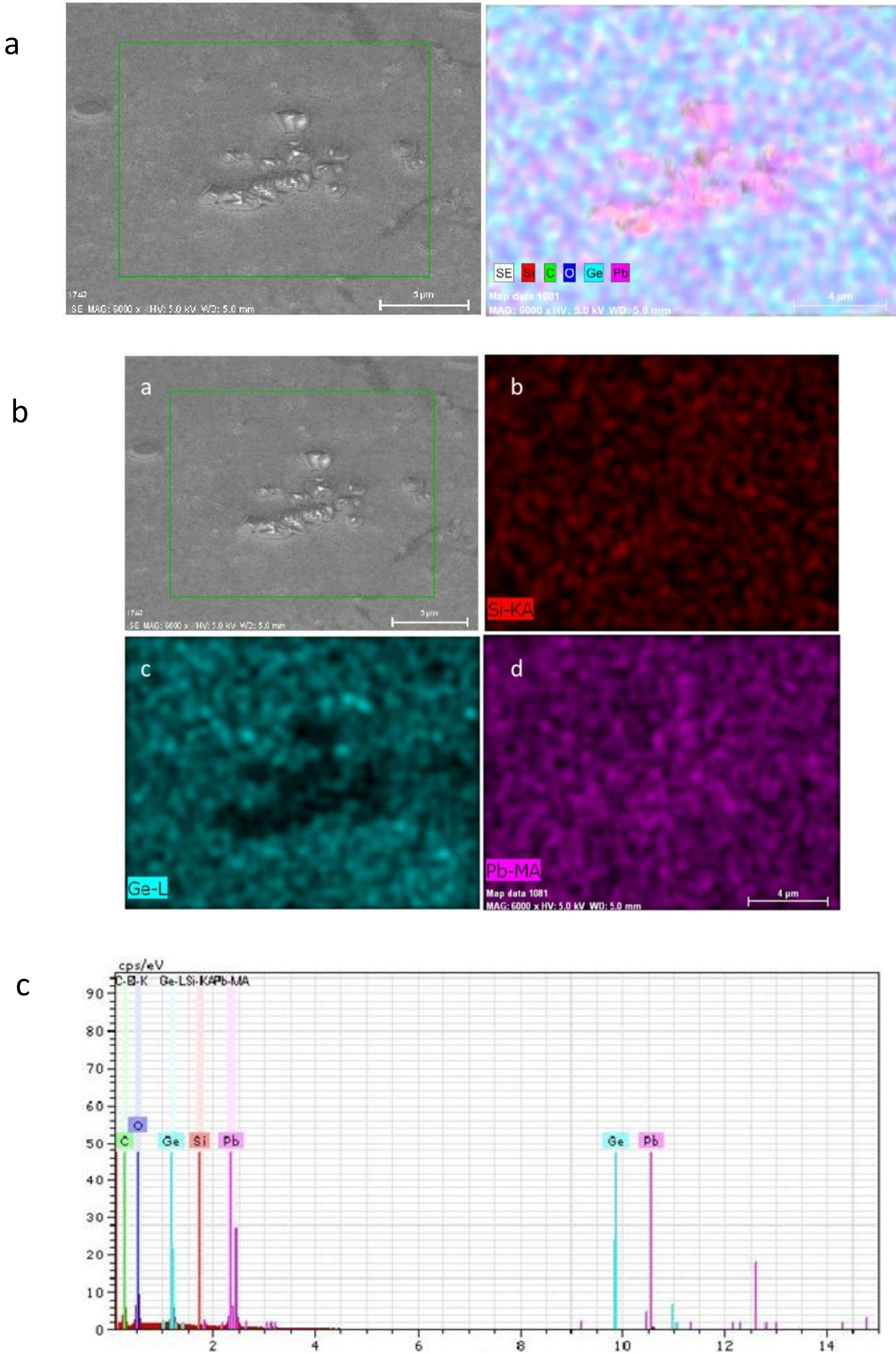

Figure 5.26. (a) and (b) are EDX images for GePb/Si annealed at 400C for 60 min, (c) GePb mapping.

In order to confirm that the GePb alloy films had layer inversion (layer exchange), a cross sectional image was taken for a GePb sample. As Figure 5.27 shows most of the Pb which was deposited first moved up above the GePb film in the EDX image; only a small amount of Pb remained underneath the Ge which was the second layer deposited. This indicated that layer inversion has been sucsseful obtained.

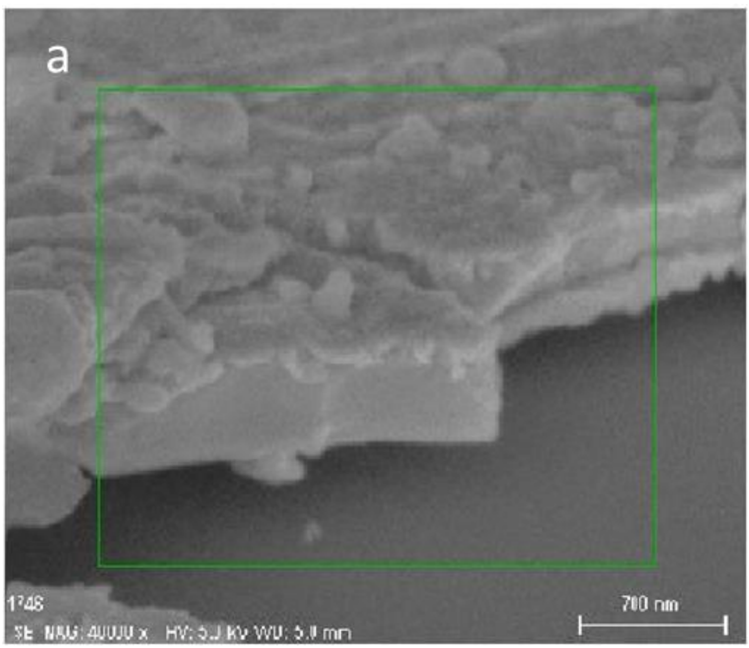

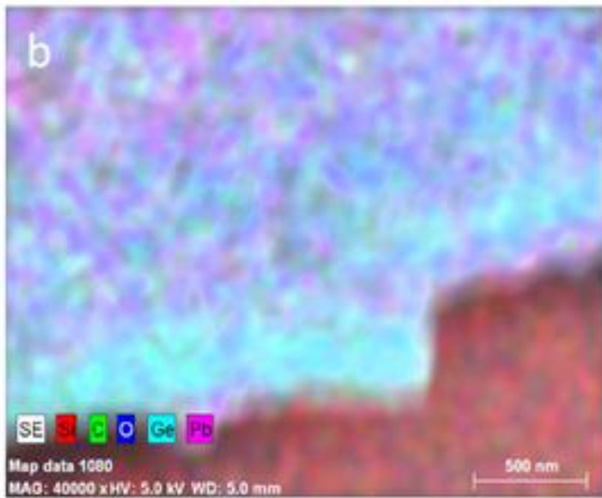

Figure 5.27. SEM images of GePb shows layer inversion.

SEM was used to measure the thickness of epitaxial layers grown for GePb annealed for 400 ºC for 1 hour as shown in Fgure 5.28 The thickness monitor was previosly calibrated, therefore, the average layer thickness obtained, around 600nm, was more than the predicted average layer thicknes which was 200 nm. However, 600 nm thickness was far beyond the critical thickness which meant that the GePb film was relaxed.

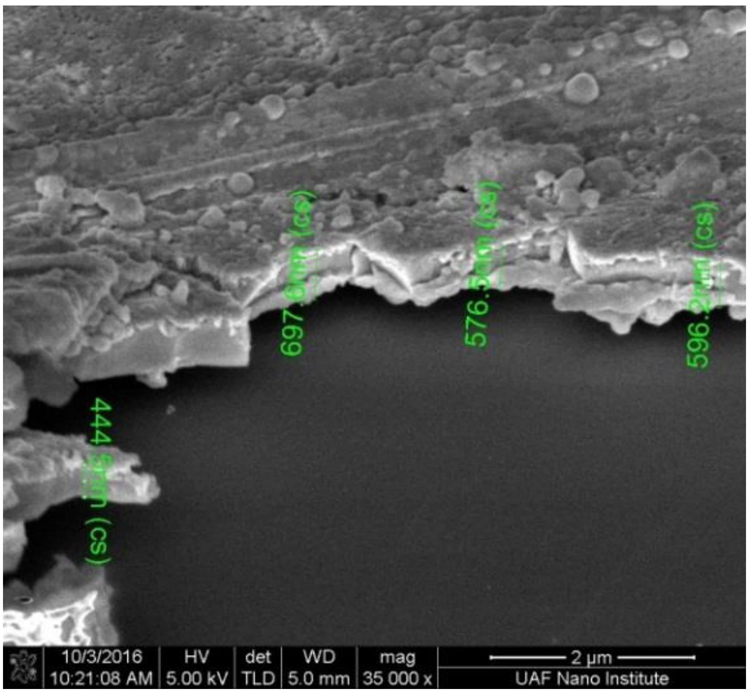

Figure 5.28. SEM images of GePb annealed at 400 ºC for 60 min with layer thickness.

Chapter 6: Conclusion

In this research, GePb and GeSn deposition using layer inversion method was studied. A systematic study on the effect of different substrates, annealing time, and temperature was done in order to maximize the crystallization of the GePb and GeSn alloys. A thermal evaporator was employed for the deposition of the layers at room temperature. The samples were annealed at 300-600 °C for 15-60 minutes. The results showed that annealing the layers resulted in inversion of the layers and the Ge layer crystallized on the Si substrate with up to 94% in the same orientation as the substrate. The incorporation of Sn and Pb in the Ge lattice occurs as the upper layer Ge diffuses through the lower layer metal and deposits on the clean Si substrate while incorporating some metal. Studying the annealing temperatures showed that increasing the temperature resulted in higher incorporation and higher material quality. However, increasing the temperature above 400 °C resulted in lower material quality and more precipitation of Pb and Sn from Ge lattice.

Material characterization of the samples using XRD showed up to 5% Pb and 14 % Sn incorporation in the Ge lattice. The SEM and EDX scanning maps showed that the layer inversion had fully happened and the Ge(Pb/Sn) was directly deposited on Si substrate. The optical characterization of the samples showed that as a result of Sn/Pb incorporation the bandgap of Ge was shrunk from indirect 0.67 eV to 0.54 eV. The shift in the Raman peak position to lower wavenumbers verified the incorporation of Pb/Sn in Ge.

References

[1] Miller, D. A. "Physical reasons for optical interconnection," Int. J. Optoelectron., vol. 11, pp. 155-168, 1997. [Accessed: 07-Nov-2016].

[2] “50 Years of Moore's Law,” Intel. Available: http://www.intel.com/content/www/us/en/silicon-innovations/moores-law-technology.html. [Accessed: 07-Nov-2016].

[3] Feldman, M. R., Esener, S. C., Guest, C. C., and Lee, S. H. "Comparison between optical and electrical interconnects based on power and speed considerations." *applied optics*27.9 (1988): 1742-1751. [Accessed: 07-Nov-2016].

[4] Miller, D. A. “Energy consumption in optical modulators for interconnects”. *Optics express*, 20(102), A293-A308. 2012. [Accessed: 07-Nov-2016].

[5] Lin, Hai. Growth and Characterization of GeSn and SiGeSn *Alloys for Optical Interconnects*. Diss. STANFORD UNIVERSITY, 2012. [Accessed: 09-Nov-2016].

[6] Huang, W., Cheng, B., Xue, C., and Li, C. "Comparative studies of clustering effect, electronic and optical properties for GePb and GeSn alloys with low Pb and Sn concentration." *Physica B: Condensed Matter* 443: 43-48, 2014. [Accessed: 26-Septmber-2016].

[7] S. M. Naidu, “2.3 The Basis and Crystal Structure,” *Safari*. Available: https://www.safaribooksonline.com/library/view/engineering-physics/9788131775073/xhtml/ch2-sub2.3.xhtml. [Accessed: 27-Septmber-2016].

[8] P. Moontragoon, R. Soref and Z. Ikonic, "The direct and indirect bandgaps of unstrained SixGe1− x− ySny and their photonic device applications," *J. Appl. Phys.,* vol. 112, pp. 073106, 2012. [Accessed: 01-Nov-2016].

[9] H. Baker and H. Okamoto, "ASM handbook," *Alloy Phase Diagrams,* vol. 3, pp. 965, 1992. [Accessed: 09-Dec-2016].

[10] Calculated Ge-Pb phase diagram,” *Calculated Ge-Sn phase diagram*. Available: http://resource.npl.co.uk/mtdata/phdiagrams/gesn.htm. [Accessed: 01-Nov-2016].

[11] Kung, P., et al. "Crystallography of epitaxial growth of wurtzite-type thin films on sapphire substrates." *Journal of applied physics* 75.9 (1994): 4515-4519. [Accessed: 09-Dec-2016].

[12] Herman, Marian A., Wolfgang Richter, and Helmut Sitter. *Epitaxy: physical principles and technical implementation*. Vol. 62. Springer Science & Business Media, 2013.PP 23-28 [Accessed: 09-Dec-2016].

[13] Ulrich, R. K., & Brown, W. D. (Eds.). (2006). *Advanced electronic packaging*. Hoboken, NJ: Wiley. pp 77-89

[14] Tsunekawa, S., Homma, Y., Morisaki, H., Okudaira, S., and Mukai, K."*Thin film deposition*." U.S. Patent No. 4,599,135. 8 Jul. 1986. [Accessed: 29-Sep-2016].

[15] Wasa, Kiyotaka, and Shigeru Hayakawa. *Handbook of sputter deposition technology*. (1992). Available: http://www.ajaint.com/what-is-sputtering.html.[Accessed: 29-Sep-2016].

[16] Mattox, Donald M. *Handbook of physical vapor deposition (PVD) processing*. William Andrew, 2010.pp 1-6.[Accessed: 04-Dec-2016].

[17] Thermal Evaporation. *Oxford Vacuum Science*, Ltd, Barton Oxfordshire, UK. Available: http://www.oxford-vacuum.com/technology/deposition/deposition.htm .[Accessed: 04-Oct-2016].

[18] Wright Center for Photovoltaics Innovation and Commercialization," *Material Deposition*. Available: http://www.utoledo.edu/research/pvic/material_deposition.html. [Accessed: 01-Dec-2016].

[19] Lin, Yuan. *Advanced Nano Deposition Methods*. John Wiley and Sons, 2016.pp33-35

[20] Hardy, N. Thin Film Deposition By Thermal Evaporation: *Essential Basics.* Available: http://www.semicore.com/news/71-thin-film-deposition-thermal-evaporation. [Accessed: 02-Oct-2016].

[21] "Thermal Evaporation in Vacuum." *Icmm.csic*. Web. 09 Dec. 2016. Available: http://www.icmm.csic.es/fis/english/evaporacion_resistencia.html. [Accessed: 02-Sep-2016].

[22] "Evaporation Sources - *PhotonExport*. Available: http://photonexport.com/en/thin-film/evaporation-sources/. [Accessed: 02-Nov-2016].

[23] Shackelford, J. F., Han, Y. H., Kim, S., & Kwon, S. H.*CRC materials science and engineering handbook*. CRC press, 2016 pp 4.

[24] Shiraki, Yasuhiro, and Noritaka Usami, eds. *Silicon-germanium (SiGe) nanostructures: Production, properties and applications in electronics*. Elsevier, 2011.

[25] Tu, King-Ning, *Solder Joint TechnologyMaterials, Properties, and Reliabilit*. 2007.

[26] Technical data for Lead. Available: http://periodictable.com/Elements/082/data.html [Accessed: 02-Oct-2016].

[27] Olesinski, R. W., & Abbaschian, G. J. (1984). The Ge− Si (germanium-silicon) system. *Journal of Phase Equilibria*, 5(2), 180-183.

28] Huang, W., Cheng, B., Xue, C., & Li, C. Comparative studies of clustering effect, electronic and optical properties for GePb and GeSn alloys with low Pb and Sn concentration. Physica B: Condensed Matter, 443, 43-48, 2014.

[29] Zhou, Q., Chan, T. K., Lim, S. L., Zhan, C., Osipowicz, T., Gong, X., and Yeo, Y. C. (2014). Single Crystalline Germanium-Lead Alloy on Germanium Substrate Formed by Pulsed Laser Epitaxy. ECS Solid State Letters, 3(8), P91-P93.

[30] Zhou, Q., Zhan, C., Gong, X., Chan, T. K., Osipowicz, T., Lim, S. L.,and Yeo, Y. C. (2014, June). Germanium-lead alloy with 0.3% substitutional lead formed by pulsed laser induced epitaxy. In 2014 7th International Silicon-Germanium Technology and Device Meeting (ISTDM).

[31] Zhou, Q., Ong, E. B. L., Lim, S. L., Vajandar, S., Osipowicz, T., Gong, X., and Yeo, Y. C. Single Crystalline Germanium-Lead Formed by Laser-Induced Epitaxy. ECS Journal of Solid State Science and Technology, 5(6), P353-P360, 2016.

[32] Li, H., Brouillet, J., Salas, A., Wang, X., and Liu, J. Low temperature growth of high crystallinity GeSn on amorphous layers for advanced optoelectronics. Optical Materials Express, 3(9), 1385-1396, 2013.

[33] Lieten, R. R., Fleischmann, C., Peters, S., Santos, N. M., Amorim, L. M., Shimura, Y., and Locquet, J. P. Structural and Optical Properties of Amorphous and Crystalline GeSn Layers on Si. ECS Journal of Solid State Science and Technology, 3(12), P403-P408, 2014.

[34] Thermo Fisher Scientific Inc, Miami, OK, Available: http://www.thermofisher.com/us/en/home.html. [Accessed: 08-Dec-2016].

[35] Edwards Inc, Albany, NY, Available: https://www.edwardsvacuum.com/Industrial_Coating/. [Accessed: 08-Dec-2016].

[36] Le Ru, Eric C., Etchegoin, Pablo G. (Pablo Gabriel), and Inc Books24x7. *Principles of Surface-Enhanced Raman Spectroscopy: And Related Plasmonic Effects*, Elsevier, Amsterdam;Boston;, , pp.31, 2009;2008.

[37] Chalmers, John M. Edwards, Howell G. M.Hargreaves, Michael D. “Infrared and Raman Spectroscopy in Forensic Science (1)”. Hoboken, GB: Wiley, 2011, pp. 3-40, ProQuest ebrary. Web. 9 December 2016.

[38] S.A. Al Ghetmiri, Nano Science and Engineering Institute, University of Arkansas, "Raman spectroscope setup," private communication, 2014.

[39] Raman Spectroscopy - A Tutorial. (n.d.). Retrieved October 21, 2016, from http://www.kosi.com/na_en/products/raman-spectroscopy/raman-technical-resources/raman-tutorial.php

[40] Raman FAQs - What are the most common applications of Raman spectroscopy? - HORIBA. (n.d.). Retrieved October 21, 2016, from http://www.horiba.com/scientific/products/raman-

[41] Photoluminescence Spectroscopy and its Applications. (n.d.). Retrieved October 21, 2016, from http://archive.cnx.org/contents/81bb0311-98ee-4cfc-b3c8-0eab6aeace37@2/photoluminescence-spectroscopy-and-its-applications

[42] What is photoluminescence? (n.d.). Retrieved October 21, 2016, from http://www.photoluminescent-signs.com/en/jalite-marine/faq-frequently-asked-questions/admin.php

[43] Department of Physics. (n.d.). Retrieved October 21, 2016, from https://www2.warwick.ac.uk/fac/sci/physics/current/postgraduate/regs/mpags/ex5/techniques/optical/pl/

[44] Yamada, K., Jifeng Liu, J., Baba, T., Vivien, L., and Xu, D. (n.d.), “Photonic Integration and Photonics-Electronics Convergence on Silicon Platform,” *Front. Mater*, October 14, 2015. | http://dx.doi.org/10.3389/fmats.2015.00065. [Accessed: 14-Oct-2016].

[45] H. zur Loye, "X-Ray Diffraction, How it Works, What it Can And What it Cannot Tell us." Available: http://www.chem.sc.edu/faculty/zurloye/xrdtutorial_2013.pdf. [Accessed: October 22, 2016].

[46] Diffraction Basics - American Crystallographic Association. (n.d.), Available: http://www.amercrystalassn.org/documents/WK05LindDiffractionBasicsCrystEd.pdf. [Accessed: October 23, 2016].

[47] How does Scanning Electron Microscopy work? (n.d.). Avillable: http://www.nanoscience.com/technology/sem-technology. Retrieved October 23, 2016.

[48] Scanning Electron Microscope - Purdue University. (n.d.). https://www.purdue.edu/ehps/rem/rs/sem.htm. [Accessed: 23-Oct-2016].

[49] "Facilities - Virginia Tech. (n.d.)," Avillable: http://www.adsel.ece.vt.edu/facilities.html. [Accessed: October 23, 2016].

[50] X-ray Diffraction (XRD). (n.d.). www.msrt.ir/fa/shaa/Documents/WikiShaa/XRD. [Accessed: 09-Dec-2016].

Appendix A: Description of Research for Popular Publication

Faster electronic devices for bright future

By: Hakimah Alahmed

Electronic chips, such as chips in computers or phones, have been developed by researchers in order to get high performance devices with higher speed at the same time. At the University of Arkansas in Fayetteville, Dr. Hameed Naseem who is a professor in the electrical engineering department and his group aim to enhance the optical properties of silicon to benefit the technology of chips. One of Dr. Hameed Naseem's group member, Hakimah Alahmed, a graduate student in the Microelectronics and Photonics program, working in silicon compatible material growth, claims that growing germanium films that is able to emit light, is capable of making chips with optical interconnect base for faster data transfer applications.

Do light emitting materials really help enhance chip interconnects? Why should material used in the chip be compatible with silicon? Is it important for the interconnect material in the chips to be optical interconnect not electrical wires? In order to obtain devices that can track the recent rapid technology, light emitting materials are very important to replace electrical wire interconnect with optical ones and then can make LEDs and laser devices. Even though silicon is not a light emitting material, it is very important for every electronic circuit due to silicon physical and electrical properties. Nowadays, wire interconnect is facing Resistance-Capacitor (RC). Therefore, transistors size on the chip decrease, yet RC does not decrease at the same rate. To overcome this issue, optical interconnect is the ideal solution.

Growing germanium lead (GePb) or germanium tin (GeSn) in silicon wafer with specific composition of Pb in germanium or tin in germanium (10% tin and half this value for lead) is capable of making germanium direct bangap materials, which have high light emitting

efficiency. Using Ge alloys (GeSn /GePb) on silicon is cheaper and better technology than using gallium arsenide (GaAs) because it is not cost effective (high cost) and is not compatible with Si (thermal mismatching between Si and GaAs).

Appendix B: Executive Summary of Newly Created Intellectual Property

There is no new intellectual property matters in this research project.

Appendix C: Potential Patent and Commercialization Aspects of listed Intellectual Property Items

There is no promising patent and commercialization aspects of the intellectual

property items.

C.1 Patentability of Intellectual Property (Could Each Item be Patented)

No potential of patentability of intellectual property in this thesis.

C.2 Commercialization Prospects (Should Each Item Be Patented)

Not applicable.

C.3 Possible Prior Disclosure of IP

Not applicable.

Appendix D: Broader Impact of Research

D.1 Applicability of Research Methods to Other Problems

After characterizing Ge alloys, it was found that crystalline GePb with direct bandgap and high light emitting efficiency could be used as laser source support beside the alloy of GeSn. Also, these alloys have the potential to be implemented in fabrication of integrated circuits, light emitting diodes, solar cells and transistors.

D.2 Impact of Research Results on U.S. and Global Society

This research shows an opportunity to benefit the U.S and global society. One major objective of this project was to grow Ge alloys films that have direct bandgap and are capable of emitting light efficiently. This is in order to replace the electronic wire interconnect with the optical interconnect for high performance devices and faster data transfer. Having Ge alloys on a Si substrate to create Si base IC provides high quality optoelectronic material with low cost and easy fabrication process.

D.3 Impact of Research Results on the Environment

A thermal evaporator is a very cheap PVD system used to deposit GeSn and GePb on a silicon substrate. Metals used in this research have very low toxicity and are safe for the environment except Pb which is toxic and need to be in a safe packaging to protect the environment from its toxicity. Also the evaporation system used in this project does not have any bad impact on the environment. Obtaining GeSn and GePb with direct bandgap and high light emitting efficiency on Si helps electronic device performance and increases their efficiency which leads to low power consumption without harming the environment at all.

Appendix E: Microsoft Project for MS MicroEP Degree Plan

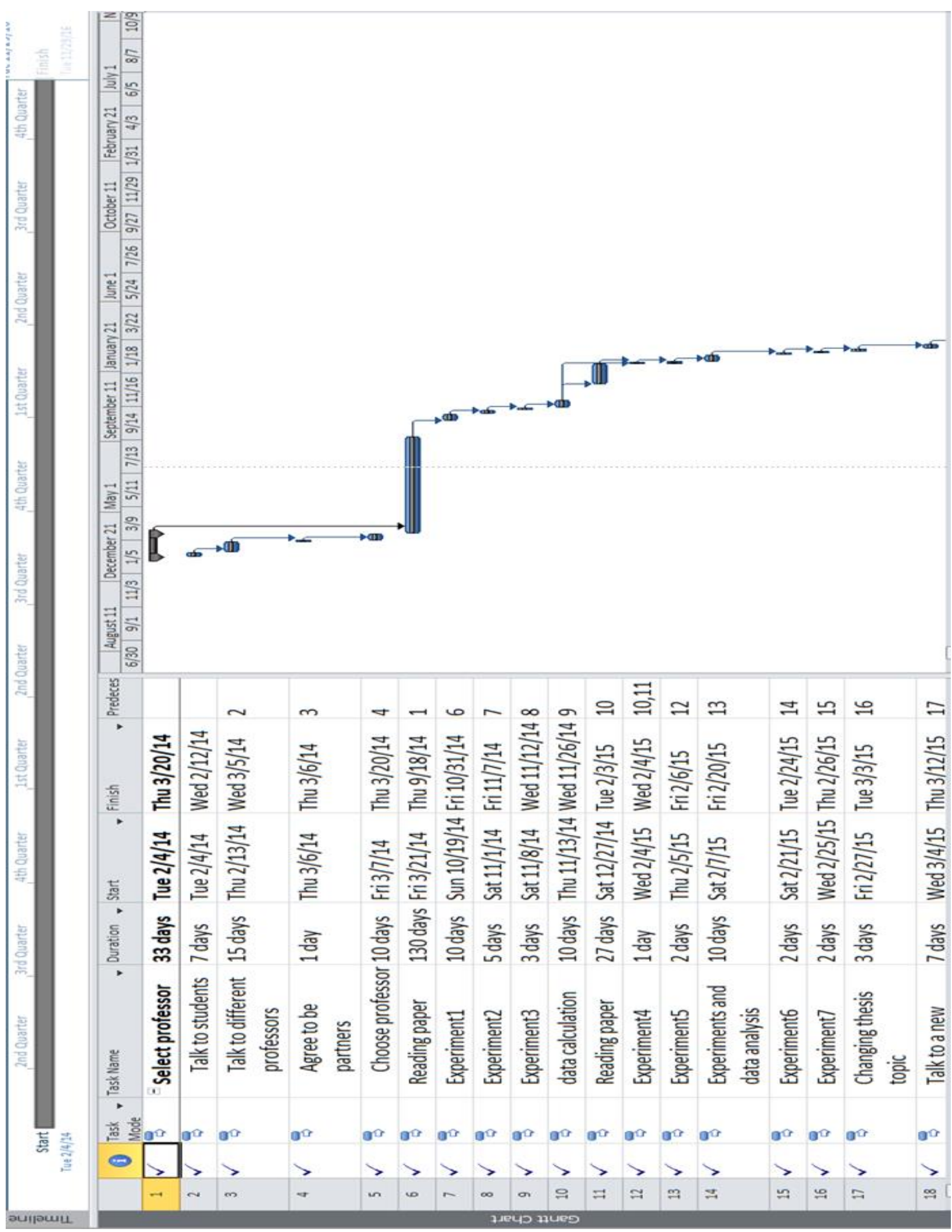

ID	Task Name	Duration	Start	Finish	Predecessors
1	Select professor	33 days	Tue 2/4/14	Thu 3/20/14	
2	Talk to students	7 days	Tue 2/4/14	Wed 2/12/14	
3	Talk to different professors	15 days	Thu 2/13/14	Wed 3/5/14	2
4	Agree to be partners	1 day	Thu 3/6/14	Thu 3/6/14	3
5	Choose professor	10 days	Fri 3/7/14	Thu 3/20/14	4
6	Reading paper	130 days	Fri 3/21/14	Thu 9/18/14	1
7	Experiment1	10 days	Sun 10/19/14	Fri 10/31/14	6
8	Experiment2	5 days	Sat 11/1/14	Fri 11/7/14	7
9	Experiment3	3 days	Sat 11/8/14	Wed 11/12/14	8
10	data calculation	10 days	Thu 11/13/14	Wed 11/26/14	9
11	Reading paper	27 days	Sat 12/27/14	Tue 2/3/15	10
12	Experiment4	1 day	Wed 2/4/15	Wed 2/4/15	10,11
13	Experiment5	2 days	Thu 2/5/15	Fri 2/6/15	12
14	Experiments and data analysis	10 days	Sat 2/7/15	Fri 2/20/15	13
15	Experiment6	2 days	Sat 2/21/15	Tue 2/24/15	14
16	Experiment7	2 days	Wed 2/25/15	Thu 2/26/15	15
17	Changing thesis topic	3 days	Fri 2/27/15	Tue 3/3/15	16
18	Talk to a new	7 days	Wed 3/4/15	Thu 3/12/15	17

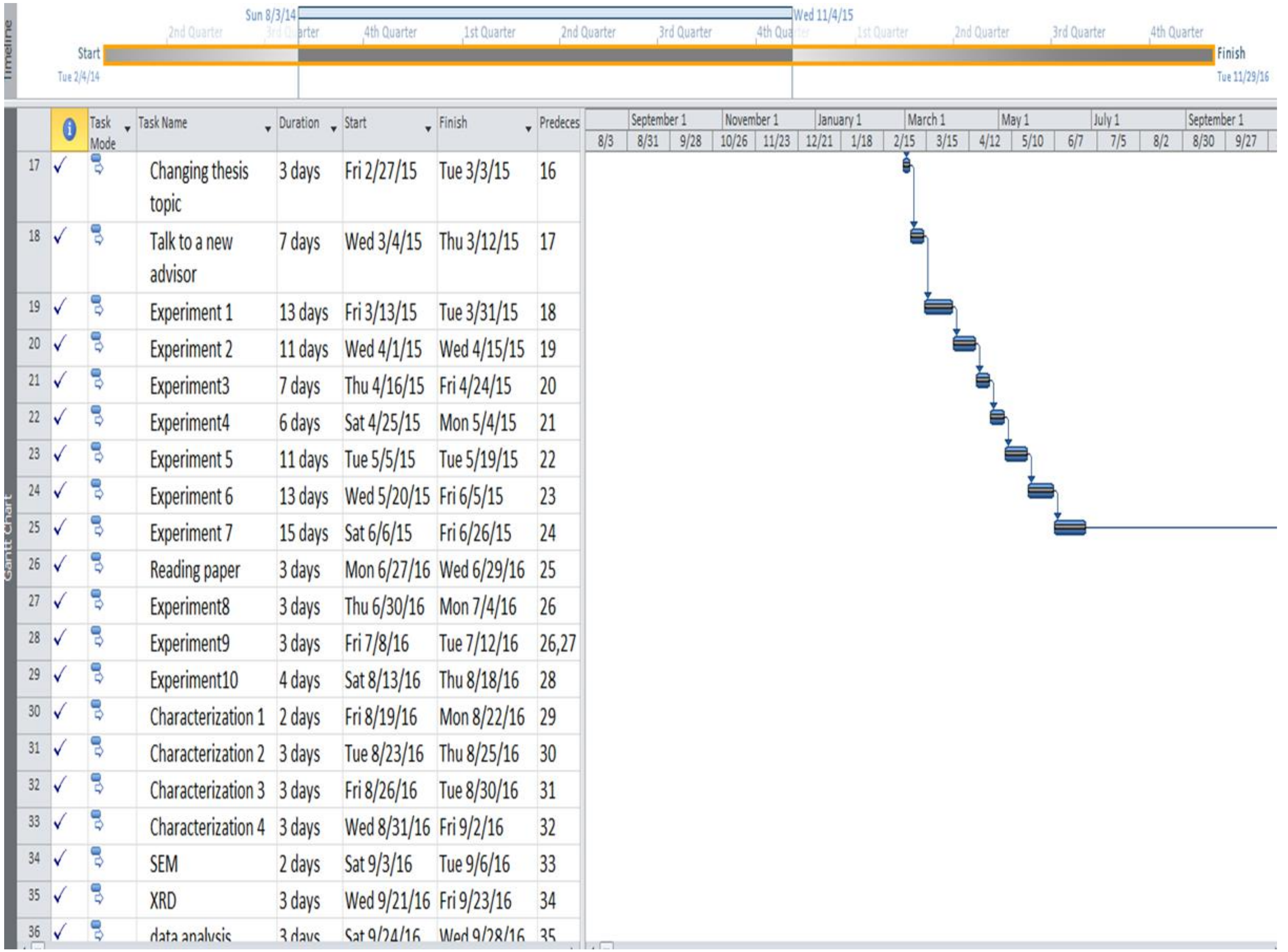

	Task Mode	Task Name	Duration	Start	Finish	Predeces
17	✓	Changing thesis topic	3 days	Fri 2/27/15	Tue 3/3/15	16
18	✓	Talk to a new advisor	7 days	Wed 3/4/15	Thu 3/12/15	17
19	✓	Experiment 1	13 days	Fri 3/13/15	Tue 3/31/15	18
20	✓	Experiment 2	11 days	Wed 4/1/15	Wed 4/15/15	19
21	✓	Experiment3	7 days	Thu 4/16/15	Fri 4/24/15	20
22	✓	Experiment4	6 days	Sat 4/25/15	Mon 5/4/15	21
23	✓	Experiment 5	11 days	Tue 5/5/15	Tue 5/19/15	22
24	✓	Experiment 6	13 days	Wed 5/20/15	Fri 6/5/15	23
25	✓	Experiment 7	15 days	Sat 6/6/15	Fri 6/26/15	24
26	✓	Reading paper	3 days	Mon 6/27/16	Wed 6/29/16	25
27	✓	Experiment8	3 days	Thu 6/30/16	Mon 7/4/16	26
28	✓	Experiment9	3 days	Fri 7/8/16	Tue 7/12/16	26,27
29	✓	Experiment10	4 days	Sat 8/13/16	Thu 8/18/16	28
30	✓	Characterization 1	2 days	Fri 8/19/16	Mon 8/22/16	29
31	✓	Characterization 2	3 days	Tue 8/23/16	Thu 8/25/16	30
32	✓	Characterization 3	3 days	Fri 8/26/16	Tue 8/30/16	31
33	✓	Characterization 4	3 days	Wed 8/31/16	Fri 9/2/16	32
34	✓	SEM	2 days	Sat 9/3/16	Tue 9/6/16	33
35	✓	XRD	3 days	Wed 9/21/16	Fri 9/23/16	34
36	✓	data analysis	3 days	Sat 9/24/16	Wed 9/28/16	35

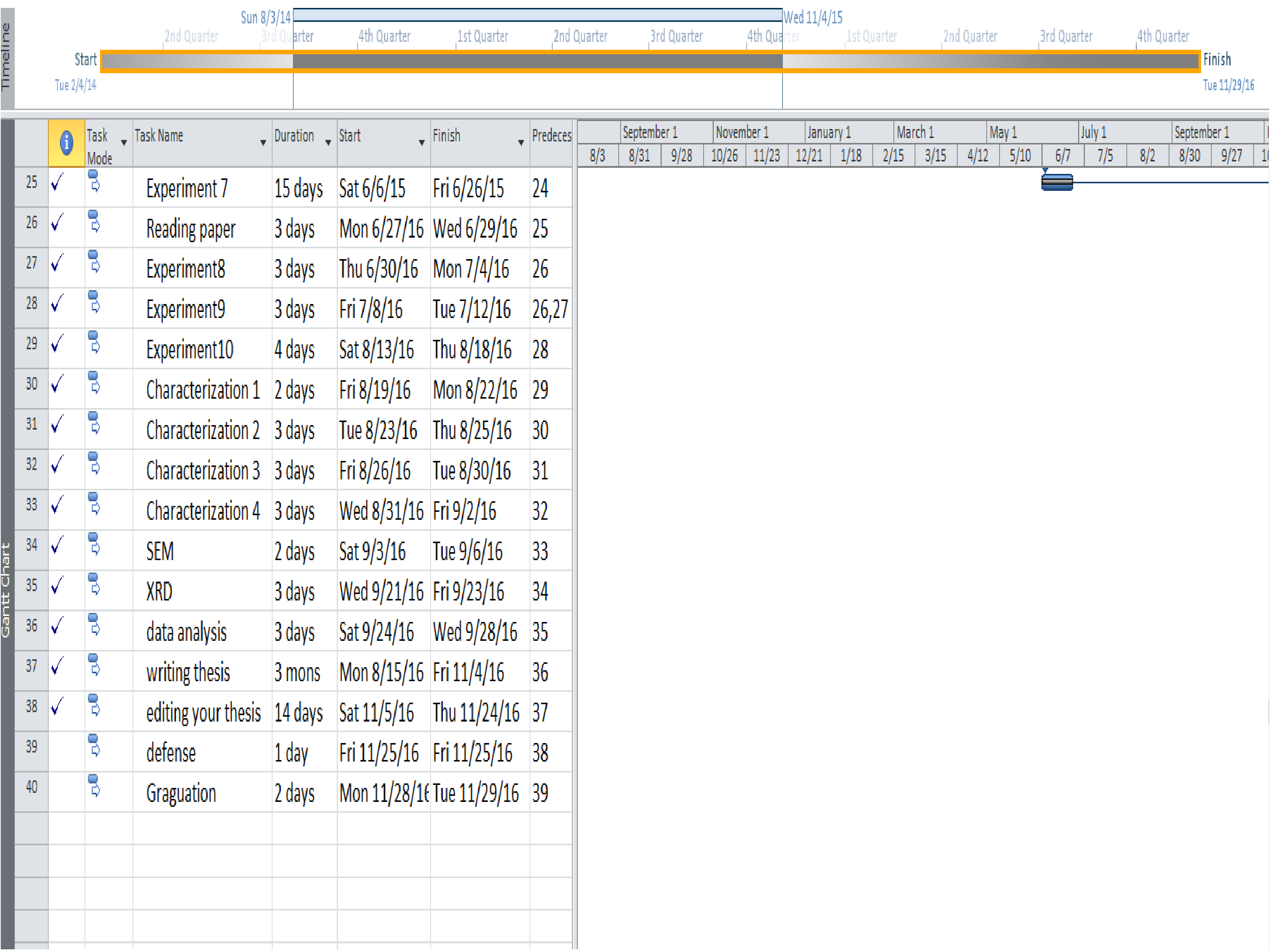

		Task Mode	Task Name	Duration	Start	Finish	Predeces
25	✓		Experiment 7	15 days	Sat 6/6/15	Fri 6/26/15	24
26	✓		Reading paper	3 days	Mon 6/27/16	Wed 6/29/16	25
27	✓		Experiment8	3 days	Thu 6/30/16	Mon 7/4/16	26
28	✓		Experiment9	3 days	Fri 7/8/16	Tue 7/12/16	26,27
29	✓		Experiment10	4 days	Sat 8/13/16	Thu 8/18/16	28
30	✓		Characterization 1	2 days	Fri 8/19/16	Mon 8/22/16	29
31	✓		Characterization 2	3 days	Tue 8/23/16	Thu 8/25/16	30
32	✓		Characterization 3	3 days	Fri 8/26/16	Tue 8/30/16	31
33	✓		Characterization 4	3 days	Wed 8/31/16	Fri 9/2/16	32
34	✓		SEM	2 days	Sat 9/3/16	Tue 9/6/16	33
35	✓		XRD	3 days	Wed 9/21/16	Fri 9/23/16	34
36	✓		data analysis	3 days	Sat 9/24/16	Wed 9/28/16	35
37	✓		writing thesis	3 mons	Mon 8/15/16	Fri 11/4/16	36
38	✓		editing your thesis	14 days	Sat 11/5/16	Thu 11/24/16	37
39			defense	1 day	Fri 11/25/16	Fri 11/25/16	38
40			Graguation	2 days	Mon 11/28/1(	Tue 11/29/16	39

Appendix F: Identification of All Software Used in Research and Thesis Generation

Computer #1:
Model Number: x86-64Full_14Sep
Serial Number: Dell 1707FP
Location: Engineering Research Center
Owner: Department of Electrical Engineering

Software #1:
Name: Microsoft Office 2013
Purchased by: Department of Electrical Engineering

Computer #1:
Model Number: HP virgin (10.0240)
Serial Number: 5CD5520K41
Location: 888. W Lawson St apt 2J
Owner: Hakimah Alahmed

Software #1:
Name: Microsoft Office 2015
Purchased by: Hakimah Alahmed

Software #2:
Name: Microsoft Project 2010
Purchased by: MSDN Academy Alliance through Engineering